

Hadron Properties and Meson Mixing Effects  
in  
Hot and Dense Strongly Interacting Matter

by

Octavian Teodorescu

A thesis submitted  
to the Faculty of Graduate Studies and Research  
in partial fulfillment of the requirements  
of the degree of

Doctor of Philosophy

Physics Department, McGill University, Montréal, Canada.  
©Octavian Teodorescu, October 2001



National Library  
of Canada

Acquisitions and  
Bibliographic Services

395 Wellington Street  
Ottawa ON K1A 0N4  
Canada

Bibliothèque nationale  
du Canada

Acquisitions et  
services bibliographiques

395, rue Wellington  
Ottawa ON K1A 0N4  
Canada

*Your file Votre référence*

*Our file Notre référence*

The author has granted a non-exclusive licence allowing the National Library of Canada to reproduce, loan, distribute or sell copies of this thesis in microform, paper or electronic formats.

The author retains ownership of the copyright in this thesis. Neither the thesis nor substantial extracts from it may be printed or otherwise reproduced without the author's permission.

L'auteur a accordé une licence non exclusive permettant à la Bibliothèque nationale du Canada de reproduire, prêter, distribuer ou vendre des copies de cette thèse sous la forme de microfiche/film, de reproduction sur papier ou sur format électronique.

L'auteur conserve la propriété du droit d'auteur qui protège cette thèse. Ni la thèse ni des extraits substantiels de celle-ci ne doivent être imprimés ou autrement reproduits sans son autorisation.

0-612-78784-2

## *Abstract*

In the present thesis, the properties of hadrons in a dense medium are studied. The collective excitations related to the propagation of scalar and vector mesons in dense nuclear matter are discussed in a relativistic mean field model. Finite temperature effects on the meson properties in nuclear matter are also considered. One of the main concerns of the present thesis is the evaluation of symmetry-breaking effects induced by the dense matter. Special emphasis is put on the study of scalar-vector meson mixing effect, a pure density-dependent effect forbidden in vacuum on account of the Lorentz symmetry. In this direction, a new symmetry-breaking effect – the  $\rho$ - $a_0$  meson mixing – is revealed and studied in detail along with a similar effect induced by the  $\omega$ - $\sigma$  mixing. The possibility of a new dilepton channel, arising from  $\pi$ - $\eta$  collisions and mediated by  $\rho$ - $a_0$  mixing, is further discussed in a relativistic kinetic model. The effects of  $\omega$ - $\sigma$  mixing on the amplitude of the dilepton production process from pion annihilation is also evaluated in a similar manner. The possibility of observing such symmetry-breaking effects in nucleus-nucleus collision experiments is investigated. For the space-time evolution of the matter formed during the collision, a thermal model is employed and the equation of state is determined from the interacting nuclear matter within the scope of a mean field model. We argue that such processes can be observed in the dilepton spectra at GSI/SIS energies, while they are not so evident at higher energy experiments performed at CERN/SPS.

## *Résumé*

Dans la thèse actuelle, les propriétés des hadrons dans un milieu dense sont étudiées. Les excitations collectives liées à la propagation des mésons scalaires et vectoriels dans la matière nucléaire dense sont discutées dans un modèle relativiste de champ moyen. Des effets de la température finie sur les propriétés des mésons dans la matière nucléaire sont également présentés. Un des principaux soucis de la thèse actuelle est l'évaluation des effets de brisure de symétrie induits par la matière dense. Nous considérons particulièrement les effets de mélange de mésons scalaire-vectoriel, des effets dépendants purement de la densité, interdits dans le vide à cause de la symétrie de Lorentz. Dans cette direction, un nouvel effet de brisure de la symétrie – le mélange de mésons  $\rho$ - $a_0$  – est indiqué et étudié en détail avec un effet semblable induit par le mélange de  $\omega$ - $\sigma$ . La possibilité d'un nouveau canal de dilepton, résultant des collisions de  $\pi$ - $\eta$  et induit par le mélange de  $\rho$ - $a_0$ , est discuté par la suite. Les effets du mélange de  $\omega$ - $\sigma$  sur l'amplitude du procédé de production de dilepton par l'annihilation des pions sont également évalués. La possibilité d'observer de tels effets de brisure de symétrie en expérience de collision de noyau-noyau est quantifiée. Pour l'évolution d'espace-temps de la matière formée pendant la collision, nous utilisons un modèle thermique et l'équation d'état déterminée à partir d'un modèle de matière nucléaire interagissant avec un champ moyen. Nous discutons du fait qu'on peut observer de tels processus dans les spectres de dilepton aux énergies de GSI/SIS, alors qu'ils ne sont pas aussi évidents à des énergies plus élevées comme à celles du CERN/SPS.

---

---

# CONTENTS

---

---

<b>1</b>	<b>INTRODUCTION</b>	<b>1</b>
1.1	Heavy Ion Collisions: Factories of Nuclear Matter under Extreme Conditions . . . . .	2
1.2	Formation and Evolution of Dense Matter in Nucleus-Nucleus Collisions	4
1.3	Dileptons as a Penetrating Probe of Heavy Ion Collisions . . . . .	7
1.4	Hadrons in Nuclear Matter . . . . .	8
1.5	Structure and Originality of the Thesis . . . . .	11
<b>2</b>	<b>NUCLEAR MATTER AT FINITE TEMPERATURE AND DENSITY</b>	<b>16</b>
2.1	Field Equations of Motion . . . . .	19
2.2	Mean Field Approximation . . . . .	20
2.2.1	Dirac Equation for Nucleons and the Field Expansion . . . . .	21
2.2.2	Nuclear Matter at Finite Density . . . . .	22
2.2.3	Thermodynamics of Nuclear Matter at Finite Temperature . . . . .	26
2.3	Nucleon Propagator at Finite Temperature . . . . .	33
<b>3</b>	<b>MESONS IN DENSE NUCLEAR MATTER</b>	<b>39</b>
3.1	Linear Response Theory . . . . .	40
3.2	Collective Excitations and the Random Phase Approximation . . . . .	44
3.3	Light Vector Mesons in Nuclear Matter: $\rho$ and $\omega$ . . . . .	47
3.4	Scalar Mesons in Nuclear Matter: $a_0$ and $\sigma$ . . . . .	56
3.5	Scalar-Vector Meson Mixing in Nuclear Matter . . . . .	58

3.6	Vector Mesons in Nuclear Matter at Finite Temperature . . . . .	67
3.6.1	Decay Widths Modification at Finite Temperature . . . . .	70
<b>4</b>	<b>DILEPTON PRODUCTION FROM THERMAL MESONS</b>	<b>74</b>
4.1	Vector Meson Dominance . . . . .	76
4.2	Thermal Rates of Dilepton Production . . . . .	79
4.3	Production from Processes $ab \rightarrow e^+e^-$ . . . . .	82
4.4	Dominant Dilepton Sources in the Low Invariant Mass Range . . . . .	83
4.5	Thermal Dileptons Produced Through Meson Mixing . . . . .	84
4.5.1	Isvector Channel Mediated by $\rho$ - $a_0$ Mixing . . . . .	85
4.5.2	Isoscalar Channel Mediated by $\omega$ - $\sigma$ Mixing . . . . .	91
4.6	Interference Between the Direct and Mixing-Induced Channel . . . . .	95
4.7	Thermal Rates at Finite Temperature and Density . . . . .	98
<b>5</b>	<b>SPACE-TIME EVOLUTION AND THE DILEPTON SPECTRA</b>	<b>102</b>
5.1	Relativistic Thermal Model . . . . .	103
5.2	Results for CERES/SPS . . . . .	104
5.3	Prediction for Experiments at HADES/GSI . . . . .	108
<b>6</b>	<b>CONCLUSIONS AND SUMMARY</b>	<b>113</b>
<b>A</b>	<b>PROPERTIES OF FINITE TEMPERATURE GREEN'S FUNCTION</b>	<b>116</b>
<b>B</b>	<b>SOME PROPERTIES OF SPIN-1 BOSON SELF-ENERGY</b>	<b>119</b>

---



---

## LIST OF FIGURES

---



---

1.1	Space-time diagram of a nucleus-nucleus collision . . . . .	5
1.2	Phase diagram of nuclear matter at extreme conditions . . . . .	6
2.1	n-n interaction through $\sigma$ and $\omega$ meson exchange . . . . .	18
2.2	Saturation curve for nuclear matter . . . . .	24
2.3	Nucleon effective mass at zero temperature . . . . .	25
2.4	Nuclear matter equation of state at zero temperature . . . . .	26
2.5	The effective mass of nucleon as function of temperature and baryonic density . . . . .	30
2.6	Specific energy as function of temperature . . . . .	32
2.7	Equation of state for different temperatures . . . . .	32
2.8	Specific entropy of nucleon as function of temperature and baryonic density . . . . .	34
3.1	Random Phase Approximation diagrams . . . . .	45
3.2	$\rho - nn$ and $\omega - nn$ loops . . . . .	48
3.3	Dispersion curves for $\rho$ and $\omega$ mesons . . . . .	56
3.4	$a_0 - nn$ and $\sigma - nn$ loops . . . . .	57
3.5	Dispersion curves for $a_0$ and $\sigma$ mesons . . . . .	59
3.6	Feynman diagrams showing $a_0$ - $\delta$ and $\omega$ - $\sigma$ mixing . . . . .	60
3.7	Dispersion curves for $\rho$ and $a_0$ mesons with mixing . . . . .	63
3.8	Dispersion curve for $\omega$ and $\sigma$ mesons with mixing . . . . .	64
3.9	The invariant mass as a function of the nuclear matter density . . . . .	65

3.10	Mixing angles as function of nuclear matter density . . . . .	66
3.11	Mixing angle as function of momentum . . . . .	67
3.12	Vector meson masses as function of temperature . . . . .	69
3.13	Scalar meson masses as function of temperature . . . . .	69
3.14	Decay of $\rho$ meson. . . . .	70
3.15	The $\rho$ decay width as a function of temperature for different values of baryon densities . . . . .	73
4.1	Schematic diagram showing the different contributions to the dilepton yield in an relativistic heavy ion collision . . . . .	76
4.2	The Feynman diagram for the process $\pi + \pi \rightarrow e^+ + e^-$ . . . . .	77
4.3	Feynman diagram for the pion annihilation into dilepton . . . . .	78
4.4	Dominant thermal dilepton channels . . . . .	85
4.5	The Feynman diagram for the process $\pi + \eta \rightarrow e^+ + e^-$ . . . . .	86
4.6	Dilepton spectrum of $\pi + \eta \rightarrow e^+ + e^-$ . . . . .	87
4.7	Dilepton spectrum of $\pi + \eta \rightarrow e^+ + e^-$ as function of momentum and density . . . . .	88
4.8	Effect of mixing on dilepton production rate in the isovector channel, T=50 MeV . . . . .	89
4.9	Effect of mixing on dilepton production rate in the isovector channel, T=75 MeV . . . . .	90
4.10	$\pi$ - $\eta$ channel with different $\Gamma_{a_0}$ widths . . . . .	91
4.11	The Feynman diagram of the process $\pi + \pi \rightarrow e^+ e^-$ mediated by $\omega$ - $\sigma$ mixing . . . . .	91
4.12	Dilepton spectrum of the isoscalar channel . . . . .	93
4.13	$\sigma$ - $\omega$ mixing effect on dilepton spectrum at T=50 MeV . . . . .	93
4.14	$\sigma$ - $\omega$ mixing effect on dilepton spectrum at T=75 MeV . . . . .	94

4.15	Interference in the $\pi\pi$ annihilation . . . . .	96
4.16	Dilepton spectrum with mixing at $T=50$ MeV . . . . .	98
4.17	Dilepton spectrum with mixing $T = 50$ MeV . . . . .	99
4.18	Dilepton spectrum with mixing $T = 150$ MeV . . . . .	99
5.1	Hadronic cocktail and p-BE, p-Au results . . . . .	105
5.2	Temperature and density dependence on time for Pb(158GeV)+Au .	106
5.3	Dilepton spectra in a CERES/SPS scenario . . . . .	107
5.4	Temperature and density dependence on time for 1GeV Au+Au . . .	109
5.5	Dilepton spectra in a HADES/SIS scenario with free masses and decay widths . . . . .	110
5.6	Dilepton spectra in a HADES/SIS scenario considering in-medium modifications . . . . .	111

---

---

## LIST OF TABLES

---

---

1.1	Properties of relevant hadrons . . . . .	14
4.1	VMD couplings . . . . .	78

## *Acknowledgment*

I would like to express sincere thanks to my supervisor, Professor Charles Gale, for his permanent guidance and help. His deep understanding of the nuclear physics and heavy ion physics in particular often amazed me. His expertise in the field made my work much easier and his pleasant attitude as supervisor transformed in joy my work at McGill. He also gave me this great opportunity to participate in several important conferences where I met and learned from experts in the field of relativistic heavy ion collisions. In the extra-curricular events of our group, I was also happy of his companion as a man of great joy and always willing to help other people, whose example I will certainly try to follow.

I would also like to address special thanks to Dr. A. K. Dutt-Mazumder. Our discussions were very helpful and I was often pleasantly surprised by his deep insights, particularly on physics problems. His enthusiasm for the study of nuclear physics also motivated my work. Last, but not least, I am grateful for our friendship that made a real pleasure my work in the last two years, and I am sure that our fruitful collaboration will continue in the future, needless to say our friendship.

I am also thankful for what I have learned during my M. Sc. studies in experimental nuclear physics specially from Professors Jean Barrette and Tommy Mark. It will always be a pleasure to thank Professor Douglas Stairs for his permanent support during my studies at McGill. My discussions with Professor Subal Das Gupta were a real pleasure and I will always remember them with great joy. I would also like to acknowledge useful discussions with Professor Sangyong Jeon. I appreciated a lot the advises received from Dr. Vasile Topor-Pop.

Finally, I would like to add that I am grateful for the stimulating environment I found in the Physics Department at McGill University. The interactions with the postdoctoral fellows and graduate students helped constantly during my studies. Special thanks to Mrs. Paula Domingues for showing me the way to such a great university.

## INTRODUCTION

---

---

Fundamental questions like

*“What happens when ordinary matter is so greatly compressed so that atomic nuclei overlap to form superdense nuclear matter, as in a neutron star?”*,

*“What happens when nuclear matter is heated to such great temperatures that nucleons and pions melt into quarks and gluons? [1]”*,

*“What are the properties and how could we study this new form of matter called Quark Gluon Plasma (QGP)?”*,

are queries that have intrigued some of the best minds of the contemporary world. Unraveling the properties of matter at normal nuclear matter density and at densities several times higher than that of ordinary nuclear matter, or at temperature sufficiently high as to unleash new phenomena, has been a fascinating field of basic research for quite some time. In fact, matter in its exotic forms naturally attracts the attention of various cross disciplinary studies, *inter alia*, gravitation, cosmology, nuclear physics, particle physics, and astrophysics coming together to untangle some of the fundamental issues concerning the early Universe, stellar and cosmic evolution.

## 1.1 *Heavy Ion Collisions: Factories of Nuclear Matter under Extreme Conditions*

Even though matter at such a high density or temperature lies ‘far outside the realm of direct human experience’, in the laboratory such an exotic state of matter, can be produced temporarily by colliding heavy nuclei at sufficiently high energy. The principal goal of this initiative is to explore the phase structure of the underlying theory of strong interactions - Quantum Chromodynamics (QCD). With this motivation, in recent years, efforts have been directed towards the design of experiments devoted to the fundamental issues concerning the equation of state of such systems, the dynamics of evolution and the possibility of the formation of a Quark Gluon Phase of matter as per the conventional wisdom of QCD [2, 3].

It has been now more than 30 years since the first heavy ion beams became available at the BEVELAC at Lawrence Berkeley National Laboratory. Alternating Gradient Synchrotron (AGS) at Brookhaven National Laboratory (BNL) came into operation more than 15 years ago and provided beams of  $^{197}\text{Au}$  ions accelerated at 11 GeV/nucleon. In the following experiments at the Super Proton Synchrotron (SPS) at CERN, more energetic ions of  $^{32}\text{S}$  and  $^{208}\text{Pb}$  at 160 GeV/nucleon were available. The Relativistic Heavy Ion Collider (RHIC) at Brookhaven has just started functioning and systematic experimental data will be available in the very near future. Also, the Large Hadron Collider (LHC) at CERN is expected to be ready in about four years from now. Heavy ion (*e.g.*  $^{208}\text{Pb}$  and  $^{197}\text{Au}$ ) collisions at the RHIC and LHC with centre of mass energies 200 AGeV and 5500 AGeV respectively are expected to produce extremely high energy densities.

The question which arises is whether one can produce a large enough and sufficiently long-lived composite system so that collective phenomena can occur and allow a statistical approach. An even bigger challenge is to extract information on the dy-

namics and the properties of the earliest and the hottest stage of such collisions, because even if QGP is produced it only has a transient existence. Due to colour confinement quarks and gluons cannot escape from the collision and must combine to colour-neutral hadrons before traveling to the detectors. Hence, all signals emerging from the QCD plasma can receive substantial contribution from the hadronic phase. Therefore, a detailed study of the hadronic phase is important in order to distinguish the emissions from the QGP.

However, the study of the hot and dense hadronic matter is also interesting in its own right. Many questions are still unanswered regarding the properties of matter in the hadronic phase in a changing environment. Beyond the fundamental theoretical challenge of this study, such investigations are also of relevance to various important issues of astrophysics. In this respect, the high-temperature region is most relevant for cosmological studies, while high baryon-density transitions are important for the structure and properties of neutron stars [4]. Furthermore, the changes of meson properties as compared to those in free space, manifest themselves in fundamental hadronic and nuclear phenomena [5]. The high-energy heavy-ion reactions can produce hadronic matter in such extreme conditions in the laboratory, and therefore provide a large amount of information. Starting with the first experiments at Bevalac [6, 7], and extending the studies to higher energies at AGS [8] and SPS [9], the study of properties of hadronic matter at extreme conditions continues to be at the forefront of nuclear physics research. New results are expected next year from the HADES experiment at GSI in Germany, an experiment dedicated to the study of in-medium properties of hadrons with special focus on the light vector mesons [10].

In the next section we will discuss the evolution of the dense matter formed in a typical collision of two heavy ions at relativistic energies. We just briefly discuss the possibility of QGP formation in such collisions, and its subsequent transition to hadronic matter. We insist more on the hadronic state of this excited nuclear matter,

since, for the energies discussed in the present thesis, the matter produced will most likely be in this form.

## 1.2 *Formation and Evolution of Dense Matter in Nucleus-Nucleus Collisions*

As the two heavy ions collide at very high energies, they deposit a substantial part of their kinetic energy into a small region of space. Depending on the energy density achieved, the initial state of the system may be either in the form of a QGP or a hot/dense hadronic gas. The evolution of an ultra-relativistic heavy ion collision with an intermediate state of QGP can roughly be described in terms of four regimes as discussed below. Since these vary widely in nature, the physics governing these stages are quite different. Figure 1.1 shows a schematic space-time diagram of such an ultra-relativistic heavy ion collision.

**a) Formation of QGP:** Immediately after the collision of the two Lorentz contracted nuclei, the scattered partons decohere and free-stream. Rescatterings of these partons can lead to locally thermalized QGP after a time generally taken to be  $\sim 1$  fm/c [11]. The value of the thermalization (realization of kinetic equilibrium) time is still rather uncertain.

**b) Expansion of the QGP:** Assuming that the interactions of quarks and gluons are sufficiently small at the temperatures achieved in ultra-relativistic heavy ion collisions, the energy density, pressure etc. can be calculated in QCD using thermal perturbation theory [12]. Driven by the high internal pressure, the thermalized QGP expands and this evolution can perhaps be described according to the laws of relativistic hydrodynamics [13, 14].

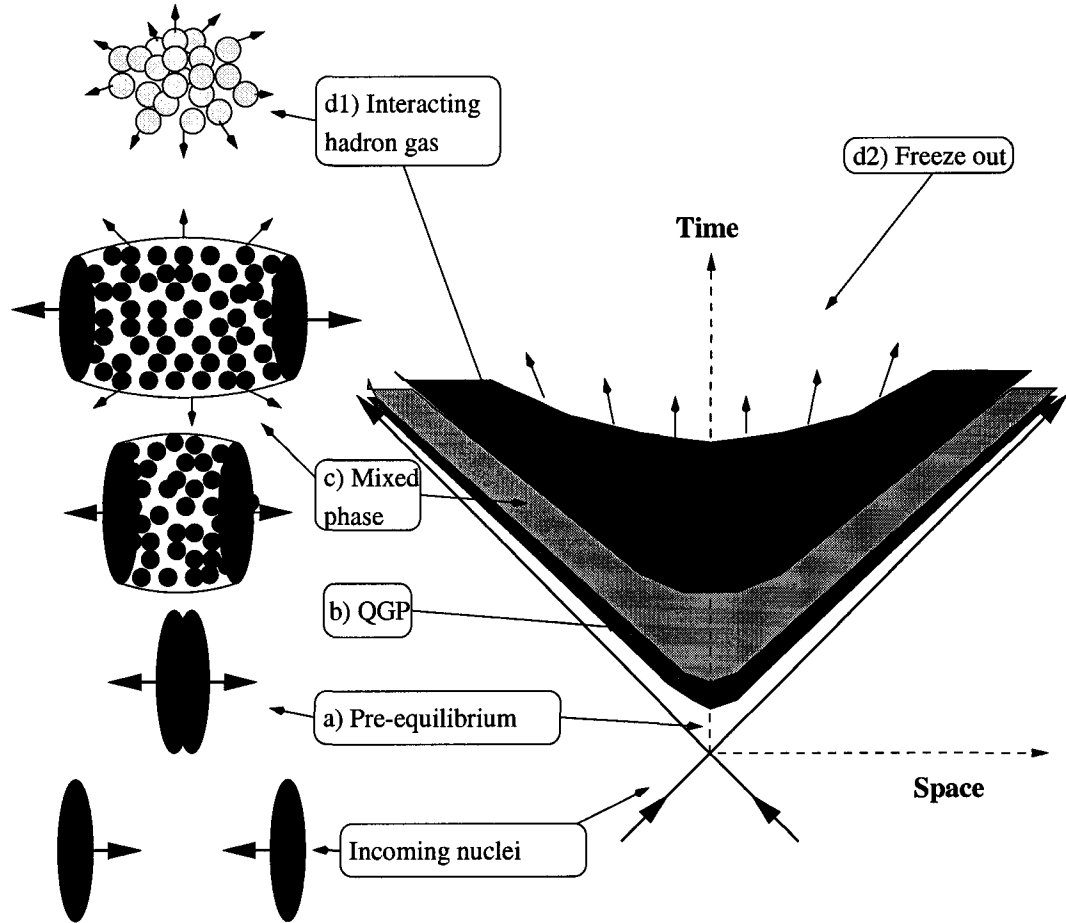


Figure 1.1: Space-time diagram of a nucleus-nucleus collision showing various phases of nuclear matter during expansion.

**c) Hadronization and the mixed phase:** Expansion of the QGP proceeds until the critical temperature  $T_c$  is reached. At this instant, a phase transition to hadronic matter starts. The order of the transition is still somewhat controversial [15]. Mostly, for the purpose of calculation of the signals of QGP a first order phase transition is considered [16], as suggested by lattice QCD calculations [17]. The value of the critical temperature is not exactly known, but values are around 150 – 200 MeV [18, 19, 20] at zero baryonic density. Of course, the critical temperature depends on the baryonic density. Figure 1.2 presents the phase diagram of nuclear

matter showing the phase transition curve in the  $(T, \rho_B)$  plane and the trajectories

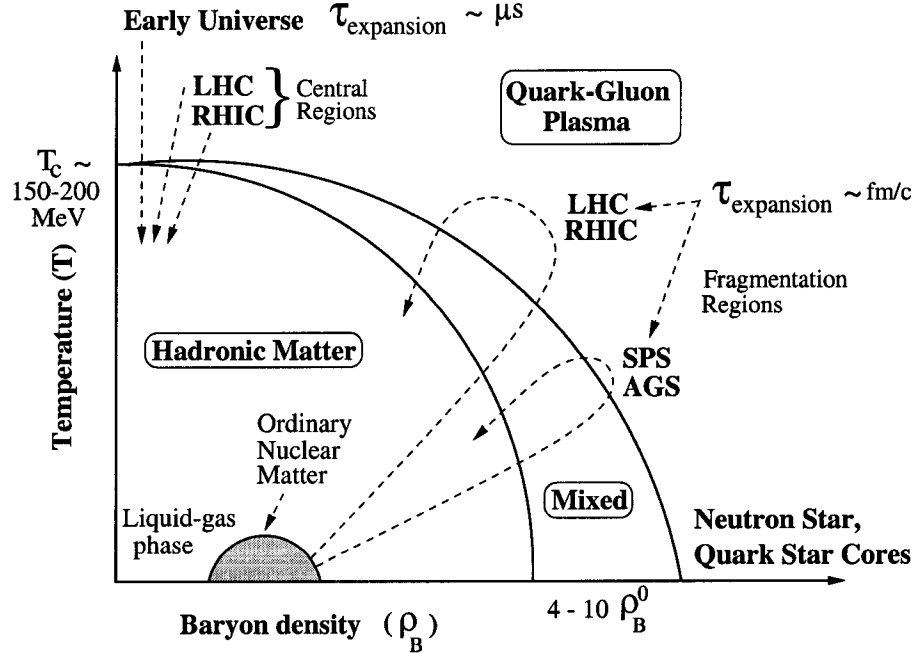


Figure 1.2: Phase diagram of nuclear matter at extreme conditions [21]

of different experiments in this plane. Through the process of hadronization, the coloured particles - quarks and gluons combine to form colour-neutral hadrons. The released latent heat maintains the temperature of the system at  $T_c$  even though the system continues to expand. During this time, quark and hadronic matter coexist until all the matter has converted to the hadronic phase.

d) **The hadronic phase and freeze-out:** The resulting hadronic matter expands and cools as long as the system can sustain interactions. As we will see later in this thesis, the properties of hadrons at high temperature are modified non-trivially due to interactions. Also, the equation of state departs from the one of a free Fermi gas and consequently influences the cooling process. During this expansion, a reasonable assumption is to consider hadrons to be thermally and chemically equilibrated.

With the dropping temperature, the chemical interactions cease between hadrons and the *chemical freeze-out* occurs [22]. The particles still undergo elastic scatterings and therefore the hadronic gas is thermally equilibrated. Once the mean free path of the hadrons becomes comparable to the dimensions of the system, they decouple and free-stream towards the detector. We therefore reach the *thermal freeze-out* when the hadrons cease to interact. The value of the freeze-out temperature is still an unsettled issue. It is of course dependent on the type of collision, energy density and size of the system formed. Still, various calculations show different values for collisions at the same energy, say SPS [23, 24]. The contribution to the signal output will depend on the freeze-out temperature, even more when transverse expansion of the fireball is considered [25].

### 1.3 *Dileptons as a Penetrating Probe of Heavy Ion Collisions*

Dileptons ( $e^+e^-$  or  $\mu^+\mu^-$ ) are considered to be by far the most direct probes of the collisions. Due to their large mean free paths they have the unique property of being less prone to secondary interactions because of their electromagnetic nature and, therefore, once produced they leave the collision area without further interactions. By the same token, real photons have a large mean free path as well, but, they face a large background produced mainly by the decay of neutral pions and also by the  $\eta$  mesons [26]. Dileptons also have the advantage of being characterized by their invariant mass, parameter which is lacking in the case of real photons.

Hadrons which reach the detectors can mostly tell us about the later stage of collision, the freeze-out zone. Moreover, unlike hadronic signals, dileptons are produced all through the evolution process therefore providing information on the whole space-time evolution of the collision. In this respect, one again must bear in mind that

even if QGP is produced in the initial stages, the quarks and gluons will eventually form colour singlet hadrons before traveling to the detectors.

In the QGP phase, if created in the collision, the dileptons are mainly produced by thermal interactions between the constituents of the plasma, like the quark-antiquark annihilation [27, 28] or other sources like  $gg \rightarrow e^+e^-$ , which can be important at finite baryonic chemical potential [29].

In the hadronic phase, dileptons come mainly from light meson annihilation processes, like pions and kaons. These processes are dynamically enhanced through the formation of light vector meson resonances, like  $\rho$ ,  $\omega$ ,  $\phi$ , which ultimately decay into lepton pairs. We will discuss this process of the hadron coupling to a virtual photon, which ultimately decays into a dilepton, in the Vector Meson Dominance model in Sec. 4.1. For now, we note that the decay of light vector mesons into dileptons constitute an important source of dileptons in the vicinity of their pole mass region.

We conclude by emphasizing that the study of the dilepton spectrum from an excited hadronic matter is important not only for the study of the in-medium modifications of hadron properties, but also an accurate estimation of the contributions from hadronic sources is critical to unmask the emission from the QGP.

## 1.4 Hadrons in Nuclear Matter

The behaviour of vector mesons in dense and/or hot nuclear medium or even at densities of normal nuclear matter has attracted widespread interest both in the arena of theory[30, 31, 32, 33] and experiment [34, 35, 36, 37, 38]. As mentioned before, in the context of heavy ion collisions or in other related experiments, the importance of light vector mesons like  $\rho, \omega$  and  $\phi$  mesons resides in the fact that they decay although not dominantly and yet importantly into lepton pairs. Particularly the  $\rho$  meson, having a large decay width and hence a short life-time, has an important

contribution to the lepton pair production from the hot medium. Aside from the information about the dynamics of heavy ion collisions, these decays could also reveal the properties and behaviour of light vector mesons at normal nuclear matter density in electron scattering experiments [38].

On the experimental front, old and current experiments have been designed to uncover the medium modifications of these vector mesons both at normal and high nuclear density. It may be mentioned that such measurements were initially carried out at the Bevalac, by the DLS collaboration [35, 36, 37]. However, poor statistics and a lack of required resolution stood in the way of detailed conclusions, although preliminary indications of the properties of vector meson masses were obtained from the invariant mass spectra of the dileptons. The High Acceptance DiElectron Spectrometer (HADES), a second generation apparatus which just has started to operate at the SIS accelerator at GSI in Germany, is dedicated to the investigation of in-medium properties of vector mesons. The experiments to be carried out at HADES are expected to settle some of the controversial points regarding the shift in masses of the vector mesons, their change of decay widths and other various related issues [34]. On the other front at the Thomas Jefferson National Accelerator Facility (TJNAF) [38], medium modifications of vector mesons at normal nuclear matter shall be studied through various scattering experiments induced by high energy electrons. These experiments are particularly well suited to the study of vector meson properties at normal nuclear matter density. At higher energies, the temperature dependence together with the corrections to the mass and decay width at non-zero baryon density characterizing the in-medium behaviour of these hadrons also acquired cardinal importance in the understanding of the low invariant mass spectrum planned to be observed at LHC or RHIC. Experimentally observed enhancements of the low invariant mass dilepton yield measured by CERES collaboration at the SPS, has made the field all the more interesting and does in fact suggest that medium modification of

vector mesons be included in order to explain the data [39, 40].

In the arena of theory at a more fundamental level, on the other hand, speculations that chiral symmetry may be restored at very high temperature or density have been put forward by Brown and Rho through their scaling hypothesis [41]. Moreover, issues such as whether the vector meson masses go down or up with temperature, have been subjects of intense debate. In fact models used to examine the in-medium properties of these particles cover a wide range, starting from hadronic models to models considering explicitly the individual parton degrees of freedom as fundamental constituents of mesons. The former involves Walecka-type of models or the non-linear sigma model where nucleons and mesons are treated as fundamental fields, while the latter constitute a wider variety including the Nambu-Jona-Lasinio (NJL) model, effective chiral Lagrangians, QCD sum rule approaches, and others [42, 43]. Results and conclusions drawn from these studies are also not free from controversy, while some of them claim that with the increase of temperature or density the vector meson masses go up, some others report the opposite. For instance, at finite density, the theory based on QCD sum rules exhibits a reduction of the vector meson masses [42, 43], while calculation based on the VMD model suggests that their masses remain almost unaltered in the medium [44]. However, according to the latter, their decay widths may change significantly. The calculation by Chin [45] predicted an increase in  $\omega$ -meson mass in nuclear matter considering the nucleon(n)-nucleon hole(h) intermediate state, where, however, the effect of the nucleon(n)-antinucleon( $\bar{n}$ ) loop had not been taken into account. On the other hand, the calculation by Jean *et al.* showed that if the effects of both the Dirac vacuum as also the Fermi sea are taken together the mass of the  $\omega$  meson decreases in matter [32]. A similar lowering of vector meson masses has also been predicted by Brown and Rho, performing calculations on the basis of dilatational symmetry in the chiral Lagrangian [41, 46]. However, it is not quite clear whether the physical mechanisms responsible for the reduction of vector meson

masses in these models are related to each other.

Nevertheless, a thorough understanding of the behaviour of different hadrons in hot and dense matter, is necessary and would pave the way to the understanding of the numerous and complex signals received by the detectors and make possible the extraction of information from heavy ion experiments.

The present effort will help not only to answer question related to the different behaviour of mesons in matter, but will also bring light on new effects which arise from the symmetry breaking in a dense medium. Mixing of different quantum states in nuclear matter are a result of such broken symmetry effects. In this work it is interesting to study the scalar-vector meson mixing via nucleon-nucleon excitations in nuclear matter which is a pure density-dependent effect [45]. Such mixing effects could bring modifications in the vector meson spectral density, and consequently, changing not only their properties in matter but also the dilepton spectrum induced by their decay. In a thermal bath,  $\pi$  mesons are abundantly produced and their collisions have a finite cross section to produce the  $\sigma$  meson. Similarly, the  $\eta$  meson is produced in large quantities and its collision with pions produce the scalar  $a_0$  meson. Therefore, scalar-vector meson mixing effects, like  $\sigma$ - $\omega$  or  $a_0$ - $\rho$ , are expected to bring important contribution to the total dilepton yield in environments with a large baryon chemical potential [47, 48, 49]. Such intriguing queries induced concentrated efforts among contemporary nuclear physicists in the last years and motivated the research described in the present thesis.

## 1.5 *Structure and Originality of the Thesis*

The thesis is structured in six chapters and begins with a short introduction into the field, showing the motivation for the present work.

Chapter 2 discusses the properties of nuclear matter at finite density and tem-

perature. After a short presentation of the formalism, we evaluate the properties of nuclear matter in the mean field approximation and review the main features of the Walecka model. Further calculations of the equation of state follow and some new thermodynamics features are presented in this model. Also, in this chapter are presented complete results for the nucleon effective mass as function of temperature and baryonic density which agree with previous calculations in the appropriate limits. A review of the in-medium nucleon propagator at finite temperature is also given.

Chapter 3 is devoted to the study of the modification of the vector meson properties in nuclear matter at finite density and temperature. We show the change in meson masses and decay widths induced in-medium by  $n$ - $n$  excitations. The nucleon propagator and effective mass is considered in the mean field model introduced in Chapter 2. In this chapter, we also explore medium-induced symmetry breaking effects, like the scalar-vector meson mixing in nuclear matter via  $n$ - $n$  excitations. In this effort, we uncover a new mixing effect,  $\rho$ - $a_0$  meson mixing, which is a purely density-driven effect, forbidden in free space on account of Lorentz symmetry. We further pursue an extensive study on the properties of this new effect showing the mixing angle as well as its effect on the dispersion curves and invariant masses. The same study has been done in this thesis for  $\omega$ - $\sigma$  meson mixing. Although we obtain good agreement with previous works, significant extension has been made in the study of this mixing effect. Selected results has been published in Phys. Rev. C. as a Rapid Communication [48].

Chapter 4 is dedicated to the study of the dilepton sources from a thermal gas of hadrons. We use Vector Meson Dominance (VMD) to describe the decay of vector mesons into lepton pairs. Special emphasizes is put on the new dilepton sources induced by meson mixing effects in both the isoscalar and isovector channels. We present for the first time a new source of dileptons mediated by  $\rho$ - $a_0$  meson mixing from a dense medium. This new channel induces a new peak in the dilepton spectrum

if the baryonic density is higher than about normal nuclear matter density. Our study at finite temperature shows that even for high temperatures this signal survives, even though a higher density is needed in this case. We are also the first to evaluate the  $\omega$ - $\sigma$  mixing effect on the dilepton spectrum at finite temperature, previous calculations being limited to the zero temperature evaluation of the cross section. The results has been published in Phys. Rev. C. [49].

Chapter 5 uses these findings in a more realistic scenario. A thermal model is used to integrate the dilepton rates over the space-time history of a nucleus-nucleus collision. Even though this scenario is not original, it was improved upon it by including the equation of state in the Walecka model. Two cases are of interest here, the Pb(158 GeV)+Au collisions studied with the CERES detector at CERN/SPS, and the 1 GeV Au+Au collisions, recently started at GSI/SIS and using the HADES detector to observe lepton pairs in the low mass region. We have shown new predictions for the dilepton spectrum where symmetry breaking effects could be observed at the upcoming experiments at GSI. The results are in preparation for the submission to Phys. Rev. C [50].

Chapter 6 contains the thesis summary and related discussions.

---

Before beginning the discussion on the properties of nuclear matter, we review some of the properties of the hadrons most frequently used in the present thesis. We also summarize this in table 1.1 [51].

As far as the origin of the signals which presently concern us, most relevant hadrons are the low lying non-strange mesons which occur in the pseudoscalar (spin-parity  $J^P = 0^-$ ) octet [*viz.* the iso-triplet pions ( $\pi^-, \pi^0, \pi^+$ ) and the isoscalar eta-meson ( $\eta$ )], the non-strange members of the vector (spin-parity  $J^P = 1^-$ ) nonet [*viz.* the iso-triplet rho mesons ( $\rho^-, \rho^0, \rho^+$ ), the isoscalar omega-meson ( $\omega$ ) and phi meson ( $\phi$ )]

Table 1.1: Properties of relevant hadrons

Hadron	$M_h$ (MeV)	$I^G(J^P)$
$\pi^\pm$ ( $\pi^0$ )	140. (135.)	$1^-(0^-)$
$\eta$	550.	$0^+(0^-)$
$\rho^{\pm,0}$	770.	$1^+(1^-)$
$a_0$	983.	$1^-(0^+)$
$\omega$	782.	$0^-(1^-)$
$\sigma$	550.	$0^+(0^+)$
$\phi$	1020.	$0^-(1^-)$
$K^\pm$	494.	$\frac{1}{2}(0^-)$
$K_{L,S}^0$	498.	$\frac{1}{2}(0^-)$

and also the  $a_0$  (former  $\delta$ ) meson with  $J^P = 0^+$  and  $I=1$ . Pseudoscalar mesons, the iso-triplet pions  $\pi^\pm$  ( $\pi^0$ ) with mass 140 (135) MeV, isoscalar eta-meson  $\eta$  (550 MeV) and the iso-doublets of strange mesons  $K^\pm$ ,  $K_{L,S}^0$ , even though do not appear as main characters, do play a role in the present context, as decay products of other mesons. Other hadrons of interest, as far as it concerns the present thesis, are of course the iso-doublet nucleons, neutrons and protons, of which nuclear matter is composed.

Lastly, though implicitly, in low energy hadron physics one invokes the  $\sigma$  meson, an isoscalar with spin parity  $J^P = 0^+$  with the requisite quantum numbers, which provides, through its exchange between nucleons, the spin and isospin independent Wigner force. We consider the pole mass of the  $\sigma$  meson 550 MeV and its decay width of 300 MeV as used in Ref. [52] for example.

It is also proper to stress some conventions and notations. The metric used every-

where in this thesis is

$$g_{\mu\nu} = \begin{pmatrix} 1 & 0 & 0 & 0 \\ 0 & -1 & 0 & 0 \\ 0 & 0 & -1 & 0 \\ 0 & 0 & 0 & -1 \end{pmatrix} \quad (1.1)$$

Repeated Greek indices mean summation over the space-time indices ( $a^\mu b_\mu = a_0 b_0 - a_1 b_1 - a_2 b_2 - a_3 b_3$ ). If the indices are Roman letters we mean summation over the space indices alone ( $a^i b_i = a_1 b_1 + a_2 b_2 + a_3 b_3$ ).

## NUCLEAR MATTER AT FINITE TEMPERATURE AND DENSITY

The properties at high density and high temperature govern the behavior of astrophysical phenomena such as supernovae and neutron stars, and are also probed in heavy ion experiments [53]. The goal of this chapter is to provide a theoretical description of nuclear matter under extreme conditions and at equilibrium, as most of the calculations done in this thesis. A proper framework to describe nuclear matter at high densities and temperatures is relativistic quantum field theory based on a local Lagrangian density. Among these theories, the ones considering hadronic degrees of freedom are represented by a generic name: Quantum Hadrodynamics (QHD). In this framework, the mean field theory, or the *Walecka model* [53], was first introduced in the early seventies to study dense nuclear matter in the context of neutron stars [54]. This model explains the properties of bulk nuclear matter such as the experimentally accessible observables: density and binding energy [55]. In this approach, one also obtain the well-known feature of nucleon-nucleon interaction known from nucleon-nucleon scattering experiments: a short range repulsion and a long-range attraction [56, 57]. We will explain these features gradually as we review the formalism of the Walecka model.

We start with a baryon field for the neutrons and protons

$$\psi = \begin{pmatrix} p \\ n \end{pmatrix} \quad (2.1)$$

a neutral scalar field  $\phi$  (coupled to the scalar density  $\bar{\psi}\psi$  with the coupling constant  $g_s$ ) and a neutral vector field  $V_\mu$  (coupled to the conserved baryon current  $\bar{\psi}\gamma_\mu\psi$  with the coupling constant  $g_v$ ).

The Lagrangian density for the present model is [53]

$$\begin{aligned} \mathcal{L} = & \bar{\psi}[\gamma^\mu(i\partial_\mu - g_v V_\mu) - (M - g_s\phi)]\psi + \frac{1}{2}[\partial^\mu\phi\partial_\mu\phi - m_s^2\phi^2] \\ & - \frac{1}{4}F^{\mu\nu}F_{\mu\nu} + \frac{1}{2}m_v^2V^\mu V_\mu \end{aligned} \quad (2.2)$$

where  $F_{\mu\nu} = \partial_\mu V_\nu - \partial_\nu V_\mu$  is the field tensor corresponding to spin-1 particles as in the case of the photon [58]. Of course,  $M$  is the nucleon mass and  $m_{s,v}$  are the scalar and vector masses respectively.

Let's evaluate the one meson exchange potential that arises from these interactions. We consider the exchange of  $\sigma$  meson, and, the interaction Lagrangian is

$$\mathcal{L}_{int} = g_s \bar{\psi}\phi\psi \quad (2.3)$$

We can write the T-matrix element for the nucleon-nucleon interaction through the exchange of a  $\sigma$  meson shown in the Feynman diagram <sup>1</sup> 2.1.

$$\begin{aligned} T_{fi} = & g_s^2 \frac{(2\pi)^4}{2E_1 2E_2} \delta^{(4)}(k_{i1} + k_{i2} - k_{f1} - k_{f2}) \frac{i}{q^2 - m_s^2} \\ & \times \bar{u}_a(k_{f1}) i u_a(k_{i1}) \bar{u}_a(k_{f2}) i u_a(k_{i2}) \end{aligned} \quad (2.4)$$

where  $q = k_{i1} - k_{f1} = k_{f2} - k_{i2}$ .

<sup>1</sup>In the present diagram the time axis is in the vertical direction. The rest of the Feynman diagrams in the present thesis have the opposite axis definition.

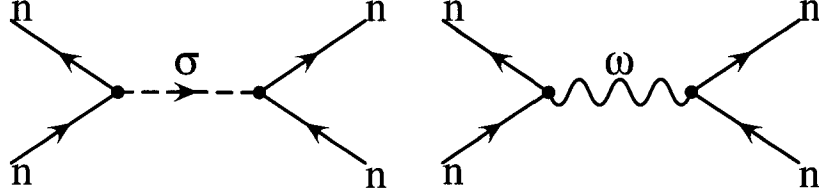


Figure 2.1: The Feynman diagram for the n-n interaction through  $\sigma$  and  $\omega$  meson exchange.

We recall the first order Born approximation result for the matrix element [59] in non-relativistic limit

$$T_{fi} = -i(2\pi)^4 \delta^{(4)}(k_{i1} + k_{i2} - k_{f1} - k_{f2}) \bar{V}_{eff}(\vec{q}) . \quad (2.5)$$

One can compare this equation with Eq. 2.4 by taking the non-relativistic limit in the last. In this limit  $M \rightarrow \infty$  and  $u^s \bar{u}^{s'} \rightarrow 2M \delta_{ss'}$ . This allows us to identify

$$\bar{V}_{eff} = -\frac{g_s^2}{\vec{q}^2 + m_s^2} . \quad (2.6)$$

The Fourier transformation of this relation provides the effective potential in coordinate space, the well-known Yukawa potential

$$\begin{aligned} V_{eff} &= \int \frac{d^3q}{(2\pi)^3} \bar{V}_{eff} e^{i\vec{q}\cdot\vec{r}} \\ V_{eff} &= -\frac{g_s^2}{4\pi} \frac{e^{-m_s r}}{r} . \end{aligned} \quad (2.7)$$

By performing the same exercise for  $\omega$  meson exchange we get the effective nucleon-nucleon interaction in the static limit

$$V_{static} = \frac{g_v^2}{4\pi} \frac{e^{-m_v r}}{r} - \frac{g_s^2}{4\pi} \frac{e^{-m_s r}}{r} . \quad (2.8)$$

One can see from the expression of potential the qualitative feature of the nucleon-nucleon interaction: a short-range repulsion between baryons coming from  $\omega$  exchange, and a long-range attraction generated by  $\sigma$  exchange. With an appropriate choice of couplings we can give also an quantitative description of nuclear matter properties as it will be emphasized later. Let's first concentrate on the field equation of motions which describe our system of particles.

## 2.1 Field Equations of Motion

We can start our study from the principle of least action [58]

$$\delta \int \mathcal{L}(q, \partial_\mu q) d^4x = 0 \quad (2.9)$$

where  $q$  is any of the field variables. Lagrange's equation follows

$$\frac{\partial}{\partial x_\mu} \frac{\partial \mathcal{L}}{\partial(\partial q / \partial x_\mu)} - \frac{\partial \mathcal{L}}{\partial q} = 0 \quad . \quad (2.10)$$

By using the Lagrangian of our model 2.3 and replacing  $q$  by the fields corresponding to our system of particle  $V_\mu, \phi, \bar{\psi}$  we get the following field equations:

$$\partial^\nu F_{\mu\nu} + m_v^2 V_\mu = g_v \bar{\psi} \gamma_\mu \psi \quad (2.11)$$

$$[\partial^\mu \partial_\mu + m_s^2] \phi = g_s \bar{\psi} \psi \quad (2.12)$$

$$(i\gamma^\mu \partial_\mu - M)\psi = (g_v \gamma^\mu V_\mu - g_s \phi)\psi \quad . \quad (2.13)$$

The first equation represents the massive spin-1 particle [58] with the conserved baryon current  $B_\mu = \bar{\psi} \gamma_\mu \psi$  as a source. The second equation can be recognized as the Klein-Gordon equation for scalar field with the baryon scalar density  $\bar{\psi} \psi$  as a source. The last equation is the Dirac equation for the baryon field with contribution from the interaction with mesonic fields.

## 2.2 Mean Field Approximation

It is evident that the field equations [2.11-2.13] are nonlinear and their exact solutions are complicated. Moreover, since we expect the couplings  $g_v$  and  $g_s$  to be large, perturbative approaches are not useful in the attempt to solve these equations. We have therefore made little progress by writing them down without a suitable solution. Still, there is an approximate solution which become increasingly valid as the nuclear density increases. When the baryonic density is large, the sources of the meson fields in the Eqs. [2.11-2.13] become strong and therefore we assume the so called *mean field approximation* by replacing the meson field operators and the sources by their expectation values [53]

$$\begin{aligned}\phi &\rightarrow \langle \phi \rangle \\ V_\mu &\rightarrow \langle V_\mu \rangle \quad .\end{aligned}\tag{2.14}$$

Because  $B_\mu$  and  $V_\mu$  are Lorentz vectors [58] and since we have no preferred spatial direction for uniform nuclear matter at rest we get

$$\begin{aligned}\langle B_\mu \rangle &= \delta_{\mu 0} \rho_B \\ \langle V_\mu \rangle &= \delta_{\mu 0} V_0\end{aligned}\tag{2.15}$$

where the baryonic density is defined as  $\rho_B = \langle \psi^\dagger \psi \rangle$ . One can observe that the meson field derivatives vanish in this approximation. The field equations become

$$\begin{aligned}V_0 &= \frac{g_v}{m_v^2} \rho_B \\ \phi_0 &= \frac{g_s}{m_s^2} \rho_s \\ (i\gamma^\mu \partial_\mu - M)\psi &= (g_v \gamma^0 V_0 - g_s \phi_0)\psi\end{aligned}\tag{2.16}$$

with the scalar density defined as the expectation value of the scalar source

$$\rho_s = \langle \bar{\psi} \psi \rangle \quad .\tag{2.17}$$

Similarly, the mean field Lagrangian density can be written as

$$\mathcal{L}_{MF} = \frac{1}{2}m_v^2V_0^2 - \frac{1}{2}m_s^2\phi_0^2 + \bar{\psi} \left[ i\gamma^\mu \partial_\mu - (M - g_s\phi_0) - g_v\gamma^0V_0 \right] \psi \quad . \quad (2.18)$$

The mean field Hamiltonian density is

$$\begin{aligned} \mathcal{H}_{MF} &= \frac{\partial \mathcal{L}_{MF}}{\partial(\dot{q}^{(\alpha)})} \dot{q}^{(\alpha)} - \mathcal{L}_{MF} \\ &= -\frac{1}{2}m_v^2V_0^2 + \frac{1}{2}m_s^2\phi_0^2 - \bar{\psi}[-i\gamma^i\partial_i + g_v\gamma_0V_0 + M^*]\psi \quad . \end{aligned} \quad (2.19)$$

### 2.2.1 Dirac Equation for Nucleons and the Field Expansion

It is worth to pay some attention to the last of the Eqs. 2.16. If one tries a solution of the form  $\psi = \Phi(\mathbf{k})e^{ik \cdot x}$ , the following equation results

$$(\alpha \cdot \mathbf{k} + \beta M^*)\Phi(\mathbf{k}) = (E - g_vV_0)\Phi(\mathbf{k}) \quad (2.20)$$

where  $\alpha = \gamma^0\boldsymbol{\gamma}$ ,  $\beta = \gamma^0$  [58] and

$$M^* = M - g_s\phi_0 \quad . \quad (2.21)$$

One recognizes the Dirac Hamiltonian of one-particle  $\mathcal{H} = \alpha \cdot \mathbf{k} + \beta M^*$  with an effective mass  $M^*$  which we find to be lower than the free value. We also notice that the solutions of the equations will have a shifted energy value so that

$$E_{\mathbf{k}}^\pm = g_vV_0 \pm (\mathbf{p}^2 + M^{*2})^{1/2} \quad . \quad (2.22)$$

In the Schrödinger picture, the baryon field operator <sup>1</sup> can be expanded in terms of complete set of solutions of the Dirac equation including both solutions corresponding to  $E_\pm$ .

---

<sup>1</sup>Henceforth we use a caret over a quantity to indicate an operator in the nuclear Hilbert space, except when this is obvious as in the case of creation and destruction operators.

$$\hat{\psi}(\mathbf{x}, t) = \frac{1}{\sqrt{V}} \sum_{\mathbf{k}, \lambda} \left[ \mathcal{U}(\mathbf{k}, \lambda) e^{i(\mathbf{k} \cdot \mathbf{x} - E_{\mathbf{k}}^+ t)} a_{\mathbf{k}, \lambda} + \mathcal{V}(-\mathbf{k}, \lambda) e^{i(\mathbf{k} \cdot \mathbf{x} - E_{\mathbf{k}}^- t)} b_{\mathbf{k}, \lambda}^\dagger \right] \quad . \quad (2.23)$$

By using the commutation relations [58] and normalizing the Dirac spinors to the unit baryonic density in the laboratory frame (*i.e.*  $\bar{\mathcal{U}}\mathcal{U} = 1$ ) we get the following baryonic and scalar density operators

$$\hat{\rho}_B = \hat{\psi}^\dagger \hat{\psi} = \frac{1}{V} \sum_{\mathbf{k}, \lambda} (a_{\mathbf{k}, \lambda}^\dagger a_{\mathbf{k}, \lambda} - b_{\mathbf{k}, \lambda}^\dagger b_{\mathbf{k}, \lambda}) \quad (2.24)$$

$$\hat{\rho}_s = \hat{\psi} \hat{\psi} = \frac{1}{V} \sum_{\mathbf{k}, \lambda} \frac{M^*}{\sqrt{\mathbf{k}^2 + M^{*2}}} (a_{\mathbf{k}, \lambda}^\dagger a_{\mathbf{k}, \lambda} + b_{\mathbf{k}, \lambda}^\dagger b_{\mathbf{k}, \lambda}) \quad (2.25)$$

$$(2.26)$$

where we have used the well-known relation [58]

$$\bar{\mathcal{U}}(\mathbf{k})\mathcal{U}(\mathbf{k}) = \frac{M^*}{\sqrt{\mathbf{k}^2 + M^{*2}}} \mathcal{U}^\dagger(\mathbf{k})\mathcal{U}(\mathbf{k}) \quad . \quad (2.27)$$

The mean field Hamiltonian will be

$$\hat{\mathcal{H}}_{MF} = -\frac{1}{2} m_v^2 V_0^2 + \frac{1}{2} m_s^2 \phi_0^2 + g_v V_0 \hat{\rho}_B + \frac{1}{V} \sum_{\mathbf{k}, \lambda} \sqrt{\mathbf{k}^2 + M^{*2}} (a_{\mathbf{k}, \lambda}^\dagger a_{\mathbf{k}, \lambda} + b_{\mathbf{k}, \lambda}^\dagger b_{\mathbf{k}, \lambda}) \quad . \quad (2.28)$$

### 2.2.2 Nuclear Matter at Finite Density

First, we discuss some properties of cold nuclear matter at finite density. It is obvious from previous discussion that the ground state of nuclear matter is obtained by filling up levels in momentum space up to  $k_F$  with nucleons having both spin and isospin states occupied. Therefore, the degeneracy of nuclear matter is  $\gamma = 4$ .

The baryon density and the energy density  $\epsilon = E/V$  can be directly obtained from the expectation values of Eqs. 2.24 and 2.28:

$$\rho_B = \frac{\gamma}{(2\pi)^3} \int_0^{k_F} d^3k = \frac{\gamma}{6\pi^2} k_F^3 \quad (2.29)$$

$$\epsilon = \frac{g_v^2}{2m_v^2} \rho_B^2 + \frac{m_s^2}{2g_s^2} (M - M^*)^2 + \gamma \int_0^{k_F} \frac{d^3k}{(2\pi)^3} \sqrt{k^2 + M^{*2}} \quad (2.30)$$

where we have used Eqs. 2.16 and 2.21 for the vector and scalar fields, respectively . The value of the effective mass can be obtained at fixed baryon density and volume by minimizing the system energy

$$\left( \frac{\partial \epsilon}{\partial M^*} \right)_{V,B} = 0 \quad . \quad (2.31)$$

By differentiation of Eq. 2.30 we get the following *self-consistency* equation whose solution provides the effective nucleon mass

$$M^* = M - \frac{g_s^2}{m_s^2} \frac{\gamma}{(2\pi)^3} \int_0^{k_F} d^3k \frac{M^*}{\sqrt{k^2 + M^{*2}}} \quad . \quad (2.32)$$

Before showing any result of our calculations, we have to discuss about the only two parameter we use in the present model, the couplings of  $\sigma$  and  $\omega$  mesons to the nucleons. We choose them to fit the experimentally accessible properties of uniform nuclear matter. Evidently, at very high and low densities, the system is unbound ( $\epsilon/\rho_B > M$ ). However, at intermediate densities, the attractive scalar interaction will dominate if coupling constants are properly chosen. To reproduce the saturation properties of nuclear matter we use the values from Ref. [60], which provide a binding energy of 15.75 MeV for a Fermi momentum  $k_F = 1.3 \text{ fm}^{-1}$  and a correspondent baryonic density  $0.15 \text{ fm}^{-3}$  at equilibrium:

$$C_s^2 = g_s^2 \frac{M^2}{m_s^2} = 357.4, \quad C_v^2 = g_v^2 \frac{M^2}{m_v^2} = 273.8 \quad . \quad (2.33)$$

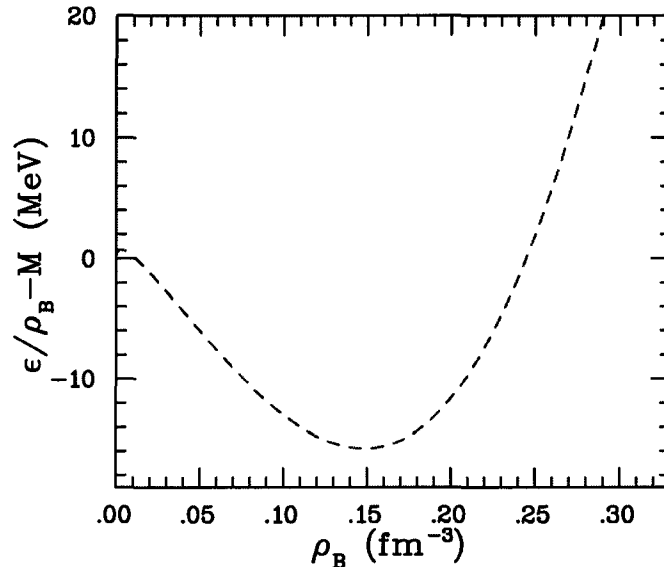


Figure 2.2: Saturation curve for nuclear matter.

With these values we present the saturation curve in Fig. 2.2. One can easily see that the energy minimum is at the experimental value of binding energy. With this choice of couplings, we show in Fig. 2.3 the effective mass dependence on baryonic density. We note that  $M^*/M = 0.6$  at saturation density.

The same expression for the energy density as in 2.30 could be obtained if we consider the analogy with continuum mechanics where we define the energy-momentum tensor [61] by

$$T_{\mu\nu} = -g_{\mu\nu}\mathcal{L} + \frac{\partial q_i}{\partial x^\nu} \frac{\partial \mathcal{L}}{\partial(\partial q_i/\partial x_\mu)} \quad (2.34)$$

where the summation over  $i$  is over the all generalized coordinates. Lagrange's equations (2.10) ensure that this tensor is conserved,

$$\partial^\mu T_{\mu\nu} = 0 \quad . \quad (2.35)$$

If we consider a perfect fluid, the energy momentum tensor has a spherical sym-

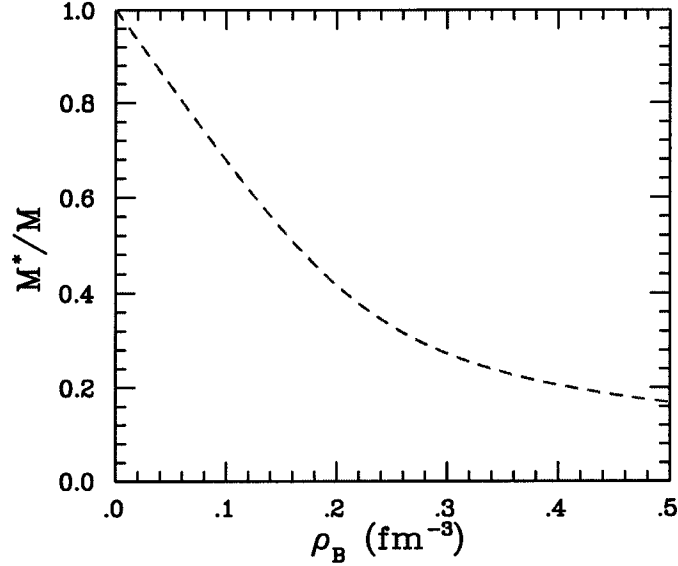


Figure 2.3: Nucleon effective mass as function of baryonic density at zero temperature.

metric form in the rest frame,

$$T_{ij} = P\delta_{ij} \quad (2.36)$$

$$T_{i0} = T_{0i} = 0$$

$$T_{00} = \epsilon \quad .$$

where  $P$  and  $\epsilon$  are the pressure and energy density of the fluid. Therefore, by using the mean field Lagrangian 2.18 along with Dirac equation 2.13 we get for pressure and energy density

$$\epsilon = -\frac{1}{2}m_v^2V_0^2 + \frac{1}{2}m_s^2\phi_0^2 + \psi^\dagger[-i\alpha \cdot \partial + \beta M^* + g_v V_0]\psi \quad (2.37)$$

$$P = \frac{1}{2}m_v^2V_0^2 - \frac{1}{2}m_s^2\phi_0^2 + \psi^\dagger(-i\alpha \cdot \partial)\psi \quad . \quad (2.38)$$

In a similar fashion with Sec. 2.2.1, through the field expansion, we recover Eq. 2.30. For the pressure we get

$$P = \frac{g_v^2}{2m_v^2} \rho_B^2 - \frac{m_s^2}{2g_s^2} (M - M^*)^2 + \frac{\gamma}{3} \int_0^{k_F} \frac{d^3k}{(2\pi)^3} \frac{k^2}{\sqrt{k^2 + M^{*2}}} . \quad (2.39)$$

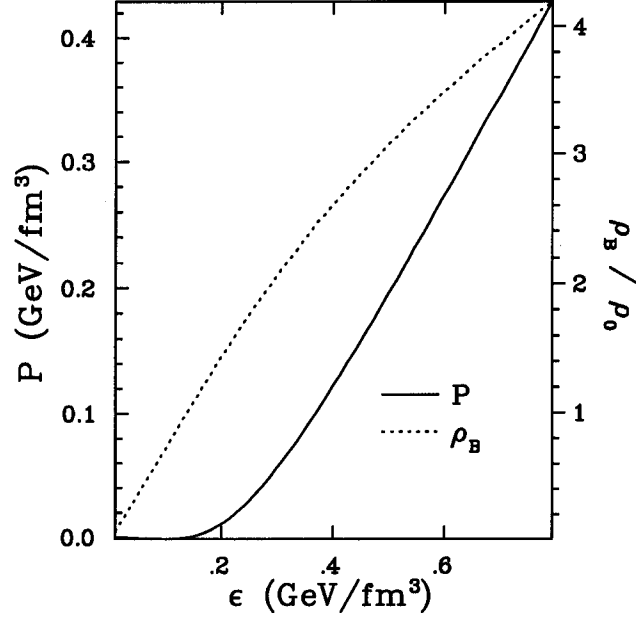


Figure 2.4: Nuclear matter equation of state at zero temperature.

This equation together with Eq. 2.30 give the nuclear matter equation of state in a parametric form:  $\epsilon(\rho_B)$ ,  $P(\rho_B)$ . We show in Fig. 2.4 our calculation for the equation of state in Walecka model for zero temperature. We notice that the causality is preserved and, at high densities, the system approaches the stiffest possible equation of state (when  $\frac{\partial P}{\partial \epsilon} = 1$ ) in the causal limit [62]. In the same plot, we also show the correspondent baryonic density.

### 2.2.3 Thermodynamics of Nuclear Matter at Finite Temperature

In the present section, the nuclear matter equation of state at finite temperature is discussed. In the grand canonical ensemble the thermodynamic potential is [63]

$$\Omega(\mu, V, T, \phi_0, V_0) = -\frac{\ln Z_G}{\beta}$$

$$\ln Z_G = Tr \left[ e^{-\beta(\hat{\mathcal{H}}_{MF} - \mu \hat{\rho}_B)} \right] \quad (2.40)$$

where  $\beta = k_B T$  and  $k_B$  is Boltzmann's constant. Before we start evaluating the grand partition function  $Z_G$ , we write down some thermodynamic identities involving the thermodynamic potential  $\Omega$

$$\Omega = -PV \quad (2.41)$$

$$\Omega = U - TS - \mu N \quad .$$

The grand partition function is given by

$$Z_G = \sum_{n_1} \cdots \sum_{\bar{n}_1} \cdots \langle n_1, \dots, \bar{n}_1, \dots | e^{-\beta(\hat{\mathcal{H}}_{MF} - \mu \hat{\rho}_B)} | n_1, \dots, \bar{n}_1, \dots \rangle \quad . \quad (2.42)$$

Replacing  $\hat{\mathcal{H}}_{MF}$  and  $\hat{\rho}_B$  with the values from Eqs. 2.24 and 2.28 we get

$$Z_G = e^{-\beta V(-\frac{1}{2}m_v^2 V_0^2 + \frac{1}{2}m_s^2 \phi_0^2)}$$

$$\times \prod_i \sum_{n_i=0,1} \langle n_i | e^{-\beta(E_i^* - \nu)n_i} | n_i \rangle \prod_j \sum_{\bar{n}_j=0,1} \langle \bar{n}_j | e^{-\beta(E_j^* + \nu)\bar{n}_j} | \bar{n}_j \rangle \quad (2.43)$$

with limiting value of one for the occupation numbers for fermions ( $n_i, \bar{n}_j = 0, 1$ ). We have introduced the following notations:  $E_k^* = \sqrt{k^2 + M^{*2}}$  is the single particle effective energy and  $\nu = \mu - g_v V_0$  is the effective chemical potential of the nucleon. In the zero temperature limit  $\nu$  is the Fermi energy of the nucleon. We can re-write the partition function by performing the first summation

$$Z_G = e^{-\beta V(-\frac{1}{2}m_v^2 V_0^2 + \frac{1}{2}m_s^2 \phi_0^2)} \prod_i [1 + e^{-\beta(E_i^* - \nu)}] \prod_j [1 + e^{-\beta(E_j^* + \nu)}] \quad . \quad (2.44)$$

By using Eq. 2.40 we get the following thermodynamic potential in the mean field approximation

$$\Omega = V(-\frac{1}{2}m_v^2 V_0^2 + \frac{1}{2}m_s^2 \phi_0^2) - \frac{1}{\beta} \sum_i \ln[1 + e^{-\beta(E_i^* - \nu)}] - \frac{1}{\beta} \sum_j \ln[1 + e^{-\beta(E_j^* + \nu)}]. \quad (2.45)$$

Once we have the thermodynamic potential, we can compute the thermodynamic variables. But first we note that the sum over all possible momentum-space states becomes in the continuum limit

$$\sum_i = V\gamma \int \frac{d^3k}{(2\pi)^3} \quad (2.46)$$

where  $\gamma$  is the spin-isospin factor ( $\gamma = 4$  for nuclear matter,  $\gamma = 2$  for neutron matter). We can write

$$\begin{aligned} \rho_B &= - \left( \frac{\partial \Omega}{\partial \mu} \right)_{T, V} \\ \rho_B &= \gamma \int \frac{d^3k}{(2\pi)^3} (n_k - \bar{n}_k) \end{aligned} \quad (2.47)$$

where we have defined the thermal occupation numbers for nucleons and anti-nucleons

$$n_k = \frac{1}{e^{\beta(E_k^* - \nu)} + 1} \quad \bar{n}_k = \frac{1}{e^{\beta(E_k^* + \nu)} + 1} \quad . \quad (2.48)$$

Similarly, pressure can be calculated

$$P = -\Omega/V$$

$$P = \left(\frac{1}{2}m_v^2V_0^2 - \frac{1}{2}m_s^2\phi_0^2\right) + \frac{1}{\beta}\gamma \int \frac{d^3k}{(2\pi)^3} \ln[1 + e^{-\beta(E_k^* - \nu)}] + \frac{1}{\beta}\gamma \int \frac{d^3k}{(2\pi)^3} \ln[1 + e^{-\beta(E_k^* + \nu)}] \quad . \quad (2.49)$$

Integrating by parts and taking  $u^\pm = \ln[1 + e^{-\beta(E_k^* \mp \nu)}]$  (“+” for the first and “-” for the second term) and  $v = \frac{k^3}{3}$  we get

$$P = \left(\frac{1}{2}m_v^2V_0^2 - \frac{1}{2}m_s^2\phi_0^2\right) + \gamma \int \frac{d^3k}{(2\pi)^3} \frac{n_k + \bar{n}_k}{3} \frac{\mathbf{k}^2}{(\mathbf{k}^2 + M^{*2})^{1/2}} \quad . \quad (2.50)$$

The energy density is obtained from

$$\begin{aligned} \epsilon + \mu\rho_B &= \frac{\partial \ln Z_G}{\partial \beta} = \frac{\partial \beta \Omega}{\partial \beta} \\ \epsilon &= -\frac{1}{2}m_v^2V_0^2 + \frac{1}{2}m_s^2\phi_0^2 + g_v V_0 \rho_B + \gamma \int \frac{d^3k}{(2\pi)^3} \sqrt{\mathbf{k}^2 + M^{*2}} (n_k + \bar{n}_k) \quad . \quad (2.51) \end{aligned}$$

In the above expressions, the value of the vector field  $V_0$  is fixed by the equation 2.16. The value of the scalar field  $\phi_0$  will be determined from the minimization of the thermodynamic potential  $\Omega$

$$\left(\frac{\partial \Omega}{\partial \phi_0}\right)_{\mu, V, T} = 0 \quad . \quad (2.52)$$

A straight forward calculation leads to

$$\begin{aligned} \phi_0 &= \frac{g_s}{m_s^2} \frac{\gamma}{(2\pi)^3} \int d^3k \frac{M^*}{\sqrt{\mathbf{k}^2 + M^{*2}}} (n_k + \bar{n}_k) \\ &\text{or} \\ \phi_0 &= \frac{g_s}{m_s^2} \rho_s \quad , \quad (2.53) \end{aligned}$$

and, by using Eq. 2.21, one can be also write the self-consistency relation:

$$M^* = M - \frac{g_s^2}{m_s^2} \frac{\gamma}{(2\pi)^3} \int d^3k \frac{M^*}{\sqrt{\mathbf{k}^2 + M^{*2}}} (n_k + \bar{n}_k) \quad . \quad (2.54)$$

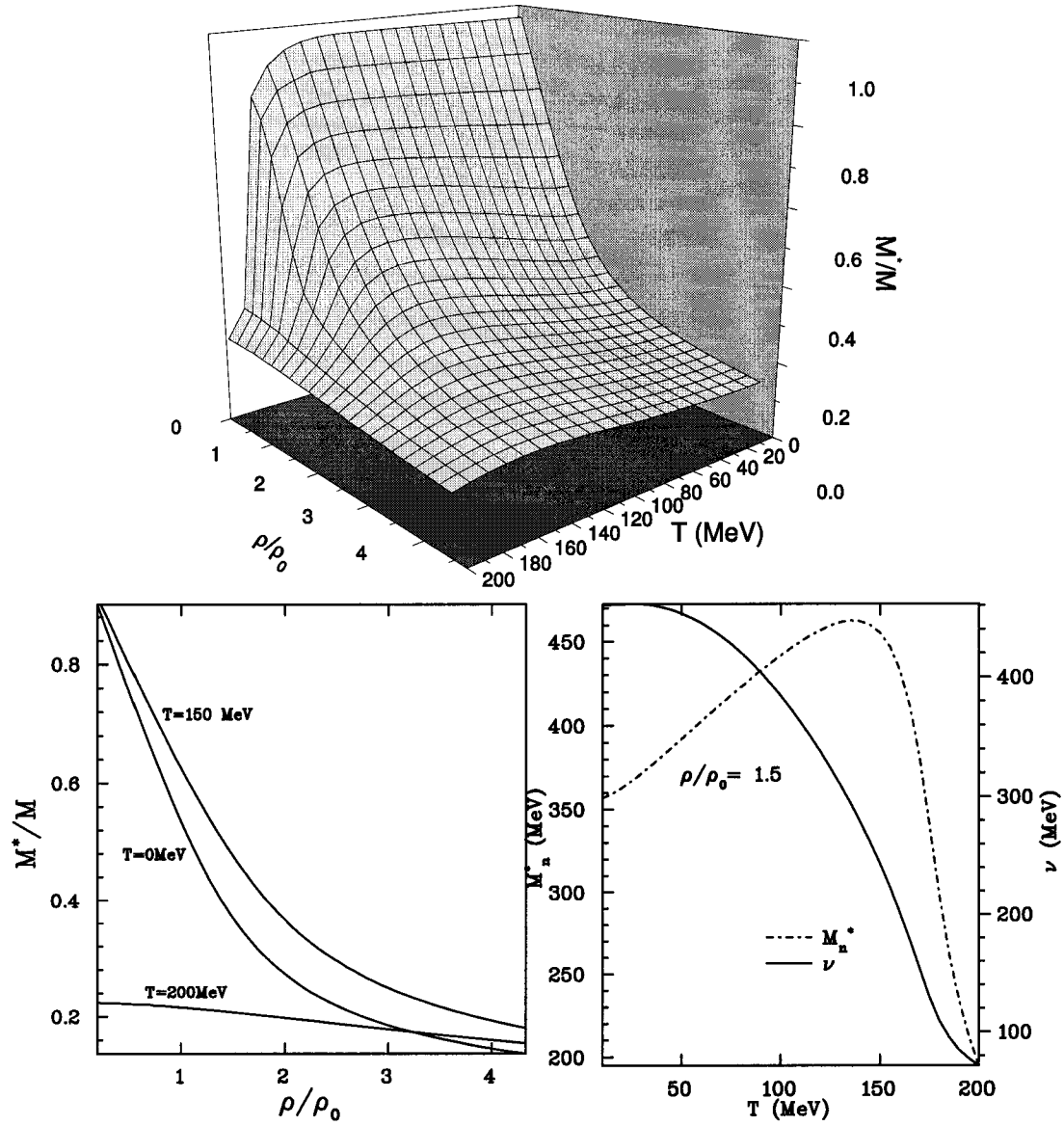


Figure 2.5: The effective mass of the nucleon as function of temperature and baryonic density. Bottom panels show results plotted against density for three different temperatures and against temperature for  $\rho_B=1.5\rho_0$  together with the correspondent effective chemical potential.

The value of the effective mass is the solution of Eq. 2.54 for a given chemical potential. To obtain the effective mass for a given baryonic density, one should self-

consistently solve the coupled Eqs. 2.47 and 2.54. One can do this by solving Eq. 2.54 for a given value of the effective chemical potential. The baryonic density can then be calculated directly using the effective mass and chemical potential. For some values of temperature and chemical potential, Eq. 2.54 develops multiple solutions [64, 65]. We assure the continuity of the effective mass as function of temperature and avoid unphysical solutions. We show in Fig. 2.5 our calculation of the effective mass for a wide range of temperatures and baryonic densities, to extend former calculations to the regions of interest to us. We notice that the effective mass drops as function of density as it should. It is interesting to notice that the nucleon mass slightly increase as function of temperature then sharply decrease when temperature increase above about 150 MeV. This is because of the pair formation which is more abundant if the temperature increases. We can see in Fig. 2.6 that the energy density rapidly increases for temperatures above about 150 MeV. This signal an abundance of pair creation above this temperature. The mass decrease is proportional to the scalar field and, consequently, to the scalar density which steeply increase due to this effect. Even at zero baryonic density we have a finite number of particle-antiparticle for non-zero temperatures and, consequently, a finite scalar density.

The nuclear matter equation of state is determined by the following equations, derived from Eqs. 2.50 and 2.51,

$$\epsilon = \frac{g_v^2}{2m_v^2}\rho_B^2 + \frac{m_s^2}{2g_s^2}(M - M^*)^2 + \gamma \int_0^\infty \frac{d^3k}{(2\pi)^3} \sqrt{\mathbf{k}^2 + M^{*2}}(n_k + \bar{n}_k) \quad (2.55)$$

$$P = \frac{g_v^2}{2m_v^2}\rho_B^2 - \frac{m_s^2}{2g_s^2}(M - M^*)^2 + \frac{\gamma}{3} \int_0^\infty \frac{d^3k}{(2\pi)^3} \frac{\mathbf{k}^2}{\sqrt{\mathbf{k}^2 + M^{*2}}}(n_k + \bar{n}_k) \quad (2.56)$$

We have a parametric form of the equation of state  $\epsilon(P)$  determined by three parameters:  $T$  and two dependent ones,  $\nu$  and  $M^*$ . Eq. 2.54 correlates  $\nu$  and  $M^*$  and therefore we solve it first for a given value of  $\nu$ . We are able then to evaluate  $\epsilon$  and  $P$  with the present parameters. In Fig. 2.7 we show the equation of state for

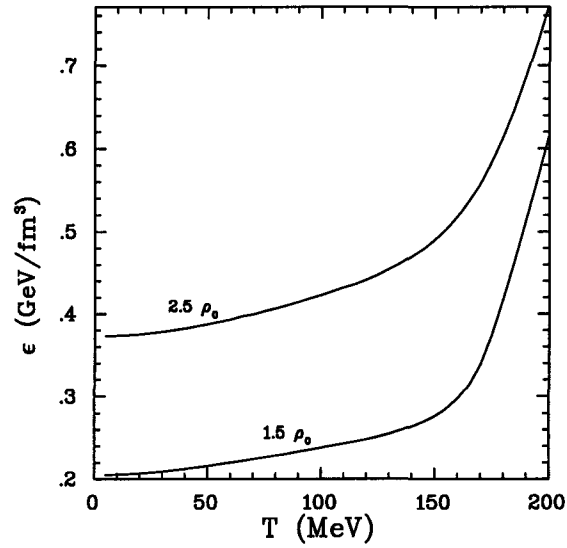


Figure 2.6: Specific energy scaled to the effective mass of nucleon as function of temperature for two baryonic densities,  $\rho_B=1.5\rho_0$  and  $\rho_B=2.5\rho_0$ .

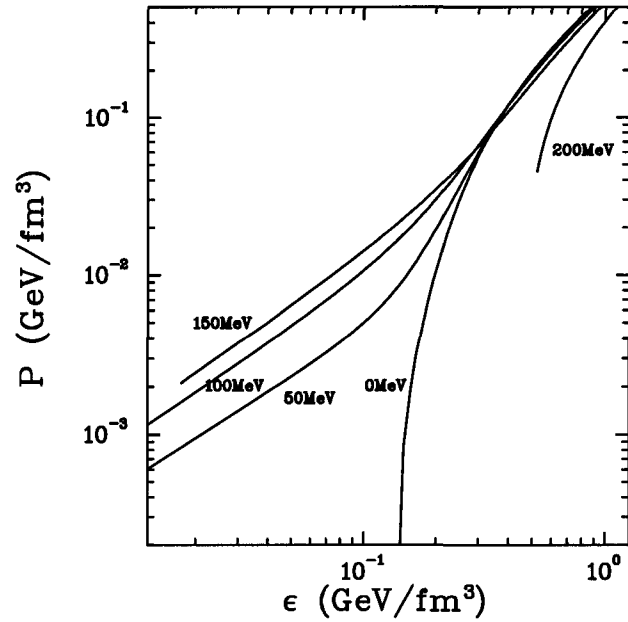


Figure 2.7: Nuclear matter equation of state for different temperatures.

different temperatures. We can notice at high temperatures a lower bound for the energy density and pressure in the equation of state. This means a finite energy density even at zero baryonic density, which is a consequence of the pair formation at high temperatures. Thus, at a given temperature, there is a finite number of nucleon-antinucleon pairs and consequently a limiting value of the energy density as the baryon density goes to zero. For low temperatures, this bound appear for values smaller than the limits of the pressure and energy shown in Fig. 2.7, and therefore they are not apparent.

Entropy is especially important for space-time analysis in relativistic heavy ion collisions where often it is assumed constant during thermal expansion. It can be determined from Eq. 2.42 where all the other variables are determined as presented before. An alternative way of calculating the entropy is by using the following identity and using 2.45

$$S = \left( \frac{\partial \Omega}{\partial T} \right)_{V, \mu} . \quad (2.57)$$

If the total baryon number is conserved, like we consider in the case of a fireball expansion following a nucleus-nucleus collision, the total entropy is proportional to  $s/\rho_B$ , the baryonic specific entropy. Therefore, this quantity is of practical importance. We plot our results for the specific entropy in Fig. 2.8.

### 2.3 Nucleon Propagator at Finite Temperature

In this section we look at the nucleon propagator at finite temperature. We start with the finite temperature Green's function that can be written as the thermal average of the time-ordered propagation amplitude

$$S_\beta(x - y) = \frac{Tr\{e^{-\beta H} T[\psi(x)\bar{\psi}(y)]\}}{Tr\{e^{-\beta H}\}}$$

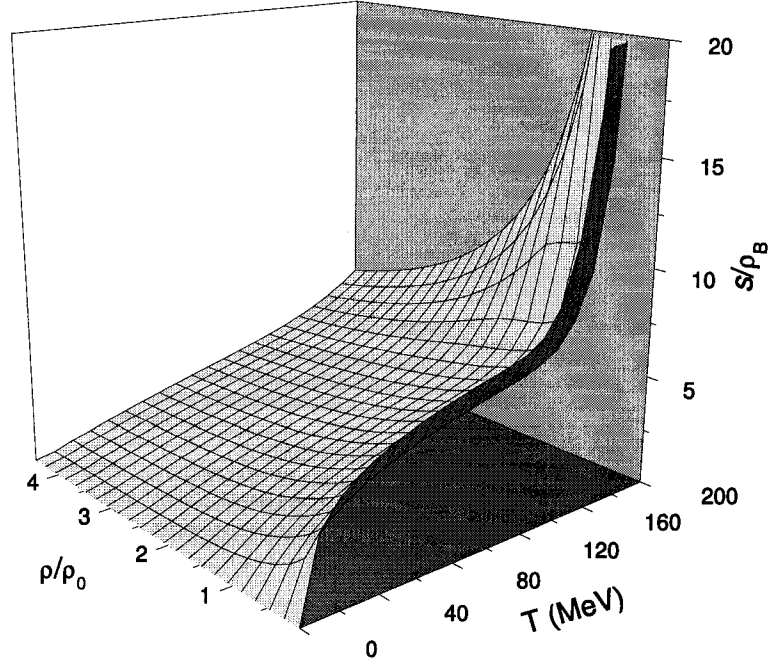


Figure 2.8: Baryonic specific entropy of nucleon as function of temperature and baryonic density.

$$= \langle T\psi(x)\bar{\psi}(y) \rangle \quad (2.58)$$

$$(i\cancel{\partial} - m)S_\beta(x - y) = i\delta^4(x - y) \quad (2.59)$$

The Fourier transformation gives the two-point function in the momentum space

$$\bar{S}_\beta(p) = \int d^4x S_\beta(x) e^{ip \cdot x} \quad (2.60)$$

where our notation ignore the first point of the Green function as being the origin of the coordinate. By using the equation of motion 2.59 we get for the free fields

$$\bar{S}_\beta(p) = \frac{i}{\cancel{p} - m} \quad (2.61)$$

We define  $S^>$  and  $S^<$  as

$$S_\beta^>(x - y) = \langle \psi(x)\bar{\psi}(y) \rangle_\beta, \quad ix_0 > iy_0$$

$$S_{\beta}^{\lessdot}(x-y) = - \langle \psi(y) \bar{\psi}(x) \rangle_{\beta}, \quad iy_0 > ix_0 . \quad (2.62)$$

$$(2.63)$$

In the real-time formalism, we define the following operators as the Fourier transformation of the Green's function (the bar denotes a Fourier transformation)

$$\bar{S}_{\beta}^{\lessdot}(p) = \int d^4x e^{ip \cdot x} S_{\beta}^{\lessdot}(x) . \quad (2.64)$$

Let's express the relationship between  $\bar{S}_{\beta}^{\lessdot}(p)$  and  $\bar{S}_{\beta}^{\gtrdot}(p)$ . By using equation A.12 from appendix A and equation 2.64 we get

$$\begin{aligned} \bar{S}_{\beta}^{\lessdot}(p) &= \int d^4x e^{i(p_0 x_0 - \mathbf{p} \cdot \mathbf{x})} S_{\beta}^{\lessdot}(x) \\ \bar{S}_{\beta}^{\gtrdot}(p) &= \int d^4x e^{i(p_0 x_0 - \mathbf{p} \cdot \mathbf{x})} S_{\beta}^{\gtrdot}(x_0 - i\beta, \mathbf{x}) \\ \bar{S}_{\beta}^{\lessdot}(p) &= e^{-\beta p_0} \int d^4x e^{ipx} S_{\beta}^{\gtrdot}(x) \\ \bar{S}_{\beta}^{\lessdot}(p) &= e^{-\beta p_0} \bar{S}_{\beta}^{\gtrdot}(p) . \end{aligned} \quad (2.65)$$

The spectral function is represented as

$$\rho(p) = \bar{S}_{\beta}^{\gtrdot}(p) + \bar{S}_{\beta}^{\lessdot}(p) \quad (2.66)$$

and can be written, by using Eq. 2.65,

$$\begin{aligned} \rho(p) &= (1 + e^{-\beta p_0}) \bar{S}_{\beta}^{\gtrdot}(p) = \frac{1}{1 - f(p_0)} \bar{S}_{\beta}^{\gtrdot}(p) \\ \rho(p) &= (1 + e^{\beta p_0}) \bar{S}_{\beta}^{\lessdot}(p) = \frac{1}{f(p_0)} \bar{S}_{\beta}^{\lessdot}(p) \end{aligned} \quad (2.67)$$

where  $f(\epsilon) = \frac{1}{e^{\beta(\epsilon - \mu)} + 1}$  is the Fermi-Dirac distribution function.

Next, we would like to relate the real-time propagator with the spectral function. For this, we write it in the following form

$$\bar{S}_{\beta}(p) = \int d^4x e^{p \cdot x} [\theta(x_0) S_{\beta}^{\gtrdot}(x) - \theta(-x_0) S_{\beta}^{\lessdot}(x)] \quad (2.68)$$

by using the following integral expansion of the  $\theta$  functions

$$\theta(\pm x_0) = \mp i \int_{-\infty}^{+\infty} \frac{d\omega}{2\pi} \frac{e^{\mp i\omega x_0}}{\omega \pm i\epsilon} , \quad (2.69)$$

and, using Eq. 2.64 we can write

$$\bar{S}_\beta(p) = i \int_{-\infty}^{+\infty} \frac{dp'_0}{2\pi} \left[ \frac{\bar{S}_\beta^>(p'_0, \mathbf{P})}{p_0 - p'_0 + i\epsilon} + \frac{\bar{S}_\beta^<(p'_0, \mathbf{P})}{p_0 - p'_0 - i\epsilon} \right] \quad (2.70)$$

where  $p'_0 = p_0 - \omega$ . We can now use Eqs. 2.67 to replace  $S_\beta^><$  propagators by the spectral function and we have

$$\bar{S}_\beta(p) = i \int_{-\infty}^{+\infty} \frac{dp'_0}{2\pi} \rho(p'_0, \mathbf{P}) \left[ \frac{1 - f(p'_0)}{p_0 - p'_0 + i\epsilon} + \frac{f(p'_0)}{p_0 - p'_0 - i\epsilon} \right] . \quad (2.71)$$

By grouping the terms containing the thermal distribution function and considering the following representation of the Dirac function ( $\delta$ )

$$\delta(k) = \lim_{\epsilon \rightarrow 0} \frac{1}{\pi} \frac{\epsilon}{k^2 + \epsilon^2} , \quad (2.72)$$

we finally get the real-time propagator in the momentum space as function of the spectral function

$$\bar{S}_\beta(p) = i \int_{-\infty}^{+\infty} \frac{dp'_0}{2\pi} \frac{\rho(p'_0, \mathbf{P})}{p_0 - p'_0 - i\epsilon} - f(p_0) \rho(p) . \quad (2.73)$$

Let's now obtain the spectral function as a imaginary-time representation of the Green's function  $S_\beta(x)$ . For this, we take the Fourier representation in the imaginary-time formalism (see appendix A)

$$\bar{S}_\beta(\omega_n, \mathbf{p}) = \int_0^\beta dx_0 e^{i\frac{(2n+1)\pi}{\beta}x_0} \int d^3x e^{-i\mathbf{p}\cdot\mathbf{x}} S_\beta(x) , \quad (2.74)$$

and, by using Eq. 2.64 and the integral representation of the delta function

$$\delta(\mathbf{k} - \mathbf{p}) = \int \frac{d^3x}{(2\pi)^3} e^{-i(\mathbf{k}-\mathbf{p})\cdot\mathbf{x}} , \quad (2.75)$$

we get

$$\bar{S}_\beta(\omega_n, \mathbf{p}) = \int_0^\beta dx_0 e^{i\frac{(2n+1)\pi}{\beta}x_0} \int_{-\infty}^{+\infty} \frac{dp_0}{2\pi} e^{-p_0 x_0} \bar{S}_\beta^>(p) . \quad (2.76)$$

If one performs the time integral, replaces the real-time Green's function with the value of Eq. 2.67 and reduces the thermal distribution terms coming from both, the Green's function and integration, the following expression is found

$$\bar{S}_\beta(\omega_n, \mathbf{p}) = i \int_{-\infty}^{+\infty} \frac{dp_0}{2\pi} \frac{\rho(p_0, \mathbf{p})}{\omega_n - p_0} . \quad (2.77)$$

By extending  $\bar{S}_\beta(\omega_n, \mathbf{p})$  to a continuous function  $\bar{S}_\beta(p)$  and evaluating in this way in both  $(k_0 \pm i\epsilon, \mathbf{k})$  one can prove that

$$\rho(p) = \bar{S}_\beta(p_0 + i\epsilon, \mathbf{p}) - \bar{S}_\beta(p_0 - i\epsilon, \mathbf{p}) . \quad (2.78)$$

For free fields Eq. 2.61 can be used and replaced into the Eq. 2.78 to get

$$\rho(p) = 2\pi\epsilon(p_0)(\not{p} + m)\delta(p^2 - m^2) . \quad (2.79)$$

The spectral function can now be replaced in Eq. 2.73 to finally get the real-time finite temperature fermion propagator

$$\bar{S}_\beta(k) = \frac{i}{\not{k} - m + i\epsilon} - \frac{2\pi(\not{k} + m)}{e^{\beta(E-\mu)} + 1} \delta(k^2 - m^2) . \quad (2.80)$$

The nucleon propagator has two terms. The first one is the vacuum propagator and involves the propagation of virtual positive and negative energy states. The second term is the medium-induced part and allows for the propagation of “holes” inside the Fermi sea and accounts for the Pauli exclusion of the occupied states in nuclear matter.

## Summary

This chapter develops a consistent framework for studying nuclear matter in a relativistic model. An approximate solution to the strongly coupled quantum field

equations can be obtained in high-density limit. We have seen that the mean field approach gives accurate description of many of the bulk features of nuclear matter. In this approximation, we reviewed the nucleon properties at finite temperature and density and the equation of state of nuclear matter, also presenting few novel calculations of some thermodynamic variables. It is interesting to notice the particularities of the nucleon mass: a decrease with baryonic density and a non-trivial behavior as function of temperature: a slow increase for low temperature followed by a sharp decrease at temperatures above about 150 MeV. Furthermore, complete results of the nucleon mass as function of temperature and density are presented. We just mention that there are other versions of the Walecka model [66], but the results relevant for our study are similar with those obtained in the original model employed here.

## MESONS IN DENSE NUCLEAR MATTER

---

---

The study of the properties of hadrons in hot and dense nuclear matter is of cardinal importance to the understanding of various signals that probe the dynamics of heavy ion collisions [5, 67]. Such investigations furthermore are of relevance to various important issues of nuclear astrophysics dealing with the properties of neutron stars, the cooling of supernovae, the gravitational collapse of massive stars, etc. [4, 68].

The essential focus of this chapter is to investigate the properties of scalar and vector mesons propagating in dense nuclear matter. The properties of these particles are modified when they propagate in a medium, as they become “dressed” by their interactions. For instance, they acquire an effective mass which is different from the mass as measured in vacuum.

The case of main interest here is the study of the light vector mesons  $\rho$  and  $\omega$ . The relevance of these vector mesons resides in the fact that their decay into lepton pairs, as shown in the VMD model described in Sec. 4.1, bringing a substantial contribution to the dilepton spectra in nucleus-nucleus collisions. Also, the collisions between thermal mesons, like  $\pi$ - $\pi$  annihilation into dileptons, proceeds through  $\rho$  as an intermediate state as we will see in the VMD model. We will also study in-medium properties of the scalar mesons  $a_0$  and  $\sigma$  for reasons that will become clear later.

Despite numerous theoretical attempts to determine the properties of vector mesons in dense nuclear matter, controversy still exists regarding their in-medium effective

masses and decay widths [32]. As mentioned earlier, various formalisms such as the NJL model, the Walecka model or QCD sum rules [69, 31, 70, 42] give different results [71, 72, 46]. Most of the mean-field models seem to indicate that in dense nuclear matter  $\rho$  meson mass drops from its vacuum values [31, 73]. On the other hand there are several calculations which show that the  $\rho$  meson mass in dense matter does not change much but its decay width shows a substantial increase [74, 40]. These two scenarios in the present literature are termed as the “dropping mass” and the “melting mass” scenarios. It might be mentioned at this point that both the scenarios can largely account for the low invariant dilepton mass spectra as reported by the CERES experiment [75]. Nevertheless, this issue is still open and efforts are being directed more to understand the in-medium properties of the  $\rho$  and  $\omega$  mesons in dense nuclear matter so as to explain the excess dilepton yield from the heavy ion collisions.

In the same time, the study of in-medium properties of mesons has attracted large interest in its own right. Experimental investigations of mass shifts and decay widths of mesons in nuclear matter have assumed a particular importance in view of proposals to make such measurements at TJNAF [38] and GSI [34].

Before we start discussing the matter-induced effects on the meson propagation we first introduce some elementary concepts used in the subsequent formalism. The general framework used to interpret physically the results of the subsequent calculations is the *linear response theory* [1, 76].

### 3.1 *Linear Response Theory*

Let's suppose there is a weak external perturbation on a system. One would like to study the response of the system to such perturbation. For this, it is useful to begin by calculating the change in the ensemble average for an operator  $\hat{O}$  to first order.

The total Hamiltonian could be written as

$$H'(t) = H_0 + H_{ext}(t) \quad (3.1)$$

where  $H_0$  is the unperturbed Hamiltonian and  $H_{ext}$  corresponds to the external perturbation which couples the external field to the system. Let's assume that the perturbation starts at  $t_0 = 0$ . The exact equation of motion in the Heisenberg picture is

$$\frac{\partial \hat{O}(\mathbf{x}, t)}{\partial t} = i[H'(t), \hat{O}(\mathbf{x}, t)] \quad (3.2)$$

Let  $|i\rangle$  be the initial eigenstate of  $H_0$ . Then, the rate of change of the expectation value of  $\hat{O}$  is

$$\begin{aligned} \frac{\langle i|\partial\hat{O}(x)|i\rangle}{\partial t} &= i \langle i|[H'(t), \hat{O}(\mathbf{x}, t)]|i\rangle \\ &= i \langle i|[H_{ext}(t), \hat{O}(\mathbf{x}, t)]|i\rangle \quad . \end{aligned} \quad (3.3)$$

This exact equation is generally not possible to be solved in a closed form and therefore is useful to consider the approximation of small perturbation. Then we can write to first order

$$\langle i|\hat{O}(\mathbf{x}, t)|i\rangle = \langle i|\hat{O}(\mathbf{x}, 0)|i\rangle + i \int_0^t dt' \langle i|[H_{ext}(t'), \hat{O}(\mathbf{x}, t)]|i\rangle \quad (3.4)$$

For finite temperature we take the ensemble average and, therefore, we have

$$\begin{aligned} \delta \langle \hat{O}(\mathbf{x}, t) \rangle_\beta &= \langle i|\hat{O}(\mathbf{x}, t)|i\rangle_\beta - \langle i|\hat{O}(\mathbf{x}, 0)|i\rangle_\beta \\ &= i \int_0^t dt' \langle [H_{ext}(t'), \hat{O}(\mathbf{x}, t)] \rangle_\beta \end{aligned} \quad (3.5)$$

where we have denoted the thermal average by

$$\langle \hat{O} \rangle_\beta = \frac{\sum_i e^{-\beta(E_i - \mu_i N_i)} \langle i|\hat{O}|i\rangle}{\sum_i e^{-\beta(E_i - \mu_i N_i)}} \quad (3.6)$$

Let's consider now that the operator  $\hat{\mathcal{O}}$  is the baryon current  $J_\mu$ , and the perturbation is described by the variation of the vector meson field coupled to the baryonic current.

$$\begin{aligned}\hat{\mathcal{O}}(x) &= J_\mu(x) \\ H_{ext}(t') &= \int d^3x' \delta V_\nu(\mathbf{x}', t') J^\nu(\mathbf{x}', t')\end{aligned}\quad (3.7)$$

according to eq. 3.5 we have

$$\delta \langle J^\mu(\mathbf{x}, t) \rangle_\beta = i \int_0^t dt' \int d^3x' \delta V_\nu(\mathbf{x}', t') \langle [J^\nu(\mathbf{x}', t'), J^\mu(\mathbf{x}, t)] \rangle_\beta \quad . \quad (3.8)$$

By using the Fourier transformation to go to the momentum space, *e. g.*,

$$\begin{aligned}V_\nu(\mathbf{x}', t') &= \int \frac{d^4q}{(2\pi)^4} e^{-iq \cdot x'} V_\nu(q) \\ J_\nu(\mathbf{x}, t) &= \int \frac{d^4q}{(2\pi)^4} e^{-iq \cdot x} J_\nu(q)\end{aligned}\quad (3.9)$$

we get the following fluctuation of the current [45, 77]

$$\delta \langle J^\mu(q) \rangle_\beta = -\Pi^{\mu\nu}(q) \delta V_\nu(q) \quad . \quad (3.10)$$

This result is particularly important to study the collective modes related to the vector meson propagation in nuclear matter. This issue will be discussed in Section 3.2.

We will just mention without going into much detail, another important result of linear response theory. If we consider now that the operator  $\hat{\mathcal{O}}$  is the vector field operator  $V_\mu$  and the perturbation is described by the vector meson coupled to the baryonic current,

$$\begin{aligned}\hat{\mathcal{O}}(x) &= V_\mu(x) \\ H_{ext}(t') &= \int d^3x' V_\nu(\mathbf{x}', t') J^\nu(\mathbf{x}', t')\end{aligned}\quad (3.11)$$

we get from Eq. 3.5

$$\delta \langle V^\mu(\mathbf{x}, t) \rangle_\beta = i \int_0^t dt' \int d^3x' \langle [V^\mu(\mathbf{x}', t'), V^\nu(\mathbf{x}, t)] \rangle_\beta J_\nu(\mathbf{x}', t') \quad . \quad (3.12)$$

Doing the same manipulations as before and by defining the retarded and advanced propagators as

$$D_{\beta}^{R\mu\nu}(x-y) = \langle [V^{\mu}(x)V^{\nu}(y)] \rangle_{\beta}, \quad x_0 > y_0$$

$$D_{\beta}^{A\mu\nu}(x-y) = \langle [V^{\mu}(x)V^{\nu}(y)] \rangle_{\beta}, \quad y_0 > x_0, \quad (3.13)$$

$$(3.14)$$

we get

$$\delta \langle V^{\mu}(x) \rangle = -i \int d^4x' D_R^{R\mu\nu}(x-x') J_{\nu}(x') \quad (3.15)$$

$$\delta \langle V^{\mu}(q) \rangle_{\beta} = -i D^{R\mu\nu}(q) J_{\nu}(q) . \quad (3.16)$$

Consider now an impulsive perturbation,

$$J^{\mu}(x) = J^{\mu}(\mathbf{q}) e^{i\mathbf{q}\cdot\mathbf{x}} \delta(t) \quad (3.17)$$

we get by replacing into eq. 3.15

$$\delta \langle V^{\mu}(x) \rangle = -i J_{\nu}(\mathbf{q}) e^{-i\mathbf{q}\cdot\mathbf{x}} \int_{-\infty}^{+\infty} \frac{dq_0}{2\pi} e^{-iq_0 t} D^{R\mu\nu}(q_0, \mathbf{q}) . \quad (3.18)$$

Since we expect the collective excitations to show as poles in the propagator we can try the following form for  $D_R$

$$D^{R\mu\nu}(q_0, \mathbf{q}) = \frac{R^{\mu\nu}}{q_0 - \omega(\mathbf{q}) + i\gamma(q_0, \mathbf{q})} . \quad (3.19)$$

Because  $D^R(q_0, \mathbf{q})$  is analytic in the upper  $q_0$ -plane ( $Im(q_0) > 0$ ),  $\gamma$  has to be positive.

We have the following response

$$\delta \langle V^{\mu}(x) \rangle = -J_{\nu}(\mathbf{q}) R^{\mu\nu}(\omega(\mathbf{q}), \mathbf{q}) \theta(t) e^{i(\mathbf{q}\cdot\mathbf{x} - \omega(\mathbf{q})t) - \gamma t} \quad (3.20)$$

where we can notice the dispersion law  $q_0 = \omega(\mathbf{q})$  and the damping rate  $\gamma(\omega(\mathbf{q}))$ . Therefore, in the next section we will start the study of collective excitations associated with the meson propagation in the nuclear matter by finding the in-medium

propagator. As we see, the contribution to the dispersion relation comes from the real part of the propagator while the imaginary part employs damping of the collective modes.

### 3.2 *Collective Excitations and the Random Phase Approximation*

Let consider a fluctuation of the scalar baryonic density  $\delta\rho_s(x)$ . The equation of motion of the scalar potential will be, in the coordinate space, similar to 2.12

$$(\partial^2 + m^2)\delta\phi(x) = \delta\rho_s(x) \quad . \quad (3.21)$$

In the momentum space we have, by taking the Fourier transformation of the above equation

$$(q^2 - m^2)\delta\bar{\phi}(q) = -\delta\bar{\rho}_s(q) \quad (3.22)$$

which can be written in terms of the free particle propagator ( $iD_0(q) = \frac{i}{q^2 - m_s^2}$ ) as

$$\delta\bar{\phi}(q) = -D^0(q)\delta\bar{\rho}_s(q) \quad . \quad (3.23)$$

We consider now a fluctuation of the baryonic current  $\delta J_\mu(x)$ . Therefore, we have for a vector potential in the Lorentz gauge when current conservation is assumed ( $\partial^\mu V_\mu = 0$ ), analogous to eq. 2.11

$$(\partial^2 + m^2)\delta V_\mu(x) = +\delta J_\mu(x) \quad . \quad (3.24)$$

In momentum space

$$(q^2 - m^2)\delta\bar{V}_\mu(q) = -\delta\bar{J}_\mu(q) \quad (3.25)$$

which can be written in terms of the free particle propagator ( $iD_0^{\mu\nu}(q) = i\frac{-g^{\mu\nu} + \frac{q^\mu q^\nu}{q^2}}{q^2 - m_V^2}$ ) as

$$\delta\bar{V}_\mu(q) = -D_\mu^{0\nu}(q)\delta\bar{J}_\nu(q) \quad . \quad (3.26)$$

This induced potential can induce further current fluctuations. In the linear density approximation, accordingly to the eq. 3.10, we have

$$\delta J'_\mu(q) = -\Pi_{\mu\nu}(q)\delta V^\nu(q) . \quad (3.27)$$

For collective modes, the current density fluctuation must be self-consistently sustained without external potential and, therefore, we must identify

$$\delta J'_\mu(q) = \delta J_\mu(q) . \quad (3.28)$$

Consequently, Eqs. [3.26-3.28] imply that

$$[\delta_\mu^\nu - D_{\mu\alpha}^0(q)\Pi^{\alpha\nu}(q)]\delta J_\nu(q) = 0 \quad (3.29)$$

which is an eigenvalue equation for the current density fluctuation. Collective modes exists only if solutions for  $\delta J_\nu(q)$  exists. Therefore, we can write the eigencondition for determining the excitation spectra of collective modes as

$$\det[\delta_{\mu\nu} - D_{\mu\alpha}^0 \Pi_\nu^\alpha] = 0 . \quad (3.30)$$

The vector meson propagator is calculated by summing over ring diagrams, a diagrammatic equivalent of the *random phase approximation* (RPA), which consist of repeated insertions of the lowest order polarization [78, 79]. Schematically this can be represented as in Fig. 3.1

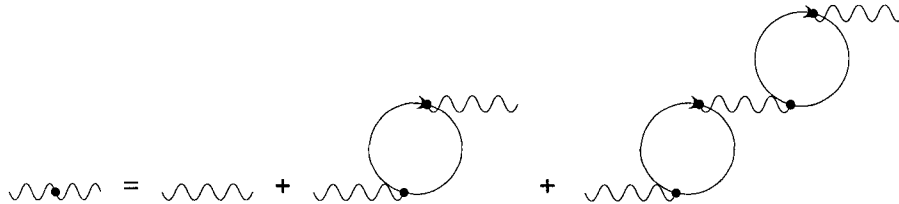


Figure 3.1: Ring diagrams relevant for the random phase approximation.

We make use of the Dyson equation to carry out the summation

$$D_{\mu\nu}(q) = D_{\mu\nu}^0(q) + D_{\mu\alpha}^0(q)\Pi^{\alpha\beta}(q)D_{\beta\nu}(q) \quad (3.31)$$

which gives

$$[\delta_{\mu}^{\nu} - D_{\mu\alpha}^0 \Pi^{\alpha\nu}] D_{\nu\beta} = D_{\mu\beta}^0 \quad . \quad (3.32)$$

Therefore, the poles of the vector meson propagator are given by

$$\det[\delta_{\mu\nu} - D_{\mu\alpha}^0 \Pi_{\nu}^{\alpha}] = 0 \quad (3.33)$$

which is the same as the equation representing the eigencondition for determining the excitation spectra of collective modes (Eq. 3.30). This equation provides the dispersion relation, *i. e.*, their energy as function of the momenta  $q_0$  ( $\vec{q}$ ). We can further define the dielectric tensor as

$$\epsilon_{\mu\nu} = \delta_{\mu\nu} - D_{\mu\alpha}^0 \Pi_{\nu}^{\alpha} \quad (3.34)$$

and its determinant will be defined as the dielectric function

$$\epsilon(q) = \det[\epsilon_{\mu\nu}] \quad . \quad (3.35)$$

Hence, the eigencondition for collective excitation will be

$$\epsilon(q) = 0 \quad . \quad (3.36)$$

So, the zeros of the dielectric function yield the dispersion relation which in turn characterizes the collective modes. For this, one should first evaluate the in-medium polarization tensor  $\Pi_{\mu\nu}$ . It should be noted here that the imaginary part in the polarization function will introduce a damping of the collective modes as we have seen. The presence of matter raises the threshold of this effect since the baryon pair production is inhibited due to the Pauli blocking. For instance, at normal nuclear matter density and in the static limit, the value of the meson energy should be

$q_0 \geq 2E_F$  (about 1.2 GeV in the present model). Detailed discussion on this issue could be found in Refs. [45, 80]. We begin with the study of vector mesons propagation in dense matter.

### 3.3 Light Vector Mesons in Nuclear Matter: $\rho$ and $\omega$

In this section we evaluate the in-medium modification on the masses of  $\rho$  and  $\omega$  vector mesons and the collective excitations set by their propagation in nuclear matter in a relativistic mean field model.

Adopting the notation and approach provided by Shiomi and Hatsuda [31], we can write the vector meson - nucleon interaction Lagrangian as

$$\mathcal{L}_{int} = g_\alpha [\bar{N} \gamma_\mu \tau^\alpha N - \frac{\kappa_\rho}{2M} \bar{N} \sigma_{\mu\nu} \tau^\alpha N \partial^\nu] V_\alpha^\mu \quad (3.37)$$

where  $V_\alpha$ ,  $\alpha$  running from 0 to 3, shows the ( $\rho$ ,  $\omega$ ) meson field and  $\tau^i$  are the isospin Pauli matrices,  $\tau^0 = 1$ . The coupling constants  $g_\rho$ ,  $g_\omega$  and the ‘‘anomalous’’ or tensor-coupling parameter  $\kappa_\rho$ ,  $\kappa_\omega$  may be estimated [31] from the VMD model [81] (discussed in Sec. 4.1) of nucleon form-factors or from the fitting of the nucleon-nucleon interaction data as done by the Bonn group [82]. In view of the relatively small value of the isoscalar anomalous magnetic moment of the nucleon as compared to the isovector part, the tensor coupling is more important for the  $\rho$  than it is for the  $\omega$ , for instance [83]. In the present calculation, the treatment of the two meson is very similar, the couplings being the only essential difference. We can write the Lagrangian 3.37 as

$$\mathcal{L}_{int} = \bar{N} (\Gamma_\mu^\alpha V_\alpha^\mu) N \quad (3.38)$$

where  $\Gamma_\mu^\alpha$  is the  $VNN$  vertex factor given by

$$\Gamma_\mu^\alpha = g_\alpha [\gamma_\mu \tau^\alpha - \frac{\kappa_\alpha}{2M} \sigma_{\mu\nu} \partial^\nu \tau^\alpha] \quad . \quad (3.39)$$

Expanding  $\Gamma_\mu^\alpha V_\alpha^\mu$  in its components, we have

$$\mathcal{L}_{int} = [\bar{p}\Gamma_\mu p - \bar{n}\Gamma_\mu n]\rho_0^\mu + \sqrt{2}g_\rho[\bar{p}\Gamma_\mu n\rho_+^\mu + p\Gamma_\mu \bar{n}\rho_-^\mu] + (\bar{n}\Gamma_0 n + \bar{p}\Gamma_0 p)\omega \quad . \quad (3.40)$$

We shall consider the propagation of vector mesons in dense nuclear matter at zero temperature. As such, we shall be following the usual methods of relativistic quantum field theory, with the vacuum replaced by the ground state of nuclear matter at zero temperature, specified by the Fermi momentum ( $k_F$ ) corresponding to its density. Such a field-theoretic approach to the study of many body problems was developed, in the context with which we are concerned, by Matsubara, Galitskii and Migdal [84, 85, 86], and the relativistic generalization provided by Fradkin [87], and most importantly in the approach of Chin [45] which is the closest to the present work.

The second order polarization tensor  $\Pi_{\mu\nu}$ , corresponding to the vector meson and arising from the nucleon loop (Fig. 3.2), is thus calculable from the Lagrangian yielding

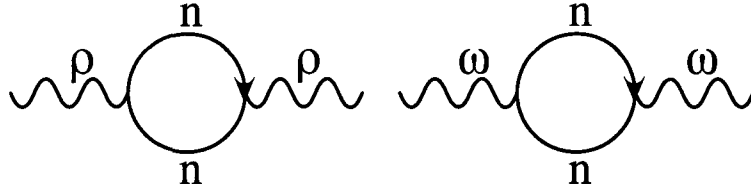


Figure 3.2:  $\rho - nn$  and  $\omega - nn$  loops

$$\Pi_{\mu\nu}^{\alpha\beta} = \frac{-i}{(2\pi)^4} \int d^4k \text{Tr}[i\Gamma_\mu^\alpha iG(k+q)i\bar{\Gamma}_\nu^\beta iG(k)] \quad (3.41)$$

where  $(\alpha, \beta)$  are the isospin indices and  $iG(k)$  is the in-medium nucleon propagator, which can easily be written from eq. 2.80 as

$$G(k) = G_F(k) + G_D(k) \quad (3.42)$$

where

$$G_F(k) = (k_\mu \gamma^\mu + M^*) \left[ \frac{1}{k^2 - M^{*2} + i\epsilon} \right] \quad (3.43)$$

and

$$G_D(k) = (k_\mu \gamma^\mu + M^*) \left[ \frac{i\pi}{E^*(k)} \delta(k_0 - E^*(k)) \theta(k_F - |\vec{k}|) \right] \quad (3.44)$$

with  $M^*$  denoting the effective mass of the nucleon in the medium and  $E^*(|k|) = \sqrt{|\vec{k}|^2 + M^{*2}}$ . The first term in  $G(k)$ , namely  $G_F(k)$ , is the same as the free propagator of a spin  $\frac{1}{2}$  fermion except for the fact that the effective mass of the nucleon is to be used. The second part,  $G_D(k)$  involving  $\theta(k_F - |\vec{k}|)$  arises from Pauli blocking and describes the modifications of the same in the nuclear matter at zero temperature [53]. It deletes the on mass-shell propagation of the nucleon in nuclear matter with momenta below the Fermi momentum.

In a similar vein the polarization insertions can also be written for any of the vector mesons as sum of two parts:

$$\Pi_{\mu\nu}(q) = \Pi_{\mu\nu}^F(q) + \Pi_{\mu\nu}^D(q), \quad (3.45)$$

$$\Pi_{\mu\nu}^F(q) = \frac{-i}{(2\pi)^4} \int d^4k \text{Tr}[\Gamma_\mu G_F(k+q) \bar{\Gamma}_\nu G_F(k)] \quad (3.46)$$

$$\Pi_{\mu\nu}^D(q) = \frac{-i}{(2\pi)^4} \int d^4k \text{Tr}[\Gamma_\mu G_F(k+q) \bar{\Gamma}_\nu G_D(k) \quad (3.47)$$

$$+ \Gamma_\mu G_D(k+q) \bar{\Gamma}_\nu G_F(k) \quad (3.48)$$

$$+ \Gamma_\mu G_D(k+q) \bar{\Gamma}_\nu G_D(k)] \quad (3.49)$$

$$(3.50)$$

$\Pi_{\mu\nu}^D(q)$  denotes the density dependent part of the polarization and  $\Pi_{\mu\nu}^F(q)$  denotes the free part, i.e., it contains the effect of ‘Dirac sea’ which we will discuss later. The density dependent part has a natural cutoff because of the  $\theta(k_F - |\vec{k}|)$  function. The real part of the density dependent polarization tensor is given by

$$\begin{aligned} \Pi_{\mu\nu}^D &= \frac{g_v^2 \pi}{(2\pi)^4} \int \frac{d^4k}{E^*(k)} \delta(k_0 - E^*(k)) \theta(k_F - |\vec{k}|) \\ &\times \left[ \frac{T_{\mu\nu}(k-q, k)}{(k-q)^2 - M^{*2}} + \frac{T_{\mu\nu}(k, k+q)}{(k+q)^2 - M^{*2}} \right] \end{aligned} \quad (3.51)$$

where  $T_{\mu\nu}$  is the trace given by

$$T_{\mu\nu}(k, k+q) = Tr[\Gamma_\mu(\not{k} + \not{q} + M)\Gamma_\nu(\not{k} + M)] . \quad (3.52)$$

Although the form of  $\Pi_{\mu\nu}^D(q)$  is the same as that of Chin [45], however, in this case it has three parts corresponding to vector-vector, vector-tensor and tensor-tensor terms. This is because the vertex factor in Eq. 3.39 is composed of two terms the first term which we call “vector”, and the tensor coupling which accounts for the effect of the magnetic interaction between vector mesons and nucleons. Hence, the self-energy can be also split in three terms

$$\Pi_{\mu\nu}^D(q) = \Pi_{\mu\nu}^{vv}(q) + \Pi_{\mu\nu}^{vt+tv}(q) + \Pi_{\mu\nu}^{tt}(q) . \quad (3.53)$$

The  $\Pi_{\mu\nu}^D(q)$  functions in this case are as follows

$$\begin{aligned} \Pi_{\mu\nu}^{vv} &= \frac{g_v^2}{\pi^3} \int_0^{k_F} \frac{d^3k}{E^*(k)} \frac{\mathcal{K}_{\mu\nu}q^2 - Q_{\mu\nu}(k \cdot q)^2}{q^4 - 4(k \cdot q)^2} \\ \Pi_{\mu\nu}^{vt+tv} &= \frac{g_v^2}{\pi^3} \left(\frac{kM^*}{4M}\right) 2q^4 Q_{\mu\nu} \int_0^{k_F} \frac{d^3k}{E^*(k)} \frac{1}{q^4 - 4(k \cdot q)^2} \\ \Pi_{\mu\nu}^{tt} &= -\frac{g_v^2}{\pi^3} \left(\frac{k}{4M}\right)^2 (4q^4) \int_0^{k_F} \frac{d^3k}{E^*(k)} \frac{\mathcal{K}_{\mu\nu} + Q_{\mu\nu}M^{*2}}{q^4 - 4(k \cdot q)^2} \end{aligned} \quad (3.54)$$

where  $\mathcal{K}_{\mu\nu} = (k_\mu - \frac{k \cdot q}{q^2} q_\mu)(k_\nu - \frac{k \cdot q}{q^2} q_\nu)$  and  $Q_{\mu\nu} = (-g_{\mu\nu} + \frac{q_\mu q_\nu}{q^2})$ .

It is clear that the form for the polarization tensor conforms to the requirement of current conservation, i.e.

$$q_\mu \Pi_{\mu\nu}^D = \Pi_{\mu\nu}^D q_\nu = 0 . \quad (3.55)$$

In order to evaluate  $\Pi_{\mu\nu}^D$  conveniently, we choose  $\vec{k}$  to be along the  $z$  axis i.e.  $q = (q_0, 0, 0, |\vec{q}|)$ , and  $k \cdot q = |\vec{k}||\vec{q}|\chi - E^*(k)q_0$ , where  $\chi$  is the cosine of the angle

between  $\vec{k}$  and  $\vec{q}$ . After  $\phi$  integration the non-vanishing components  $\Pi_{\mu\nu}^D$  are as shown below

$$\begin{pmatrix} \Pi_{00} & 0 & 0 & \Pi_{03} \\ 0 & \Pi_{11} & 0 & 0 \\ 0 & 0 & \Pi_{22} & 0 \\ \Pi_{30} & 0 & 0 & \Pi_{33} \end{pmatrix} . \quad (3.56)$$

Also for isotropic nuclear matter we have

$$\Pi_{11}^D = \Pi_{22}^D \quad (3.57)$$

$$\Pi_{03}^D = \Pi_{30}^D . \quad (3.58)$$

This, along with the current conservation relation 3.55, leaves us only with two non-vanishing independent component of  $\Pi_{\mu\nu}^D$ . It might be worthwhile to say here that the  $\rho$  meson being a vector, the collective oscillations set by its propagation through matter would have longitudinal (L) and transverse (T) components depending upon whether its spin is aligned along or perpendicular to the direction of propagation. Of course, these modes should coincide in the static limit when there is no preferred direction in the matter. Accordingly, with our choice of z-axis along the direction of the momenta ( $\vec{q}$ ), one can define the longitudinal and transverse polarization as linear combinations of the two independent components:

$$\Pi_L = -\Pi_{00} + \Pi_{33} \quad (3.59)$$

$$\Pi_T = \Pi_{11} = \Pi_{22} . \quad (3.60)$$

If we perform the angular integration in relations 3.55 we can write two independent components  $\Pi_{00}$ ,  $\Pi_{11}$  as

$$\Pi_{00}(q) = \frac{g_v^2 q^2}{2\pi^2} \left[ I_{00}^{vv}(q) - \frac{kM_n^*}{2M_n} I_{00}^{vt}(q) + \left(\frac{kM_n^*}{2M_n}\right)^2 I_{00}^{tt}(q) \right] \quad (3.61)$$

where

$$I_{00}^{vv}(q) = I_{00}^k(q) + \frac{q_z^2}{q^2} I_{02}(q) \quad (3.62)$$

$$\begin{aligned}
I_{00}^{vt}(q) &= \frac{q_z^2}{q^2} I_{00}(q) \\
I_{00}^{tt}(q) &= I_{00}^k(q) + \frac{q_z^2 M^{*2}}{q^4} I_{00}(q) \\
I_{00}^k(q) &= \int_0^{k_F} \frac{k dk}{E_k q_z} \left[ -\frac{E_k^2}{q^2} I_0(k, q) + \frac{E_k q_0}{q^2} I_1(k, q) - \frac{q_0^2}{q^2} I_2(k, q) \right] \\
I_{00}(q) &= \int_0^{k_F} \frac{k dk}{E_k q_z} I_0(k, q) \\
I_{02}(q) &= \int_0^{k_F} \frac{k dk}{E_k q_z} I_2(k, q) \\
I_0(k, q) &= \ln \left[ \frac{4E_k^2 q_0^2 - (q^2 - 2|\vec{k}|q_z)^2}{4E_k^2 q_0^2 - (q^2 + 2|\vec{k}|q_z)^2} \right] \\
I_1(k, q) &= \ln \left[ \frac{4(E_k q_0 + k q_z)^2 - q^4}{4(E_k q_0 - k q_z)^2 - q^4} \right] \\
I_2(k, q) &= 2 \frac{k q_z}{q^2} + I_0(k, q) \quad .
\end{aligned} \tag{3.63}$$

Similarly we have for  $\Pi_{11}$

$$\Pi_{11}(q) = \frac{g_v^2 q^2}{2\pi^2} \left[ I_{11}^{vv}(q) - \frac{k M_n^*}{2M_n} I_{11}^{vt}(q) + \left( \frac{k M_n^*}{2M_n} \right)^2 q^4 I_{11}^{tt}(q) \right] \tag{3.64}$$

where

$$\begin{aligned}
I_{11}^{vv}(q) &= I_{11}^k(q) + I_{02}(q) \\
I_{11}^{vt}(q) &= I_{00}(q) \\
I_{11}^{tt}(q) &= I_{11}^k(q) + \frac{M^{*2}}{q^2} I_{00}(q) \\
I_{11}^k(q) &= \int_0^{k_F} \frac{k dk}{E_k q_z} \left[ (E_k^2 \frac{q_0^2}{q_z^2} - k^2) \frac{I_0(k, q)}{q^2} - \frac{2E_k q_0}{q_z^2} I_1(k, q) + \frac{q^2}{q_z^2} I_2(k, q) \right] \quad .
\end{aligned} \tag{3.65}$$

As mentioned before,  $\Pi_{\mu\nu}^F(q)$  in Eq. 3.46 is the vacuum polarization. This is a bilinear function of  $G_F^H$  and hence describes the correction to the meson propagator

due to coupling to  $N\bar{N}$  excitations. The  $N\bar{N}$  pairs can be excited only if the four-momentum carried by the mesons is in the time-like region ( $k^2 > 0$ ). Hence the shift in the mass of the vector mesons due to vacuum polarization is caused by processes like  $V \rightarrow N\bar{N} \rightarrow V$  where  $N$  represents nucleons in the modified Dirac sea having an effective mass  $M_N^*$ , smaller than what it would be in free space. From Eq. (3.46) we have

$$\Pi_F^{\mu\nu}(k) = -2ig_{VNN}^2 \int \frac{d^4p}{(2\pi)^4} \frac{\text{Tr}[\Gamma^\mu(\not{p} + M_N^*)\Gamma^\nu(\not{p} + \not{k} + M_N^*)]}{(p^2 - M_N^{*2})[(p+k)^2 - M_N^{*2}]} . \quad (3.66)$$

From naive power counting it can be seen that this part of the self-energy is ultraviolet divergent and has to be renormalized. A few comments about renormalizability of the interaction given by Eq. (3.38) is in order here. At very large momenta the propagator for massless bosons  $\sim O(k^{-2})$ , whereas for massive vector bosons it goes as  $\sim O(1)$ . This poses severe problems to the renormalizability of the theory with massive vector bosons. However, in a gauge theory with spontaneous symmetry breaking the vector gauge bosons acquire mass in such a way that the renormalizability of the theory is always preserved [88]. The theory which involves neutral massive vector bosons coupled to a conserved current is also renormalizable. This is because in a physical process the propagator  $iD_0^{\mu\nu} = i(-g^{\mu\nu} + k^\mu k^\nu/m^2)/(k^2 - m^2 + i\epsilon)$  appears between two conserved currents  $J_\mu$  and  $J_\nu$  and the offending term  $k^\mu k^\nu/m^2$  does not contribute because of current conservation ( $k_\mu J^\mu = 0$  or  $\partial^\mu J_\mu(x) = 0$  in coordinate space). Now, the power counting is similar with the case of massless vector fields and the theory is renormalizable. This is the case for the  $\omega$  meson [32, 89] which we shall consider first. The counter term required in this case is [90]

$$\mathcal{L}_{VNN}^{CT} = -\frac{1}{4}\zeta F^{\mu\nu} F_{\mu\nu} . \quad (3.67)$$

We use dimensional regularization to separate the divergent and the finite parts. The divergences now appear as a pole in the  $\Gamma$ -function at the physical dimension

$n = 4$  [58]. The renormalized vacuum polarization tensor for the  $\omega$  is then given by

$$\Pi_F^{\mu\nu}(k) = (g^{\mu\nu} - k^\mu k^\nu / k^2) \Pi_F^{ren}(k^2) \quad , \quad (3.68)$$

where

$$\begin{aligned} \Pi_F^{ren}(k^2) = \frac{g_{\omega NN}^2}{\pi^2} k^2 \left\{ \Gamma(2 - n/2) \int_0^1 dz z(1-z) \right. \\ \left. - \int_0^1 dz z(1-z) \ln[M_N^{*2} - k^2 z(1-z)] \right\} - \zeta \end{aligned} \quad (3.69)$$

in which the counter term contribution

$$\Pi_F^{\mu\nu CTC} = -\zeta k^2 (g^{\mu\nu} - k^\mu k^\nu / k^2) \quad (3.70)$$

has been included.  $\zeta$  is determined by the renormalization condition [90, 48]

$$\Pi_F^{ren}(k^2)|_{M_N^* \rightarrow M_N} = 0 \quad . \quad (3.71)$$

Finally, we arrive at

$$\begin{aligned} \Pi_F^\omega(k^2) &= \frac{1}{3} \text{Re}(\Pi_F^{ren})^\mu{}_\mu \\ &= -\frac{g_{\omega NN}^2}{\pi^2} k^2 \int_0^1 dz z(1-z) \ln \left[ \frac{M_N^{*2} - k^2 z(1-z)}{M_N^2 - k^2 z(1-z)} \right] \quad . \end{aligned} \quad (3.72)$$

It might be mentioned that, because of the tensor interaction in Eq. 3.38 which involves derivative couplings, the renormalizability of the Lagrangian is lost. We, however, employ a phenomenological subtraction procedure [31, 90] to extract the finite part using the condition:

$$\left. \frac{\partial^n \Pi_F^\rho(k^2)}{\partial (k^2)^n} \right|_{M_N^* \rightarrow M_N} = 0 \quad (3.73)$$

with  $n = 0, 1, 2, \dots, \infty$ . By using dimensional regularization and the above subtraction procedure we arrive at the following expression:

$$\Pi_F^\rho(k^2) = -\frac{g_{\rho NN}^2}{\pi^2} k^2 \left[ I_1 + M_N^* \frac{\kappa_\rho}{2M_N} I_2 + \frac{1}{2} \left( \frac{\kappa_\rho}{2M_N} \right)^2 (k^2 I_1 + M_N^{*2} I_2) \right] \quad (3.74)$$

where

$$\begin{aligned} I_1(k^2) &= \int_0^1 dz z(1-z) \ln \left[ \frac{M_N^{*2} - k^2 z(1-z)}{M_N^2 - k^2 z(1-z)} \right] \\ I_2(k^2) &= \int_0^1 dz \ln \left[ \frac{M_N^{*2} - k^2 z(1-z)}{M_N^2 - k^2 z(1-z)} \right] . \end{aligned} \quad (3.75)$$

With the polarization functions calculated, we can now study the properties of the collective excitations in dense matter. Following the procedure described in Sec. 3.2 we can write the dielectric function (Eq. 3.35) as

$$\epsilon(q_0, |\vec{q}|) = \det(1 - \mathcal{D}^0 \Pi) = \epsilon_T^2 \times \epsilon_L \quad (3.76)$$

where  $\epsilon_T$  corresponds to two identical transverse (T) modes and  $\epsilon_L$  corresponds to the longitudinal mode depending upon whether its spin is aligned along or perpendicular to the direction of propagation. They can be written as

$$\begin{aligned} \epsilon_T &= 1 - d_0 \Pi_T \\ \epsilon_L &= 1 - d_0 \Pi_L \end{aligned} \quad (3.77)$$

where  $d_0 = \frac{1}{q^2 - m_V^2 + i\epsilon}$  is the non-tensorial part of the vector meson free propagator. The zeros of the dielectric functions characterize the dispersion relation for the meson propagation. Fig. 3.3 shows in the left panel the dispersion curves for the  $\rho$  meson in nuclear matter at density  $\rho=2.5\rho_0$ . One can notice that in the static limit, at low momentum, the longitudinal and transversal mode coincides as it should. Also, the gap between the two modes increase with momentum. The same feature can be seen in the right panel for the  $\omega$  meson but the difference is slightly larger. Even though the longitudinal and transversal modes coincide when the particle is at rest, its mass differ from its vacuum value. One could notice a non-zero value of the polarization function at finite density even in the static limit as evident from the modified dispersion function.

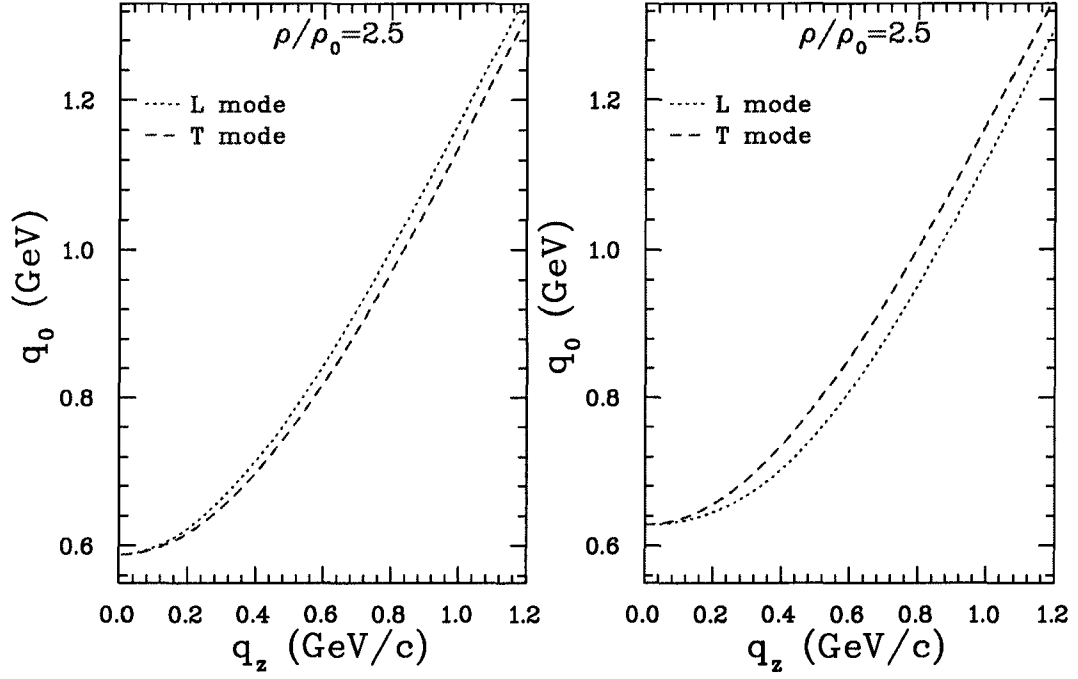


Figure 3.3: The dispersion curves for  $\rho$  and  $\omega$  mesons at  $\rho=2.5\rho_0$ .

### 3.4 Scalar Mesons in Nuclear Matter: $a_0$ and $\sigma$

The Lagrangian describing the scalar meson interaction with nucleons could be written as

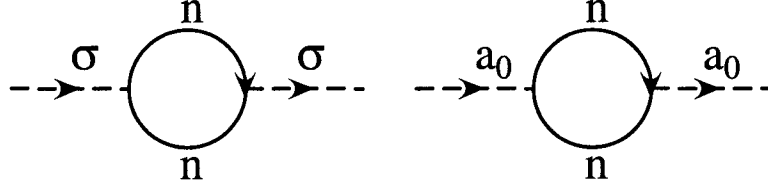
$$\mathcal{L}_{int} = g_{a_0} \bar{\psi} \phi_{a_0, a} \tau^a \psi + g_{\sigma} \bar{\psi} \phi_{\sigma} \psi \quad (3.78)$$

where  $\psi$ ,  $\phi_{a_0}$  and  $\phi_{\sigma}$  correspond to nucleon,  $a_0$  and  $\sigma$  fields, and  $\tau_a$  is a Pauli matrix. The values used for the coupling parameters are obtained from Ref. [82].

The polarization tensor can be calculated by evaluating the Feynman diagrams 3.4, and, it takes the form

$$\Pi_{a_0, \sigma}(q_0, |\vec{q}|) = -i g_{a_0, \sigma}^2 \int \frac{d^4 k}{(2\pi)^4} \text{Tr}[G(k)G(k+q)] \quad (3.79)$$

where the nucleon propagator is again given by Eq. 3.42. The two-fold structure of

Figure 3.4:  $a_0 - nn$  and  $\sigma - nn$  loops

this propagator permits to write the self-energy as sum of two parts

$$\Pi_s(q) = \Pi_s^F(q) + \Pi_s^D(q), \quad (3.80)$$

$$\Pi_s^F(q) = \frac{-i}{(2\pi)^4} \int d^4k \text{Tr}[G_F(k+q)G_F(k)] \quad (3.81)$$

$$\Pi_s^D(q) = \frac{-i}{(2\pi)^4} \int d^4k \text{Tr}[G_F(k+q)G_D(k) \quad (3.82)$$

$$+ G_D(k+q)G_F(k) + G_D(k+q)G_D(k)] \quad (3.83)$$

$$(3.84)$$

The dense part of the scalar meson self-energy takes the form

$$\Pi_{a_0,\sigma}^D(q) = \frac{g_{a_0,\sigma}^2}{\pi^3} \int \frac{d^3k}{E_k} \frac{q^2 m^{*2} - (k \cdot q)^2}{q^4 - 4(k \cdot q)^2} \quad (3.85)$$

After performing the angular integration, the self-energy involves only an integral over the internal momentum of the nucleon loop in the following manner:

$$\begin{aligned} \Pi_{a_0,\sigma}^D(q_0, |\vec{q}|) &= \frac{g_{a_0,\sigma}^2}{\pi^2} \int \frac{k dk}{E_k q_z} \quad (3.86) \\ &\times \left[ k q_z + \frac{q^2/2 - M^{*2}}{2} \ln \left( \frac{4E_k^2 q_0^2 - (q^2 - 2|\vec{k}|q_z)^2}{4E_k^2 q_0^2 - (q^2 + 2|\vec{k}|q_z)^2} \right) \right] \end{aligned}$$

It should be mentioned that Eq. 3.79 also involves a free part stemming from the  $G_F(k)G_F(k)$  combination which is divergent. This therefore needs to be regularized. The regularization condition employed again is [48]:

$$\partial^n \Pi^F(q^2) / \partial (q^2)^n |_{m_n^* \rightarrow m, q^2 = m_s^2} = 0 \quad (n = 0, 1, 2, \dots, \infty) \quad (3.87)$$

The free part of the self-energy is given by

$$\begin{aligned} \Pi_{a_0,\sigma}^F(q^2) = & \frac{3g_{a_0,\sigma}^2}{2\pi^2} \{ 3(m_n^{*2} - m_n^2) - 4(m_n^* - m_n)m_n \\ & - (m_n^{*2} - m_n^2) \int_0^1 dx \ln \left[ \frac{m_n^{*2} - x(1-x)q^2}{m_n^2} \right] \\ & - \int_0^1 dx (m_n^2 - x(1-x)q^2) \ln \left[ \frac{m_n^{*2} - x(1-x)q^2}{m_n^2 - x(1-x)q^2} \right] \} . \end{aligned} \quad (3.88)$$

The dielectric function for the scalar meson can be written as

$$\epsilon_s = 1 - d_0 \Pi^s \quad (3.89)$$

where

$$\begin{aligned} \Pi^s &= \Pi^F + \Pi^D \\ id_0 &= \frac{i}{q^2 - m_s^2 + i\epsilon} . \end{aligned} \quad (3.90)$$

We are now in the position to evaluate the dispersion curves corresponding to the  $a_0, \sigma$  scalar mesons in the nuclear matter. Fig. 3.5 presents the dispersion curve correspondent to the  $a_0$  and  $\sigma$  mesons for a density 2.5 times larger than normal nuclear matter density. It is understood that scalar mesons, being spinless particles, do not have two components as in the vector case.

### 3.5 Scalar-Vector Meson Mixing in Nuclear Matter

As mentioned before at the beginning of Chapter 3, several theoretical studies have sought to investigate the in-medium properties of vector mesons. Their possible mixing with other mesons has only started to receive attention in the context of dense baryonic matter. An exception is the case of  $\rho$ - $\omega$  [91, 92]. This isospin symmetry breaking effect is possible when there is an asymmetry in the number of protons and neutrons. Technically speaking,  $\rho_0$  (unlike  $\omega$ ), couples with opposite sign to the proton and neutron, as can be seen from Eq. 3.40. Therefore, the contribution from

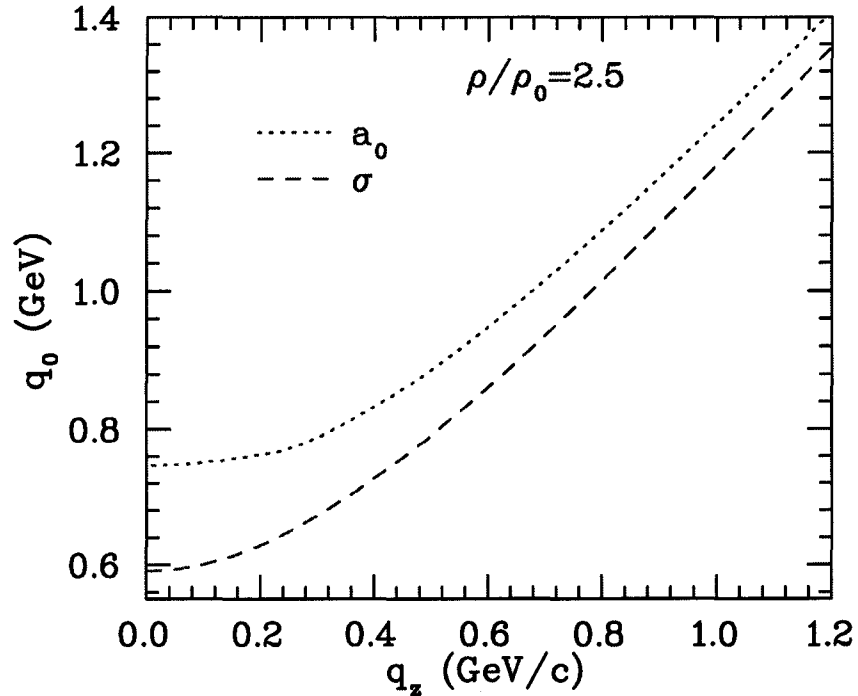


Figure 3.5: The dispersion curve for  $a_0$  and  $\sigma$  mesons at  $\rho=2.5\rho_0$ .

the proton and neutron loops to the self-energy diagram corresponding to the  $\rho$ - $\omega$  mixing, exactly cancel in symmetric matter. Consequently, this specific mixing can be omitted when dealing with symmetric nuclear matter, as assumed in the present calculation.

We explore here the possibility of  $\rho$ - $a_0$  ( $\delta$  in the old notation [51]) mixing via nucleon(n)-nucleon(n) excitations in nuclear matter [48]. This effect is a pure density-dependent effect and is forbidden in free space on account of Lorentz symmetry. Such a mixing, in effect, is similar to the known  $\omega$ - $\sigma$  mixing [45, 53, 52, 47]. We will also show some particularities of  $\omega$ - $\sigma$  mixing not explored before. As evident from the previous discussion, we will not consider the effect of nuclear resonances in the present model. A discussion of this issue is postponed until later.

The polarization vector through which the  $a_0$  ( $\sigma$ ) couples to  $\rho$  ( $\omega$ ) via the n-n

loop, as shown in the diagram 3.6, is given by

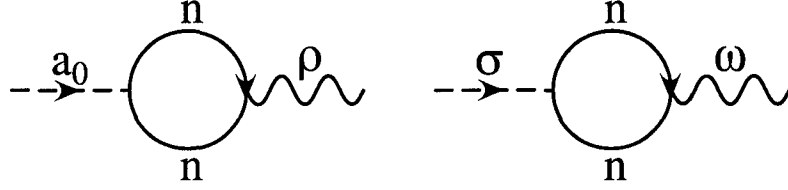


Figure 3.6: Feynman diagrams showing  $a_0$ - $\delta$  and  $\omega$ - $\sigma$  mixing via n-n loops

$$\Pi_\mu(q_0, |\vec{q}|) = 2ig_{a_0,\sigma}g_{\rho,\omega} \int \frac{d^4k}{(2\pi)^4} \text{Tr}[G(k)\Gamma_\mu G(k+q)] \quad . \quad (3.91)$$

where 2 is an isospin factor, and, the vertex for  $\rho$  ( $\omega$ )-nn coupling is:

$$\Gamma_\mu = \gamma_\mu - \frac{\kappa_{\rho,\omega}}{2m_n} \sigma_{\mu\nu} q^\nu \quad . \quad (3.92)$$

$G(k)$  is the in-medium nucleon propagator (eq. 3.42)

With the evaluation of the trace and after a little algebra Eq. (3.91) can be cast into a suggestive form:

$$\Pi_\mu(q_0, |q|) = \frac{g_{\rho,\omega}g_{a_0,\sigma}}{\pi^3} 2q^2 \left( 2m_n^* - \frac{\kappa_{\rho,\omega}q^2}{2m_n} \right) \int_0^{k_F} \frac{d^3k}{E^*(k)} \frac{k_\mu - \frac{q_\mu}{q^2}(k \cdot q)}{q^4 - 4(k \cdot q)^2} \quad . \quad (3.93)$$

This immediately leads to two conclusions. First, it manifestly respects the current conservation condition, namely  $q^\mu \Pi_\mu = 0 = \Pi_\nu q^\nu$ . Secondly, there are only two components which survive after the integration over azimuthal angle:  $\Pi_0$  and  $\Pi_3$ . In fact, this shows that it is only the longitudinal component of the  $\rho$  meson which couples to the scalar meson while the transverse mode remains unaltered, as we will also see later reflected in the dielectric function. Furthermore, current conservation implies that out of the two non-zero components of  $\Pi_\mu$ , only one is independent. It should also be noted here that the tensor interaction, as evident from Eq. 3.93, inhibits the mixing. After performing the angular integration  $\Pi_0$  takes the form:

$$\begin{aligned} \Pi_0 &= \frac{g_{\rho,\omega}g_{a_0,\sigma}}{8\pi^2|\vec{q}|} \left(2m_n^* - \frac{\kappa_{\rho,\omega}q^2}{2m_n}\right) \\ &\times \int_0^{k_F} \frac{kdk}{E_k^*} \left[ 2E_k^* \ln \left[ \frac{(q^2 + 2k|\vec{q}|)^2 - 4E_k^{*2}E_q^{*2}}{(q^2 - 2k|\vec{q}|)^2 - 4E_k^{*2}E_q^{*2}} \right] - q_0 \ln \left[ \frac{q^4 - 4(E_k^*E_q^* - 4k|\vec{q}|)^2}{q^4 - 4(E_k^*E_q^* + 4k|\vec{q}|)^2} \right] \right] . \end{aligned} \quad (3.94)$$

In presence of mixing the combined meson propagator can be written in a matrix form where the dressed propagator is no longer diagonal:

$$\mathcal{D} = \mathcal{D}^0 + \mathcal{D}^0 \Pi \mathcal{D} \quad . \quad (3.95)$$

It is to be noted that the free propagator is a block-diagonal  $5 \times 5$  matrix and has the form

$$\mathcal{D}^0 = \begin{pmatrix} D_{\mu\nu}^0 & 0 \\ 0 & \Delta_0 \end{pmatrix} \quad . \quad (3.96)$$

In Eq. (3.96) the non-interacting propagator for the  $a_0$  and  $\rho$  are given respectively by

$$i\Delta_0(q) = \frac{i}{q^2 - m_{a_0,\sigma}^2 + i\epsilon}, \quad (3.97)$$

$$iD_{\mu\nu}^0(q) = i \frac{-g_{\mu\nu} + \frac{q_\mu q_\nu}{q^2}}{q^2 - m_{\rho,\omega}^2 + i\epsilon} \quad . \quad (3.98)$$

The mixing is characterized by the polarization matrix which now contains non-diagonal elements

$$\Pi = \begin{pmatrix} \Pi_{\mu\nu}^{\rho,\omega}(q) & \Pi_\nu(q) \\ \Pi_\mu(q) & \Pi^{a_0,\sigma}(q) \end{pmatrix} \quad . \quad (3.99)$$

In the above expression,  $\Pi^{a_0,\sigma}$  and  $\Pi_{\mu\nu}^{\rho,\omega}$  refer to the diagonal self-energies of the  $a_0$  ( $\sigma$ ) and  $\rho$  ( $\omega$ ) mesons induced by the n-n polarization as written in Eqs. 3.41 and 3.79. After the  $\phi$  integration, the non-vanishing components  $\Pi$  are as shown below

$$\Pi = \begin{pmatrix} \Pi_{00} & 0 & 0 & \Pi_{03} & \Pi_0 \\ 0 & \Pi_{11} & 0 & 0 & 0 \\ 0 & 0 & \Pi_{22} & 0 & 0 \\ \Pi_{30} & 0 & 0 & \Pi_{33} & \Pi_3 \\ \Pi_0 & 0 & 0 & \Pi_3 & \Pi^{a_0} \end{pmatrix} . \quad (3.100)$$

To determine the collective modes, one defines the dielectric function as [45]:

$$\epsilon(q_0, |\vec{q}|) = \det(1 - \mathcal{D}^0 \Pi) \quad (3.101)$$

which, after a little algebra, can be cast into the form

$$\epsilon(q_0, |\vec{q}|) = \epsilon_T^2 \times \epsilon_{mix} \quad (3.102)$$

where  $\epsilon_T$  corresponds to two identical transverse (T) modes, unmodified by mixing as expected, and  $\epsilon_{mix}$  is the longitudinal dielectric function with the corresponding changes induced by mixing. The latter, of course, also characterizes the mode relevant for the  $a_0$  and  $\sigma$  meson propagation.

$$\begin{aligned} \epsilon_T &= 1 - d_0 \Pi_T \\ \epsilon_{mix} &= (1 - d_0 \Pi_L)(1 - \Delta_0 \Pi_s) - \frac{q^2}{|\vec{q}|^2} \Delta_0 d_0 (\Pi_0)^2 . \end{aligned} \quad (3.103)$$

The zeros of the dielectric functions yield the dispersion relation for the meson propagation. Fig. 3.7 shows the relevant dispersion curves for  $\rho$  and  $a_0$  with and without mixing at density  $\rho=2.5\rho_0$ .

As only the longitudinal mode mixes with the scalar, transverse modes are not considered here. The later in fact are the same as presented for free  $\rho$  ( $\omega$ ) meson. The effect of mixing on the pole masses, as evident from Fig. 3.7, are found to be small. However, the mixing can be large when the mesons involved go off-shell. It

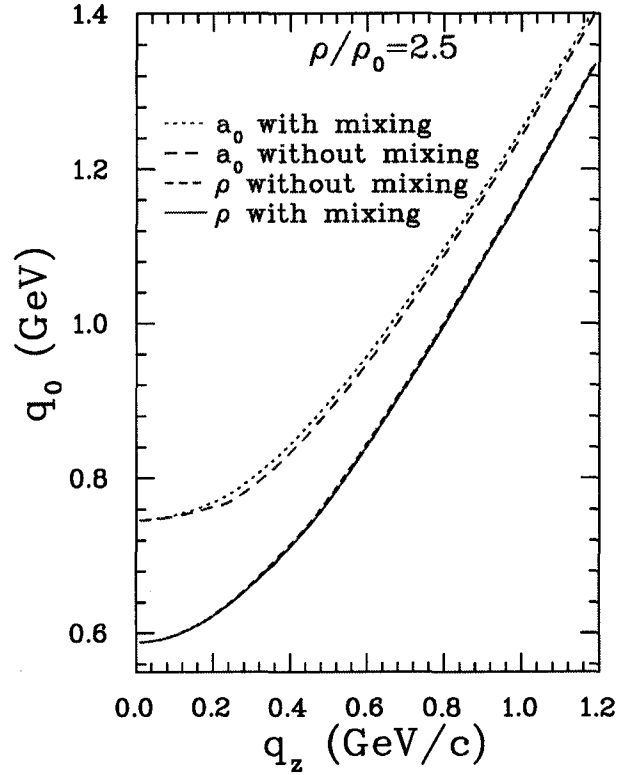


Figure 3.7: The dispersion curves for  $\rho$  and  $a_0$  meson with and without mixing at  $\rho=2.5\rho_0$ .

should be noted that the modes with mixing move away from each other compared to what one obtains without mixing. This can be understood in terms of “level-level” repulsion driven by the off-diagonal terms of the dressed propagator [93].

This effect could be seen better in the same kind of plot in Fig. 3.8 for  $\omega$  and  $\sigma$ . Without mixing, the two modes corresponding to the scalar and vector meson propagation cross each other. They will not cross each other when mixing induces the “level-level” repulsion.

Fig. 3.9 shows the dependence of the invariant masses ( $M_i = \sqrt{q_{0(i)}^2 - |\vec{q}_i|^2}$ ,  $i=\rho, \omega, a_0, \sigma$ ) on nuclear densities where the  $q_0$ 's are determined from the zeros of the dielectric function (Eq. 3.103). It is evident that the difference of the invariant masses

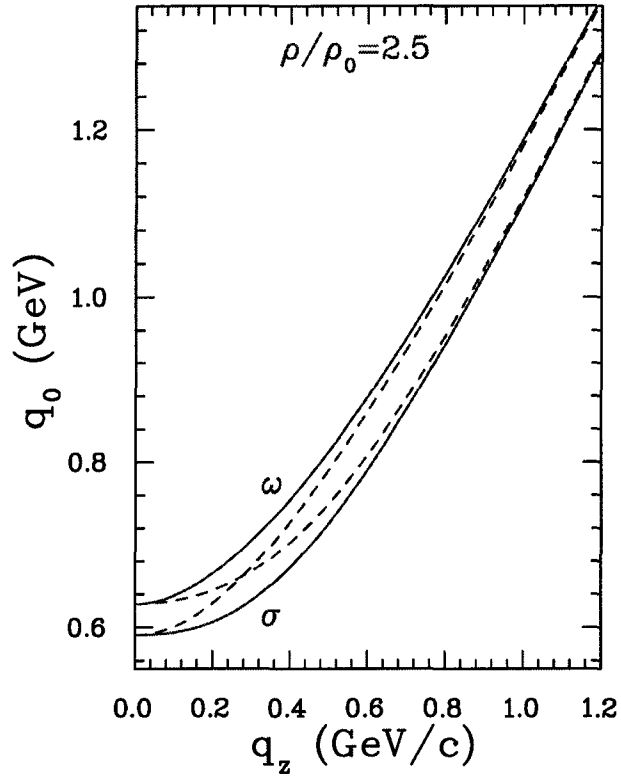


Figure 3.8: The dispersion curve for  $\omega$  and  $\sigma$  meson with (solid lines) and without (dashed lines) mixing at  $\rho=2.5\rho_0$ .

first decreases with density reaching a minima and then again starts increasing. This behaviour arises from the non-monotonic density dependence of the polarization functions.

To calculate the mixing angle, one diagonalizes the mass matrix with the mixing effect included [94]

$$\begin{pmatrix} m_v^2 + \Pi_v^{\mu\nu} & \Pi_M^\nu \\ \Pi_M^\mu & m_s^2 + \Pi_s \end{pmatrix}. \quad (3.104)$$

The mixing angle will be defined as the shift of the basis vectors, representing scalar and vector particles, which diagonalizes the mass matrix, i.e.,

$$|\tilde{\psi}_v\rangle = \cos\theta_{mix}|\psi_v\rangle - \sin\theta_{mix}|\psi_s\rangle \quad (3.105)$$

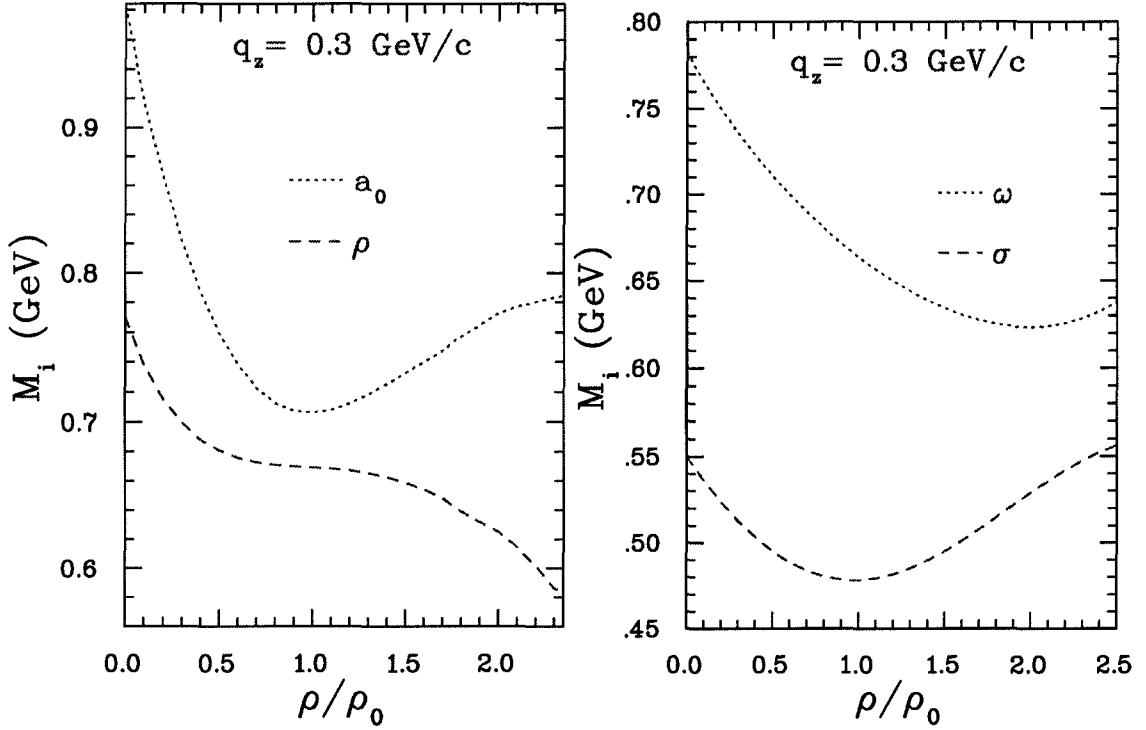


Figure 3.9: The invariant mass as a function of the relative nuclear matter density.

$$|\tilde{\psi}_s\rangle = \sin\theta_{mix}|\psi_v\rangle + \cos\theta_{mix}|\psi_s\rangle .$$

The value of the angle for which the new base diagonalizes the mass matrix is

$$\theta_{mix} = \frac{1}{2} \arctan\left(\frac{2\Pi_{mix}^{vs}}{m_s^2 - m_v^2 - \Pi_L^v + \Pi^s}\right) . \quad (3.106)$$

In eq. (3.106)  $\Pi_{mix}^{vs} = M_i/|\vec{q}|\Pi_0$  which increases with density.  $\Pi_0$  is the zero component of eq. (3.93). Eq. (3.106) clearly shows that the mixing angle depends not only on the mixing amplitude ( $\Pi_0$ ) but also on the “energy denominator”. The latter, as seen in Fig. 3.9, first decreases as a function of density then again shows an increase characterizing the density dependence of the mixing angle as presented in Fig. 3.10. The mixing angle in Fig. 3.10 corresponds to  $|\vec{q}|=0.3$  GeV/c. For each case, there are two mixing angles corresponding to the two poles representing the scalar and vector meson respectively. We also note that the “energy denominator” has different sign

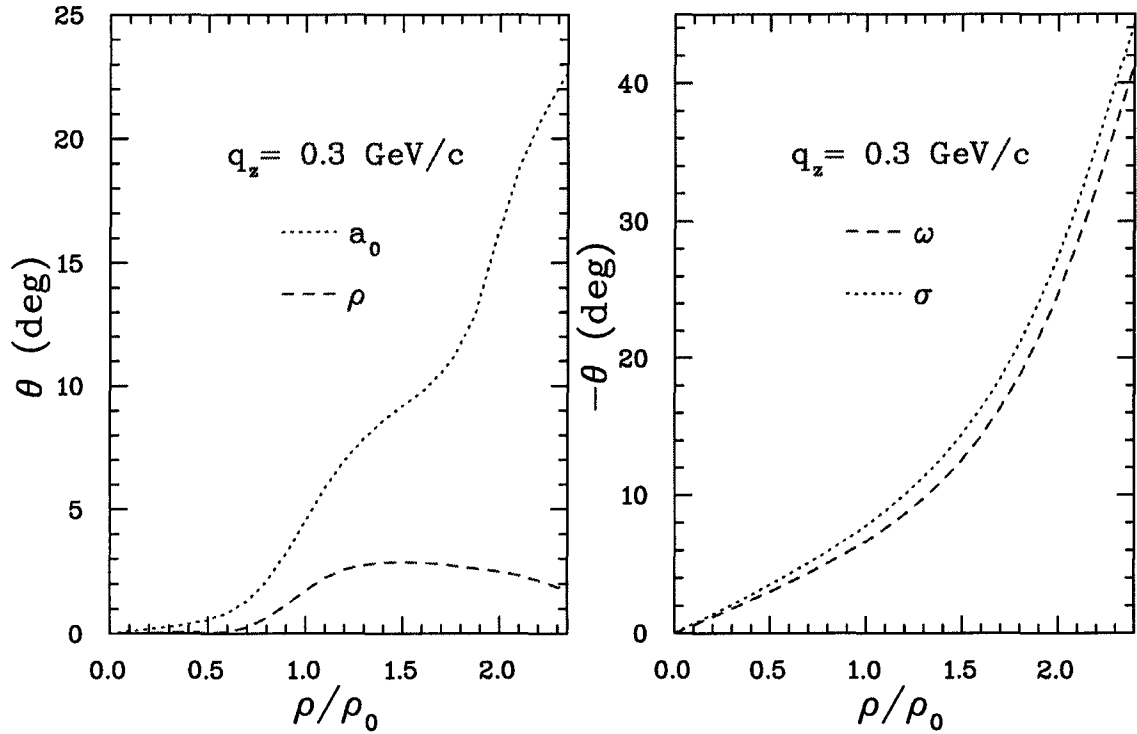


Figure 3.10: The mixing angle as function of the relative nuclear matter density for  $\rho - a_0$  (left panel) and  $\omega - \sigma$  (right panel).

for the two mixing cases as can be seen from Fig. 3.9. Therefore, the mixing angle will have opposite sign for  $\rho - a_0$  as compared to  $\omega - \sigma$  mixing.

The momentum dependence for a density of 1.5 times higher than the normal nuclear matter density is shown in Fig. 3.11. One could notice that even for momenta as low as  $|\vec{q}| \approx 0.2$  GeV/c the mixing is quite appreciable. It should also be noted that the mixing angle vanishes at  $|\vec{q}| = 0$  or at  $\rho = 0$ , as it should.

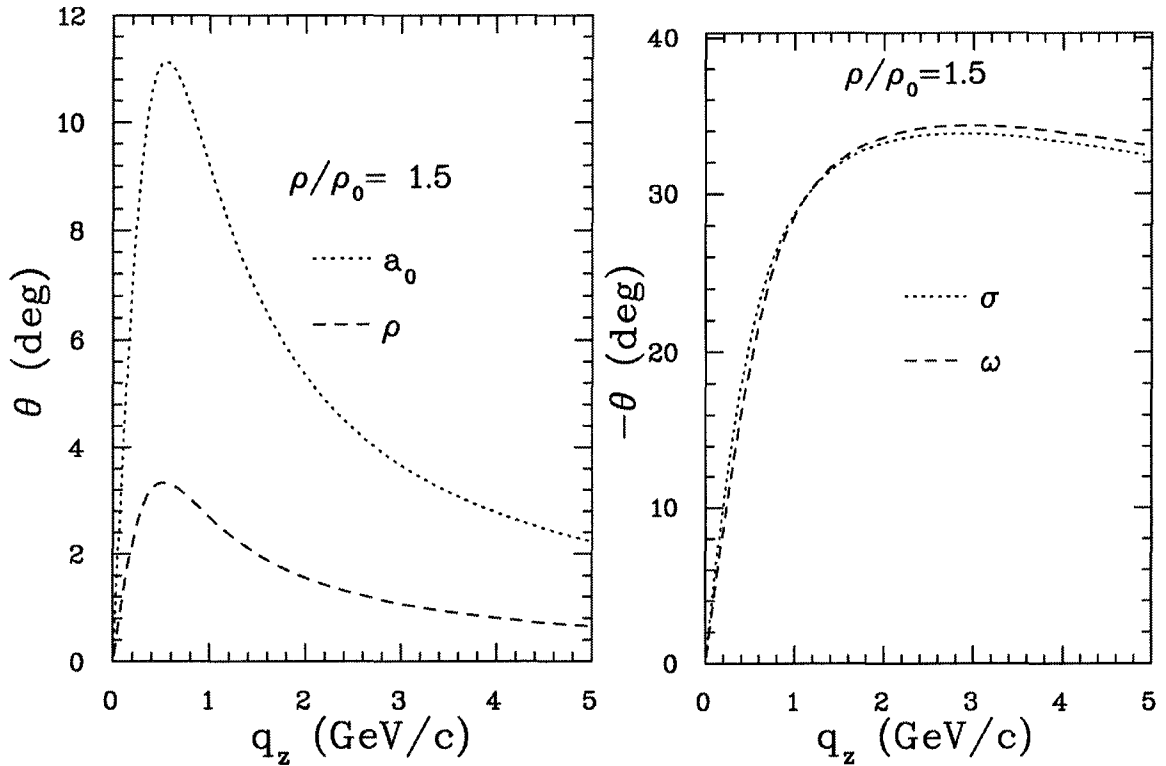


Figure 3.11: The mixing angle as a function of the momentum for a fixed baryonic density in the two mixing cases  $\rho - a_0$  (left panel) and  $\omega - \sigma$  (right panel).

### 3.6 Vector Mesons in Nuclear Matter at Finite Temperature

The literature at finite temperature is also plagued with diverse, if not contradictory results. If the phase transition to a QGP phase is primarily one of deconfinement, argues Pisarski [95], then this may be modeled by an effective bag constant which decreases with temperature and the effective mass of the  $\rho$  meson, like all hadronic bound states, should then decrease with temperature. The nonlinear sigma model [96], shows an opposite trend, the effective mass of the  $\rho$  meson increasing with temperature. A similar qualitative behaviour of the  $\rho$  mass has been observed in the hidden local symmetry approach [97]. The Walecka type of model, which is

the base of our study, however, shows a reduction of vector meson mass with density and temperature [98, 73, 99] as we shall see.

At finite temperature, the two independent components of the polarization tensor  $\Pi_{00}$  and  $\Pi_{11}$  become

$$\Pi_{00}(q) = \frac{g_v^2 q^2}{2\pi^2} \left[ I_{00}^{vv}(q) - \frac{kM_n^*}{2M_n} I_{00}^{vt}(q) + \left( \frac{kM_n^*}{2M_n} \right)^2 q^4 I_{00}^{tt}(q) \right] \quad (3.107)$$

$$\Pi_{11}(q) = \frac{g_v^2 q^2}{2\pi^2} \left[ I_{11}^{vv}(q) - \frac{kM_n^*}{2M_n} I_{11}^{vt}(q) + \left( \frac{kM_n^*}{2M_n} \right)^2 q^4 I_{11}^{tt}(q) \right] \quad (3.108)$$

where

$$I_{00}^k(q) = \int_0^\infty \frac{kdk}{E_k q_z} \left[ -\frac{E_k^2}{q^2} I_0(k, q) + \frac{E_k q_0}{q^2} I_1(k, q) - \frac{q_0^2}{q^2} I_2(k, q) \right] (n_k + \bar{n}_k) \quad (3.109)$$

$$I_{00}(q) = \int_0^\infty \frac{kdk}{E_k q_z} I_0(k, q) (n_k + \bar{n}_k)$$

$$I_{02}(q) = \int_0^\infty \frac{kdk}{E_k q_z} I_2(k, q) (n_k + \bar{n}_k)$$

$$I_{11}^k(q) = \int_0^\infty \frac{kdk}{E_k q_z} \left[ \left( E_k^2 \frac{q_0^2}{q_z^2} - k^2 \right) \frac{I_0(k, q)}{q^2} - \frac{2E_k q_0}{q_z^2} I_1(k, q) + \frac{q^2}{q_z^2} I_2(k, q) \right] (n_k + \bar{n}_k) .$$

The other expressions used in Eqs. 3.107 and 3.108 are same as previously defined in Eqs. 3.61 and 3.64.  $n_k$  and  $\bar{n}_k$  are the nucleon and anti-nucleon distribution functions as defined by Eq. 2.48.

The physical mass ( $m_v^*$ ) is defined as the zero of the dielectric function 3.77 in the limit  $\vec{k} \rightarrow 0$ . In this limit, of course, the longitudinal and transversal modes are degenerate. Fig. 3.12 shows the physical mass of the vector mesons as function of temperature for two baryonic densities. We notice a similar behaviour as in the case of the nucleon mass. For completeness, we show in Fig. 3.13 the mass dependence on temperature of the scalar mesons  $a_0$  and  $\sigma$ .

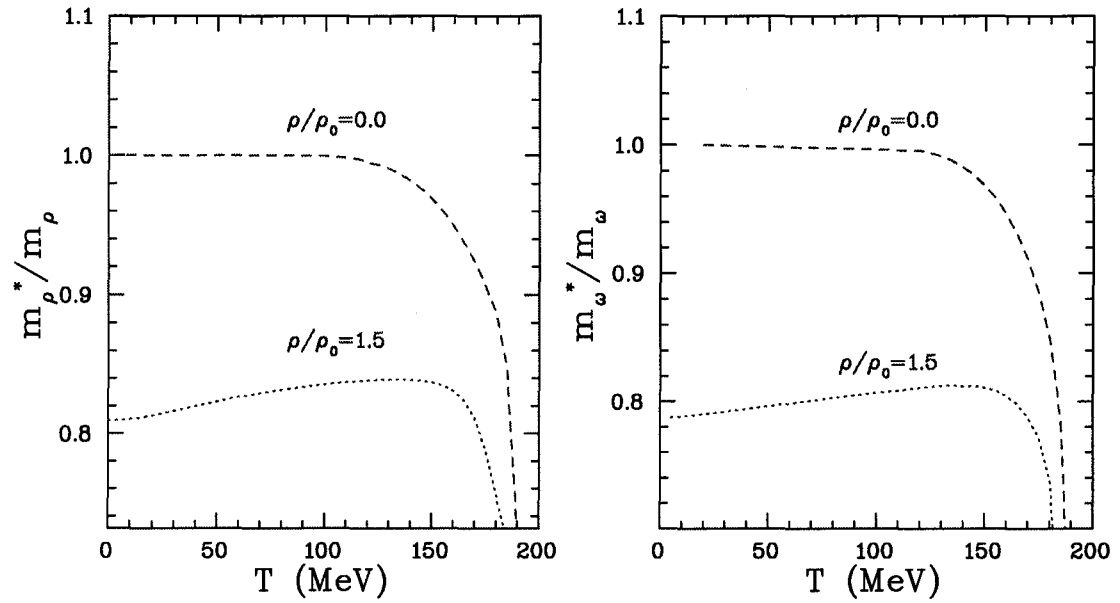


Figure 3.12: Vector meson masses as function of temperature for two baryonic densities.  $\rho$  meson is on the left panel and  $\omega$  on the right one.

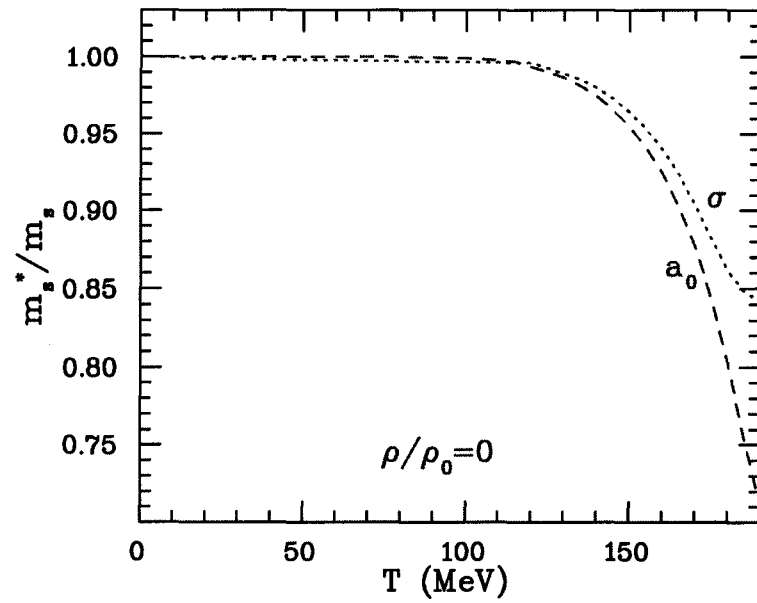
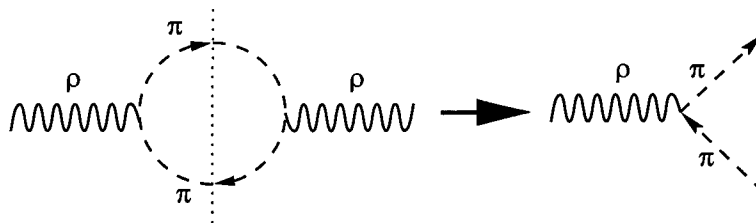


Figure 3.13: Scalar meson ( $a_0$  and  $\sigma$ ) masses as function of temperature.

Figure 3.14: Decay of  $\rho$  meson.

### 3.6.1 Decay Widths Modification at Finite Temperature

In this section we will study the finite temperature effect on the  $\rho$  meson decay width for reasons which will become clear in Chapter 5, where we evaluate the dilepton production from environments at high temperatures. It may be stressed here that the observed dilepton yield in the low invariant mass region is not only sensitive to the in-medium masses of the vector mesons but also depends on the decay widths. The particles having a large decay width are likely to decay mostly in the central region of the collisions while particles having very long life times are not likely to contribute to that part of the spectrum substantially.

More precisely, we will include here the Bose-Einstein effect on the decay width of the  $\rho$  meson. This particle predominantly decays into a pion pair and, therefore, we expect that the finite density of pions at high temperatures to modify  $\rho$  meson decay width. We are not presently concerned with these effects on the decay width of  $\omega$  and  $\phi$ . Because of their small widths, even a modification by a factor of two, will not importantly change the dilepton spectrum except in a limited range around their mass poles. Instead,  $\rho$  has a large decay width, and, a change in its width influences a wide range in the dilepton spectrum.

The decay width can be calculated using the Cutkosky rules at finite temperature [100, 101] which provide a simple and systematic way to calculate the imaginary

part of the self-energy. This is related to the physical decay width as

$$\text{Im}\Pi(k_0) = -k_0\Gamma(k_0) \quad (3.110)$$

where  $k_0$  is the energy of the decaying particle,  $\rho$  in our case. The self-energy function develops cuts along the real axis when the particles in the internal loop become on-mass shell. The discontinuity across these cuts is pure imaginary for real  $k_0$  so that we have

$$\text{Disc}\Pi(k_0) = [\Pi(k_0 + i\epsilon) - \Pi(k_0 - i\epsilon)] = 2i\text{Im}\Pi(k_0) \quad . \quad (3.111)$$

For the  $\rho$  meson, the imaginary part of the self-energy is totally dominated by the pion loop which is borne out by the fact that the two pion decay mode of the  $\rho$  has a branching ratio of  $\sim 100\%$ . In contrast, the real part of the  $\rho$  self-energy which is responsible for the mass modification has a negligible role to play as far as the pion loop is concerned. The  $\rho$ - $\pi$  interaction is described by the Lagrangian

$$\mathcal{L}_{\rho\pi\pi}^{\text{int}} = -g_{\rho\pi\pi}\vec{\rho}^\mu \cdot (\vec{\pi} \times \partial_\mu \vec{\pi}) \quad . \quad (3.112)$$

The self-energy of the  $\rho$  meson due to pion loop (Fig. (3.14)) is given by

$$-i\Pi_{\rho\pi\pi}^{\mu\nu}(k) = -g_{\rho\pi\pi}^2 \int \frac{d^4p}{(2\pi)^4} (2p+k)^\mu i\Delta_{11}^\beta(p) (2p+k)^\nu i\Delta_{11}^\beta(p+k) \quad , \quad (3.113)$$

where the pion propagator is [102]

$$i\Delta_{11}^\beta(q) = \frac{i}{q^2 - m_\pi^2 + i\epsilon} + 2\pi\delta(q^2 - m_\pi^2) \left[ \theta(q_0)f_{BE}(q_0) + \theta(-q_0)f_{BE}(-q_0) \right] \quad .$$

We notice again that we have two distinctive parts in the pion propagator, the free propagator and the last part which accounts for the in-medium effects. Consequently, the  $\rho$  self-energy also has two distinctive contributions in a similar fashion as we had for the nucleon loop in Sec. 3.3. The vacuum part of the self-energy arises when the off-shell parts of the two pion propagators contribute. Its correspondent imaginary part in the rest frame of  $\rho$  ( $\vec{k} = 0$ ) is given by [103]

$$\text{Im}\Pi_{\rho\pi\pi}^{\text{F}}(k_0) = -\frac{g_{\rho\pi\pi}^2}{48\pi k_0} (k_0^2 - 4m_\pi^2)^{3/2} \quad . \quad (3.114)$$

The other terms involving the on-shell propagator gives the in-medium contribution. Straightforward calculation in the rest frame gives the following imaginary part:

$$\text{Im}\Pi_{\rho\pi\pi}^{\text{D}}(k_0) = -\frac{g_{\rho\pi\pi}^2}{48\pi k_0}(k_0^2 - 4m_\pi^2)^{3/2} 2f_{BE}\left(\frac{k_0}{2}\right) \quad (3.115)$$

where  $\Pi(k_0) = \Pi_\mu^\mu(k_0, \vec{k} = 0)/3$ . On addition we have

$$\text{Im}\Pi_{\rho\pi\pi}(k_0) = -\frac{g_{\rho\pi\pi}^2}{48\pi k_0}(k_0^2 - 4m_\pi^2)^{3/2} \left[ 2f_{BE}\left(\frac{k_0}{2}\right) + 1 \right] \quad (3.116)$$

Using Eq. (3.110) the  $\rho$  decay width is obtained as

$$\Gamma_\rho(k_0) = \frac{g_{\rho\pi\pi}^2}{48\pi} \frac{(k_0^2 - 4m_\pi^2)^{3/2}}{k_0^2} \left[ \left(1 + f_{BE}\left(\frac{k_0}{2}\right)\right) \left(1 + f_{BE}\left(\frac{k_0}{2}\right)\right) - f_{BE}\left(\frac{k_0}{2}\right)f_{BE}\left(\frac{k_0}{2}\right) \right] \quad (3.117)$$

with the Bose-Einstein distribution function  $f_{BE}(x) = [e^x - 1]^{-1}$ . It is interesting to note that the phase space factor  $(2f_{BE} + 1)$  when written in this form clearly shows that the in-medium width is actually the difference between the rates of decay and formation of the resonance. Fig. 3.15 presents the  $\rho$  meson decay width as function of temperature for two baryonic densities. The decay width of the vector meson present the same feature as in the case of meson mass due to the correspondent modification of the phase space: for a higher  $\rho$  mass, the phase space correspondent to the decay into two pions is larger as well.

## Summary

In the present chapter we have investigated the modification of vector and scalar mesons properties in nuclear matter by studying the collective modes corresponding to density fluctuations. We have shown that the collective modes, in the present relativistic many-body system, can be characterized as poles in the meson propagator. We have presented the modified dispersion curves and the invariant mass dependence

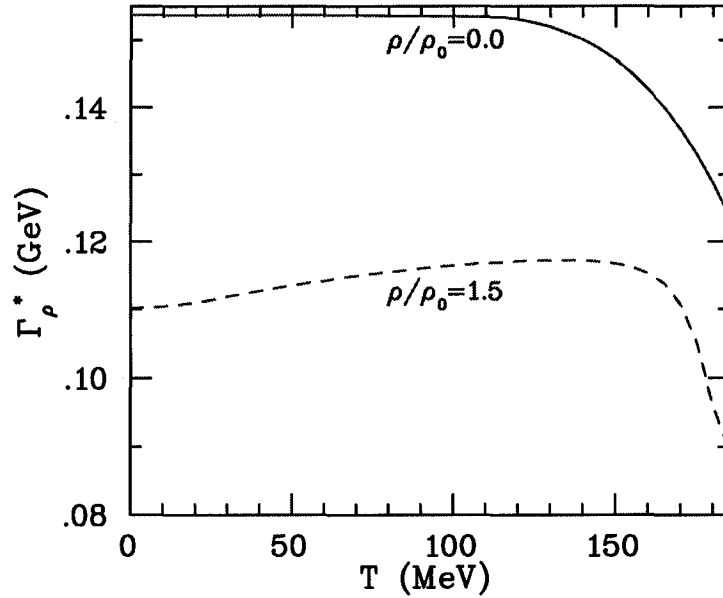


Figure 3.15: The  $\rho \rightarrow \pi\pi$  decay width as a function of temperature for different values of baryon densities.

on baryonic density. In our relativistic mean field model, we find that vector meson masses drop from their vacuum values at finite density. We extensively studied the scalar-vector mixing effect on the collective excitations, and a new mode,  $\rho$ - $a_0$  mixing, has been uncovered. We also addressed issues like the temperature modifications on the vector meson mass and decay width. It has been shown that the vector mesons mass,  $\rho$  and  $\omega$ , have the same qualitative temperature dependence as the nucleons: a slight increase for low temperatures followed by a steep drop above temperatures of about 150 MeV. It should be mentioned here that the mass of  $\phi$  meson has been treated elsewhere, and it has been shown that it changes only slightly in a hot hadronic gas [104, 105].

---



---

## DILEPTON PRODUCTION FROM THERMAL MESONS

---



---

The experimentally measured dilepton spectra can be chronologically divided into several phases. Before the nuclear surfaces actually touch dileptons are produced through coherent bremsstrahlung [106] in the decelerating Coulomb field of the approaching nuclei. Their contribution is concentrated at low  $p_T$  and negligible for our purposes as compared to subsequent sources [107, 108]. Before the first 1 fm/c or so of the nuclear interaction, the excited hadronic system is far from thermal equilibrium and the corresponding ‘pre-equilibrium’ dilepton radiation mostly consists of hard processes such as Drell-Yan annihilation [109], leaving its trace mainly at large invariant masses  $M_{ll} > 3$  GeV [110]. A rapid thermalization [111] is expected to subsequently establish the QGP phase, sometimes also called the ‘partonic phase’, where dilepton production proceeds predominantly via (perturbative) quark-antiquark annihilation or other thermal processes [29]. It should reflect a thermal spectrum even though, towards smaller masses, radiative corrections from gluons as well as thermal loop effects are likely to become important [112, 113]. At later stages when, upon expansion and cooling, the QGP has converted into a hot hadron gas, dileptons are preferentially radiated from pion and kaon annihilation processes as well as other collisions between various hadrons. The two-body annihilation processes are dynamically enhanced through the formation of (light) vector meson resonances, such as the  $\rho$ ,  $\omega$  and  $\phi$  mesons, which directly couple to  $l^+l^-$  pairs. Thus the invariant mass of the

lepton pair directly reflects the mass distribution of the vector meson at the moment of decay. This explains the distinguished role that vector mesons – in conjunction with their in-medium modifications – play for dilepton measurements in heavy-ion reactions. The situation is somewhat different for the heavy quarkonium states such as the  $J/\Psi$ : in contrast to the light vector mesons, their lifetime is substantially longer than the typical one of the hadronic fireball such that they will predominantly decay after freezeout, and therefore, the in-medium modifications are less important [114]. In the invariant mass region, the dileptons from correlated decays of “open charm” mesons  $D\bar{D}$  [115], pairwise produced followed by individual semileptonic decays, have a dominant contribution just below about 2 GeV in the invariant mass spectrum. Finally, when the freezeout stage is reached, the dominant sources are hadronic resonance as well as Dalitz decays, mostly from  $\pi^0$ ,  $\eta$  and  $\omega$  mesons, all feeding into the low-mass region,  $M_{ll} < 1$  GeV [116, 117]. A schematic view of characteristic dilepton sources in ultra-relativistic heavy-ion collisions is given in Fig. 4.1.

As we mentioned before, we are mainly interested in the low mass region and around 1 GeV. We will focus on the dilepton sources from thermal meson collisions which we will see that dominates the spectrum in this region at invariant masses above about 0.5 GeV in nucleus-nucleus collision experiments. As several hundreds of pions are produced in these collisions, we expect a large contribution from  $\pi^+\pi^- \rightarrow e^+e^-$  annihilation during the interacting phase of the hadronic fireball.

The central subject of the present chapter and the next one is to study the possible non-conventional sources which arise as consequence of meson mixing effects, discussed in chapter 3, and to compare them with the known sources. In order to proceed further we need to model the coupling of the hadron current to a virtual photon which ultimately decays into a lepton pair.

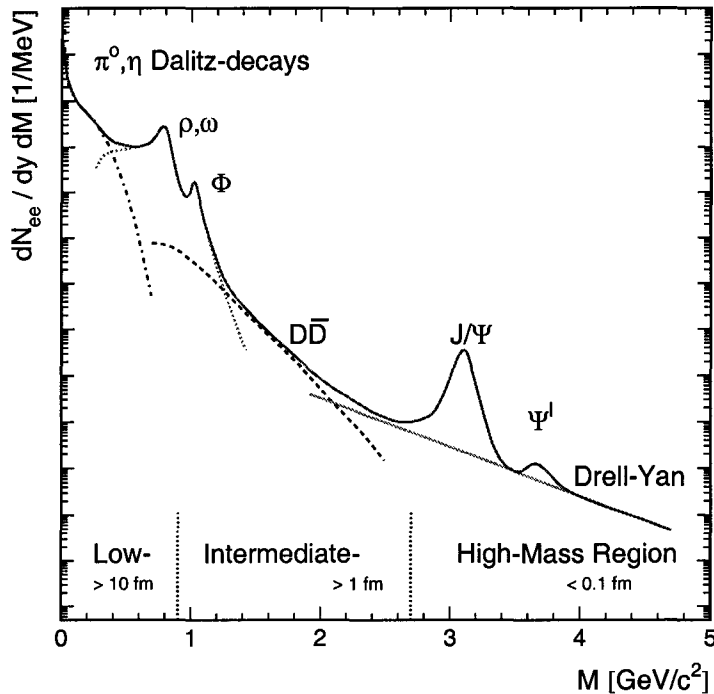


Figure 4.1: Schematic diagram showing the different contributions to the total dilepton yield in an ultra-relativistic heavy ion collision [40, 21].

## 4.1 Vector Meson Dominance

The Vector Meson Dominance (VMD) was born as an attempt of J. J. Sakurai to model strong interactions as a gauge theory where vector mesons  $\rho$ ,  $\omega$  and  $\phi$  played the role of gauge bosons [81, 118]. This model, at a phenomenological level, has been very successful in the areas of hadronic form factors, photoabsorption and absorption cross sections, and in the vector meson exchange contribution to  $\pi N$  and  $NN$  scattering [119]. In fact both isoscalar and isovector vector mesons were predicted in late fifties from a study of the nucleon form factors [120].

The VMD content of interest to us is the connection to the interaction of a virtual photon to a hadron. VMD asserts that a virtual photon converts to a neutral vector



Figure 4.2: The Feynman diagram for the process  $\pi + \pi \rightarrow e^+ + e^-$ .

meson first then couples to the hadron as shown in Fig. 4.2 for the  $\pi$ - $\pi$  annihilation to dileptons,  $\rho$  being the neutral meson in this case. To accommodate such an hypothesis within a theoretical framework, it is necessary to have an interaction term in the Lagrangian that allows a photon to be annihilated and a vector meson created, or vice versa. The interaction Lagrangian will have the form

$$\mathcal{L}_{int} = \gamma_v V_\mu A^\mu \quad (4.1)$$

where  $\gamma_v$  is a coupling constant. The problem with 4.1 is that it is not gauge invariant as  $A_\mu \rightarrow A_\mu - \partial\phi$ . However, it was shown [121] that this kind of interaction could be included in a gauge invariant theory involving the photon and the  $\rho$  meson if we have the so called *current-field identity*

$$ej_\mu^a = -\gamma_\rho \rho_\mu^a \quad (4.2)$$

where  $a$  is the isospin indices.

In order to define the electromagnetic form factor we redraw the diagram 4.2. All the strong interaction effects at the  $\gamma^*\pi\pi$  vertex are represented by the black square box in Fig. 4.3 denoting the electromagnetic structure of the pion. Of course, the amplitudes of these diagrams could be equated. We evaluate them using Feynman rules and get by omitting the common current factors

$$e \frac{1}{q^2} \gamma_\rho \frac{1}{m_\rho^2 - q^2 + im_\rho \Gamma_\rho} g_{\rho\pi\pi} = e \frac{1}{q^2} eF_\pi(q^2)$$

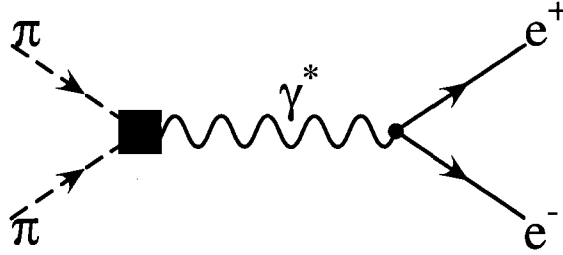


Figure 4.3: Pion annihilation into dilepton.

$$eF_\pi(q^2) = \frac{\gamma_\rho g_{\rho\pi\pi}}{m_\rho^2 - q^2 + im_\rho\Gamma_\rho} \quad . \quad (4.3)$$

A real photon with  $q^2 = 0$  must see a charge  $e$  of the  $\pi^+$ -meson and, therefore,

$$F_\pi(0) = 1 \quad . \quad (4.4)$$

Combining the above equations and assuming universality ( $g_\rho = g_{\rho\pi\pi}$ ) we get

$$\gamma_\rho = \frac{em_\rho^2}{g_\rho} \quad . \quad (4.5)$$

The same applies for  $\omega$  and  $\phi$ . We could express now hadronic electromagnetic current by the *current field identity*

$$J_\mu = -\frac{em_\rho^2}{g_\rho}\rho_\mu - \frac{em_\omega^2}{g_\omega}\omega_\mu - \frac{em_\phi^2}{g_\phi}\phi_\mu \quad . \quad (4.6)$$

The couplings,  $g_\rho, g_\omega, g_\phi$  can be determined from the vector meson decay widths into

Table 4.1: VMD couplings

Vector meson	$\Gamma_{V \rightarrow e^+e^-}$ (KeV)	$g_V$
$\rho$	6.7	5.5
$\omega$	0.6	17.0
$\phi$	1.37	12.9

dileptons:

$$\Gamma_{V \rightarrow e^+e^-} = \frac{4\pi}{3} \left(\frac{\alpha}{g_v}\right)^2 \frac{p_{e^\pm}^3}{m_v^2} \quad (4.7)$$

$$p_{e^\pm} = \sqrt{m_v^2 - 4m_e^2}$$

and we get the values in table 4.1

Before we start the evaluation of some of the dilepton sources produced through thermal meson collisions in VMD model, it is proper to introduce first the notion of thermal rate of dilepton production and then focus on the formalism of two meson collisions.

## 4.2 Thermal Rates of Dilepton Production

If we consider a hot hadron gas at a given temperature, the rate of the thermal lepton pair production is defined as the number of reactions per unit time, per unit volume

$$R^{e^+e^-} = dN^{e^+e^- \text{ pairs}} / d^4x \quad . \quad (4.8)$$

Therefore we can write this as the summation of the transition amplitude  $\mathcal{M}_{i \rightarrow f}$  over the final states and thermally averaged over initial states. In other words

$$R^{e^+e^-} = \prod_i \int d^4k_i f_{a_i}(k_i) \int d^4p_+ \int d^4p_- \prod_f \int d^4p_{b_f} \quad (4.9)$$

$$|\mathcal{M}_{a_1 a_2 \dots \rightarrow e^+ e^- b_1 b_2 \dots}|^2 \delta(\sum_i p_i - \sum_f p_f - p_+ - p_-)$$

where  $f_{a_i}(k_i)$  is the thermal distribution of the initial particles.

Next, a short review of the connection between the thermal dilepton rate of production and the photon self-energy is presented. Later, it is also shown in VMD model, how this relates to the imaginary part of the vector meson self-energy.

Let's assume a process of the form  $i \rightarrow f e^+ e^-$  where there is a hadron in the initial state and a hadron and a pair of dileptons in the final state. The hadron current  $j_\mu$

is coupled to the leptonic current through a photon. Following the Feynman rules for such process [58] we get for the following transition amplitude of the process

$$S_{fi}(k_1, k_2) = -\frac{ie}{q^2} \bar{u}(\mathbf{k}_1) \gamma^\mu v(\mathbf{k}_2) \int d^4x e^{iq \cdot x} \langle f | j_\mu(x) | i \rangle \quad . \quad (4.10)$$

The matrix element of the process can be written after the summation over the final spin states as

$$\begin{aligned} |\mathcal{M}_{fi}|^2 &= S_{fi}^\dagger S_{fi} \\ |\mathcal{M}_{fi}|^2 &= \frac{e^4}{q^4} l_{\mu\nu} \int d^4y e^{-iq \cdot y} \langle i | j^\mu(y) | f \rangle \int d^4x e^{iq \cdot x} \langle f | j^\nu(x) | i \rangle \end{aligned} \quad (4.11)$$

where [58]

$$l_{\mu\nu} = \sum_{spins} [\bar{u}(\mathbf{k}_1) \gamma^\mu v(\mathbf{k}_2)]^\dagger [\bar{u}(\mathbf{k}_1) \gamma^\nu v(\mathbf{k}_2)] = 4[k_{1\mu} k_{2\nu} + k_{1\nu} k_{2\mu} - (p_1 \cdot p_2) g_{\mu\nu}] \quad . \quad (4.12)$$

In order to obtain the rate of production one has to average over the initial states with the thermal weight  $\frac{e^{-\beta K_i}}{\mathcal{Z}}$ ,  $\mathcal{Z} = \sum_i e^{-\beta K_i}$ ,  $\hat{K} = \mathcal{H} - \mu \hat{N}$  and sum over final states

$$\begin{aligned} R^{e^+e^-} &= \frac{e^2}{q^4} \int \frac{d^3k_1}{2E_1(2\pi^3)} \int \frac{d^3k_2}{2E_2(2\pi^3)} l_{\mu\nu} \\ &\times \sum_i \frac{e^{-\beta K_i}}{\mathcal{Z}} \sum_f \int d^4y e^{-iq \cdot y} \langle i | j^\mu(y) | f \rangle \int d^4x e^{iq \cdot x} \langle f | j^\nu(x) | i \rangle \quad . \end{aligned} \quad (4.13)$$

By applying translation invariance, *i.e.*,

$$\langle f | j^\nu(y) | i \rangle = e^{i(p_i - p_f) \cdot y} \langle f | j^\nu(0) | i \rangle \quad , \quad (4.14)$$

and, after the integration over  $y$  coordinates, the thermal rate of dilepton production takes the form

$$R^{e^+e^-} = \frac{e^4}{(2\pi)^4 q^4} L_{\mu\nu} \sum_i \frac{e^{-\beta K_i}}{\mathcal{Z}} \sum_f \int d^4x e^{iq \cdot x} \langle i | j^\mu(0) | f \rangle \langle f | j^\nu(x) | i \rangle \quad (4.15)$$

where we denote

$$L_{\mu\nu} = \int \frac{d^3k_1}{2E_1(2\pi)^3} \int \frac{d^3k_2}{2E_2(2\pi)^3} (2\pi)^4 \delta^4(Q - k_1 - k_2) l_{\mu\nu} = \frac{1}{6\pi} (Q_{\mu\nu} - q^2 g_{\mu\nu}) \quad (4.16)$$

and  $q = p_i - p_f$ . Performing the summation over the final hadron states one gets

$$R^{e^+e^-} = \frac{dN^{e^+e^-}}{d^4x} = \frac{e^4}{(2\pi)^4 q^4} \Pi^{<\mu\nu} L_{\mu\nu} \quad (4.17)$$

where the  $\Pi^{<>}$  functions are defined as

$$\begin{aligned} \Pi^{<\mu\nu}(q) &= \sum_i \frac{e^{-\beta K_i}}{\mathcal{Z}} \int d^4x e^{iq \cdot x} \langle i | j^\mu(0) j^\nu(x) | i \rangle \\ \Pi^{>\mu\nu}(q) &= \sum_i \frac{e^{-\beta K_i}}{\mathcal{Z}} \int d^4x e^{iq \cdot x} \langle i | j^\mu(x) j^\nu(0) | i \rangle \quad . \end{aligned}$$

Following [122], we can represent the imaginary part of the photon self-energy as

$$Im \Pi_{\mu\nu}(q) = \Pi_{\mu\nu}^{>}(q) - \Pi_{\mu\nu}^{<}(q) \quad (4.18)$$

where there is the following relationship (see appendix B)

$$\Pi_{\mu\nu}^{>}(q) = e^{\beta q_0} \Pi_{\mu\nu}^{<}(q) \quad . \quad (4.19)$$

We finally get the following relationship between the dilepton rate and the imaginary part of the photon self-energy

$$R^{e^+e^-} = \frac{e^2}{(2\pi)^4 q^4} \frac{Im \Pi^{\mu\nu}(q)}{e^{\beta\omega} - 1} L_{\mu\nu} \quad . \quad (4.20)$$

In VMD model described in sec. 4.1 the hadronic electromagnetic current operator is given in the *current field identity* (eq. 4.6)

$$\hat{J}_\mu = -\frac{e}{g_\rho} m_\rho^2 \hat{\rho}_\mu - \frac{e}{g_\phi} m_\phi^2 \hat{\phi}_\mu - \frac{e}{g_\omega} m_\omega^2 \hat{\omega}_\mu \quad . \quad (4.21)$$

The couplings could be evaluated from the partial decay widths into dileptons for the three particles in VMD model (Sec. 4.1). As discussed in Ref. [123] the main contribution comes from the first term and, therefore, the imaginary part of the self-energy it is simply proportional to the imaginary part of the  $\rho$ -propagator. One can

therefore prove the following relationship for the dilepton rate as function of the  $\rho$  propagator

$$R^{e^+e^-} = \frac{e^4 m_\rho^4}{(2\pi)^4 g_\rho^2 q^4} \frac{-Im \mathcal{D}_\rho^{\mu\nu}(q)}{e^{\beta\omega} - 1} L_{\mu\nu} \quad (4.22)$$

where the  $\rho$ -propagator is

$$\mathcal{D}_\rho^{\mu\nu}(q) = \sum_i \frac{e^{-\beta K_i}}{\mathcal{Z}} \int d^4x e^{iq \cdot x} \langle i | T[\hat{\rho}^\mu(x) \hat{\rho}^\nu(0)] | i \rangle \quad . \quad (4.23)$$

Therefore, a complete calculation of the  $\rho$  meson spectral density, provides complete information on the various hadronic processes having a lepton pair in the final state. However, at the one loop level, the evaluation of dilepton yields from processes of the type  $a \rightarrow be^+e^-$ ,  $ab \rightarrow ce^+e^-$  or, more interesting for us  $ab \rightarrow e^+e^-$ , can be readily computed in relativistic kinetic calculations. Because the general field-theoretic treatment presented above agrees to a large extent with the latter approach, the results being identical at one loop level [123], we use kinetic theory in the present calculations. In the next section, we develop the formalism for  $ab \rightarrow e^+e^-$ , a reaction of particular interest in the present study as it will become clear later.

### 4.3 Production from Processes $ab \rightarrow e^+e^-$

The rate production can be estimated in the independent particle approximation of kinetic theory for the process  $ab \rightarrow e^+e^-$  as [124, 125]

$$\begin{aligned} dR_{12}^{e^+e^-} &= \int dM^2 \int \frac{d^3k_1}{(2\pi)^3} f_1(\mathbf{k}_1) \int \frac{d^3k_2}{(2\pi)^3} f_2(\mathbf{k}_2) \int d^4p_+ \int d^4p_- \quad (4.24) \\ &\times |\mathcal{M}_{ab \rightarrow e^+e^-}|^2 \delta[M^2 - (p_+ + p_-)^2] \delta(k_1 + k_2 - p_+ - p_-) \quad . \end{aligned}$$

If we know the cross section of the process, the differential rate of dilepton production can be written as

$$\frac{dR_{12}^{e^+e^-}}{dM^2} = \int \frac{d^3k_1}{(2\pi)^3} f_1(\mathbf{k}_1) \int \frac{d^3k_2}{(2\pi)^3} f_2(\mathbf{k}_2) \frac{d\sigma_{12}^{e^+e^-}}{dM^2}(s, M^2) v_{rel} \quad (4.25)$$

where  $f_1, f_2$  are the thermal distributions of the 1,2 species and the relative speed is

$$\begin{aligned} v_{rel} &= \frac{\vec{p}_1}{E_1} - \frac{\vec{p}_2}{E_2} \\ &= \frac{\lambda^{1/2}(s, m_1^2, m_2^2)}{2E_1E_2} \end{aligned} \quad (4.26)$$

and  $\lambda(x, y, z) = x^2 + y^2 + z^2 - 2xy - 2xz - 2yz$  is the triangle function. This can be cast into the form:

$$\frac{dR_{12}^{e^+e^-}}{dM^2} = \frac{\lambda^{1/2}(M^2, m_1^2, m_2^2)}{2} \Phi(s) \quad (4.27)$$

$$\Phi(s) = \int \prod_{i=1,2} \frac{d^3p_i f_i(E_i)}{(2\pi)^3 E_i} \delta[s - (p_1 + p_2)^2] \sigma_{12}^{e^+e^-}(E_1, E_2, M^2) \quad (4.28)$$

where  $f_i(E_i) = \frac{1}{e^{\beta E_i} + 1}$  are the distribution functions for  $\pi$  and  $\eta$  mesons assuming thermal equilibrium. A departure from the standard notation should be noticed here. Usually,  $\Phi(s)$  represents only the phase space factor [125]. In our case, the invariant mass cross-section also depends on the particle energies through  $\Pi_0$  and we include that in the definition of  $\Phi(s)$ .

After performing the angular integrations we get

$$\Phi(s) = \frac{1}{(2\pi)^4} \int_{m_1}^{\infty} dE_1 f_1(E_1) \int_{E_2^-}^{E_2^+} dE_2 f_2(E_2) \sigma_{12}^{e^+e^-}(E_1, E_2, M^2) \quad (4.29)$$

where  $E_2^{\pm} = \frac{1}{2m_1^2} [E_1(s - m_1^2 - m_2^2) \pm p_1 \lambda^{1/2}(s, m_1^2, m_2^2)]$ .  $\Phi(s)$  is then calculated numerically.

#### 4.4 Dominant Dilepton Sources in the Low Invariant Mass Range

In this section we will refer only to the most important dilepton sources in the invariant mass range  $M = 0.5 - 1.2$  GeV. We limit ourselves to the lepton pairs from

thermal mesons produced in collisions through processes  $a+b \rightarrow e^+e^-$ . There are two main sources contributing in this mass region:  $\pi\text{-}\pi$  annihilation and  $K\bar{K}$ ,  $K^+K^-$  annihilation [124, 125]. The rate production for this processes can be evaluated by using Eqs. [4.27-4.29]. As discussed in the VMD model, the pion annihilation into dileptons proceeds through the  $\rho$  meson as intermediate state. For the cross section corresponding to the process  $\pi\pi \rightarrow e^+e^-$ , one can evaluate the Feynman diagram (Fig. 4.2) and gets the following expression

$$\sigma_{\pi\pi \rightarrow \rho \rightarrow e^+e^-}(M) = \frac{4\pi\alpha^2}{3} \left( \frac{g_{\rho\pi\pi}}{g_\rho} \right)^2 \frac{m_\rho^4}{(M^2 - m_\rho^2)^2 + m_\rho^2\Gamma_\rho^2(M)} \frac{\sqrt{M^2 - 4m_\pi^2}}{M^3} . \quad (4.30)$$

For the strange meson annihilation into dileptons ( $K\bar{K}$ ,  $K^+K^- \rightarrow e^+e^-$ ), the intermediate state is the  $\phi$  meson. We get the following cross section

$$\sigma_{K\bar{K} \rightarrow \phi \rightarrow e^+e^-}(M) = \frac{4\pi\alpha^2}{3} \frac{g_{\phi K\bar{K}}^2}{g_\phi^2} \frac{m_\phi^4}{(M^2 - m_\phi^2)^2 + m_\phi^2\Gamma_\phi^2(M)} \frac{\sqrt{M^2 - 4m_K^2}}{M^3} \quad (4.31)$$

$$\Gamma_\phi(M) = \frac{1}{6\pi} g_{\phi K\bar{K}}^2 \frac{(m_\phi^2/4 - m_K^2)^{3/2}}{M^2} \quad (4.32)$$

where the currently used mass values of the mesons are presented in the introduction. The couplings,  $g_{\phi K\bar{K}}=5.8$  and  $g_{\phi K^+K^-}=4.5$ , are fitted to reproduce the free decay widths  $\Gamma_{\phi K\bar{K}}=1.5$  MeV and  $\Gamma_{\phi K^+K^-}=2.2$  MeV as quoted in Ref. [51].

We present in Fig 4.4 the dilepton spectrum created by these two channels for two temperatures  $T = 50$  MeV and  $T = 150$  MeV. We see that the second is in agreement with [125].

## 4.5 Thermal Dileptons Produced Through Meson Mixing

In chapter 3 we have already discussed the possibility of scalar-vector meson mixing in nuclear matter. We will show in this section that these mixing could open some new dilepton channels [48]. Of course these are pure density-dependent effects. Thus these channels could become important when there is a high baryonic density. Such

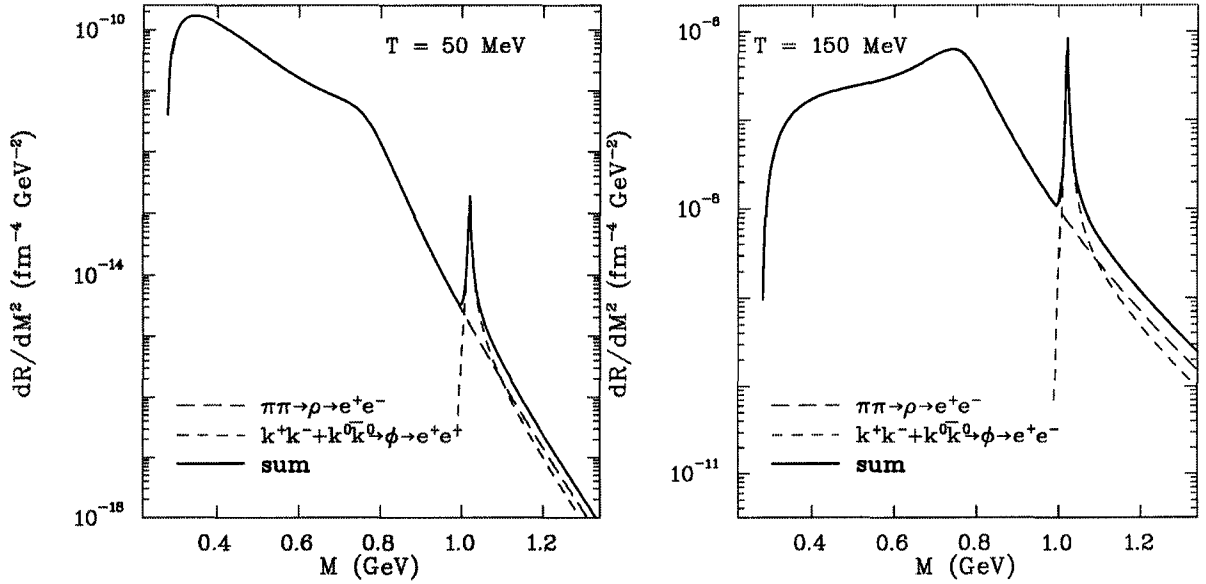


Figure 4.4: The dominant thermal dilepton channels in the invariant mass range  $M = 0.5 - 1.2$  GeV.

dense nuclear matter is very likely to be achieved in heavy ion collisions. For instance, the initial baryonic density is predicted to be  $\rho_B^i \approx 2.5\rho_0$  by transport calculations (RQMD [126]) for  $S+Au$  collisions (200 GeV/u) produced at CERN. These results are in good agreement with studies in other models [33]. A even higher initial baryonic density,  $\rho_B^i \approx 4\rho_0$  was calculated by these groups for central collisions  $Pb+Au$  (158 GeV/u).

The present finite temperature estimations will consider the free spectral functions. However, in chapter 5 we will also estimate the dilepton production by considering in-medium effects on the meson masses.

#### 4.5.1 Isovector Channel Mediated by $\rho$ - $a_0$ Mixing

Next, we discuss the process mediated by the mixing of isovector meson  $\rho$  with the isoscalar  $a_0$  which opens up a new channel *viz*  $\pi + \eta \rightarrow e^+ + e^-$  in dense nuclear matter through n-n excitations. The Feynman diagram of the process is depicted in

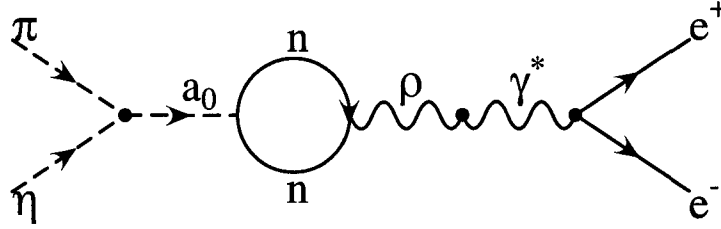


Figure 4.5: The Feynman diagram for the process  $\pi + \eta \rightarrow e^+ + e^-$ .

Fig. 4.5.

To describe the  $\pi a_0 \eta$  vertex we use [48]

$$\mathcal{L}_{a_0 \pi \eta} = f_{a_0 \pi \eta} \frac{m_{a_0}^2 - m_\eta^2}{m_\pi} \phi_\eta \vec{\phi}_\pi \cdot \vec{\phi}_{a_0} \quad . \quad (4.33)$$

For later convenience we define  $g_{\pi a_0 \eta} = f_{a_0 \pi \eta} (m_{a_0}^2 - m_\eta^2) / m_\pi$ . It should be noted here that this coupling has mass dimension.

We should also mention here that there is an uncertainty involved with the coupling parameter  $f_{a_0 \pi \eta}$  as discussed in Refs. [127, 51]. This arises from the fact that  $a_0$  lies close to the opening of the  $K\bar{K}$  channel leading to a cusp-like behavior in the resonant amplitude, therefore a naive Breit-Wigner form for the decay width is inadequate. Furthermore, as mentioned before, there is also uncertainty involved with the  $a_0$ NN coupling which renders the precise extraction of  $a_0$ - $\pi$ - $\eta$  coupling even more difficult [127]. We take  $f_{a_0 \pi \eta} = 0.44$  [127] which gives  $\Gamma_{a_0 \rightarrow \pi \eta}(m_{a_0}) = 59$  MeV, while the experimental vacuum width of  $a_0$  is between 50 – 100 MeV [51].

The zero temperature cross-section involving mixing in the isovector channel can be written in terms of momentum-dependent mixing amplitude (Eq. 3.95):

$$\sigma_{\pi \eta \rightarrow e^+ e^-}(M, |\vec{q}|) = \frac{2\pi\alpha^2}{3q_z^2 M} \frac{g_{a_0 \pi \eta}^2}{g_\rho^2} \frac{F_\rho(M^2) G_{a_0}(M^2)}{k_{a_0}} |\Pi_0(M, |\vec{q}|)|^2$$

where

$$F_\rho(M^2) = \frac{m_\rho^4}{(M^2 - m_\rho^2)^2 + m_\rho^2 \Gamma_\rho^2(M)} \quad G_{a_0}(M^2) = \frac{1}{(M^2 - m_{a_0}^2)^2 + m_{a_0}^2 \Gamma_{a_0}^2(M)} .$$

The decay width of the  $\rho$  meson is given by Eq. 3.117 and the decay width of the  $a_0$  meson is:

$$\Gamma_{a_0}(M) = \frac{f_{a_0\pi\eta}^2}{8\pi} \left( \frac{m_{a_0}^2 - m_\eta^2}{m_\pi} \right)^2 \frac{\mathbf{k}_{a_0}}{M^2} \quad (4.34)$$

$$\mathbf{k}_{a_0} = \frac{\sqrt{(M^2 - (m_\pi + m_\eta)^2)(M^2 - (m_\pi - m_\eta)^2)}}{2M} .$$

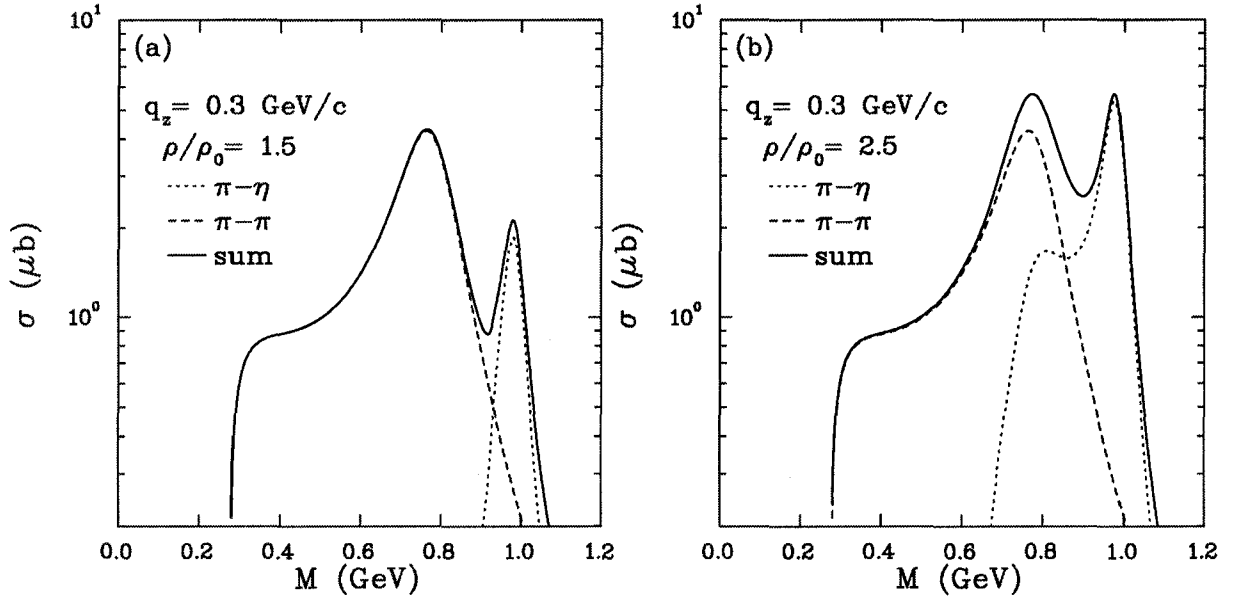


Figure 4.6: Dilepton spectrum of  $\pi + \eta \rightarrow e^+ + e^-$  considering matter induced  $\rho - a_0$  mixing and the direct channel

We compare our new channel with  $\pi - \pi$  annihilation into lepton pairs, a dominant channel in this invariant mass region [125]. The  $\pi + \pi \rightarrow e^+ + e^-$  cross section was presented in Eq. 4.30.

One can notice in Fig. 4.6 that the process,  $\pi + \eta \rightarrow e^+ + e^-$ , at densities higher than  $\rho_0$ , not only enhances the overall production of lepton pairs but also induces an additional peak near the  $\phi$  mass region. The contribution at the  $a_0$  mass is comparable to that of  $\pi + \pi \rightarrow e^+ + e^-$  near the  $\rho$  peak, for densities higher than  $\rho_0$ . Fig. 4.6 also shows that as the density goes higher the dilepton yield arising out of the mixing also increases further.

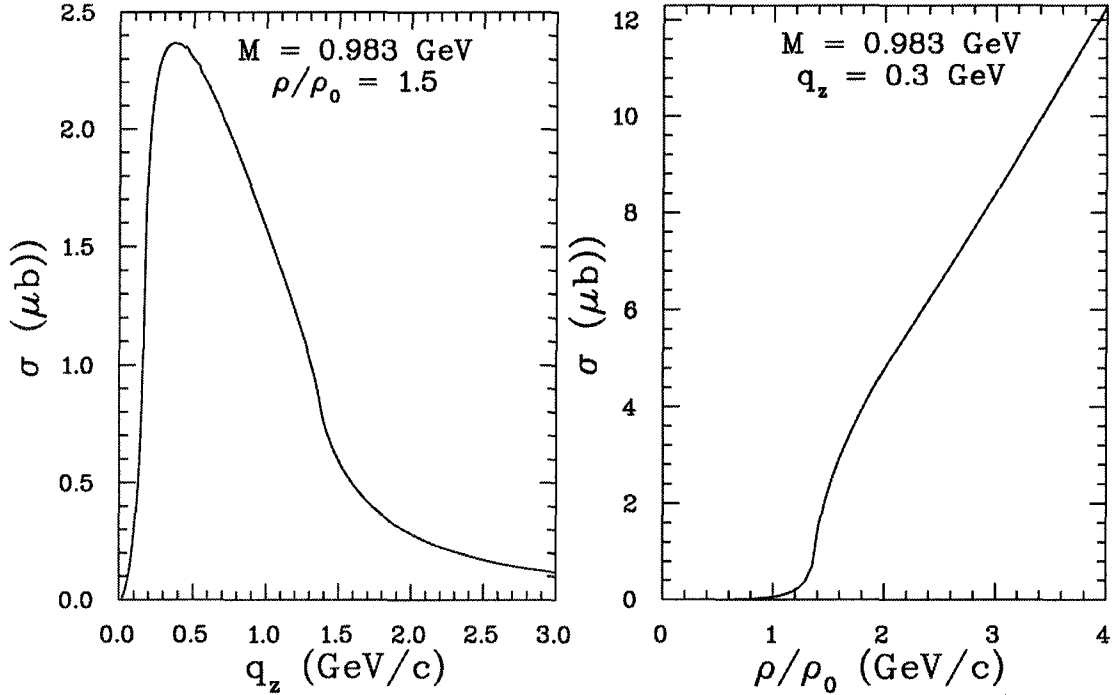


Figure 4.7: Cross section of  $\pi + \eta \rightarrow e^+ + e^-$  as function of momentum and density for  $M = 0.983$  GeV

In the left-hand side of fig. 4.7 we see the cross section of  $\pi + \eta \rightarrow e^+ + e^-$  mediated by  $\rho$ - $a_0$  mixing as function of momentum for the invariant mass  $M = 0.983$  GeV. We see that the cross-section increases with increasing momenta of the mesons in keeping with the mixing angle as shown in fig. 3.11. We also can notice that the cross section has a steep increase for densities higher than normal nuclear matter density. It is proper to point out that the effect of mixing disappear at zero baryonic density,

expected since this is a pure density-dependent effect forbidden in vacuum on account of the Lorentz symmetry.

Next, we discuss the effect of mixing in the isovector channel at finite temperature and density [49]. We show in Fig. 4.8 the  $\rho$ - $a_0$  mixing effect on the thermal rates of dilepton production at a temperature of  $T = 50$  MeV. This induces again the  $a_0$  bump just below the  $\phi$  peak.  $\rho$ - $a_0$  channel seems to be important since it induces additional contribution beyond the tail of  $\rho$  spectral function. One can easily observe from Fig. 4.8 that even at density  $\rho/\rho_0 = 1.5$  the contribution of the mixing wins over the  $\pi$ - $\pi$  annihilation rate in the vicinity of  $M = 1.0$  GeV. Naturally at higher density this goes up as evident from the right panel of Fig. 4.8.

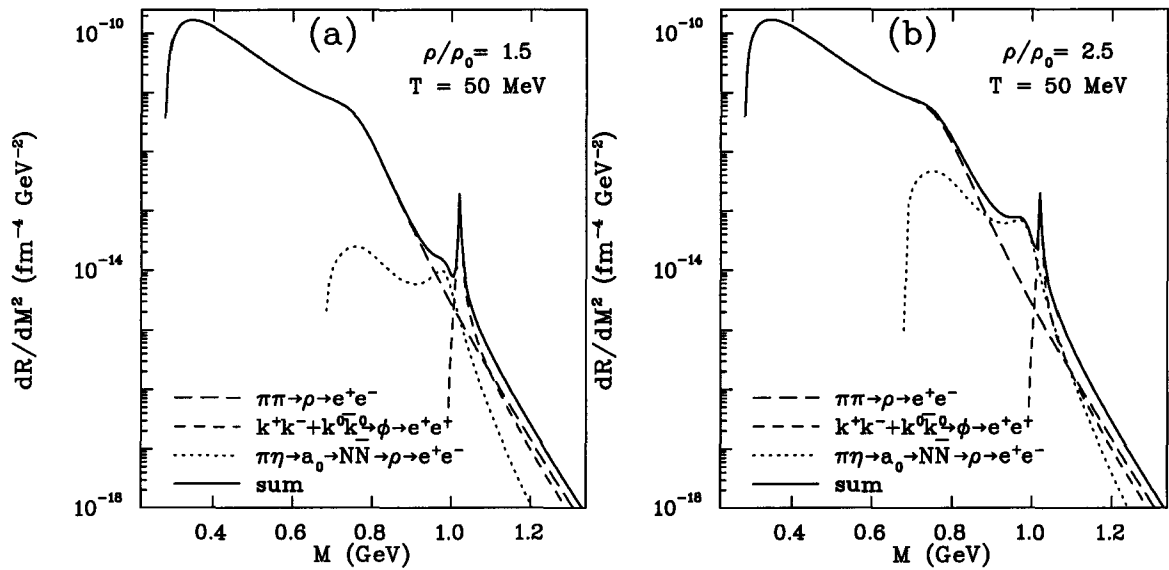
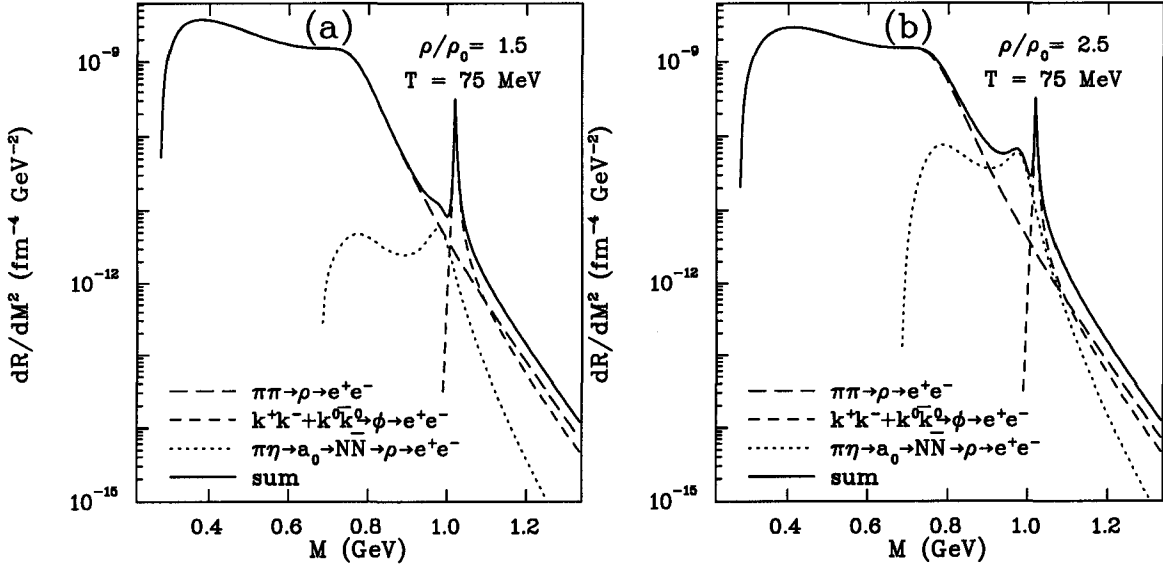


Figure 4.8: Effect of mixing on dilepton production rate in the isovector channel involving  $\rho$ - $a_0$  mixing at  $T=50$  MeV.

The dilepton yield induced by this mixing effect mixing presents the same features at a higher temperature of 75 MeV as appears in Fig. 4.9.

It should be noted that, unlike  $\omega$  [47], the broadening induced by the mixing on  $\rho$  decay width has been found to be marginal. One can understand this physically.

Figure 4.9: Same as Fig. 4.8 but for  $T=75$  MeV

Mixing opens up a new channel for  $\rho$  to decay into  $\pi$ - $\eta$ .  $\eta$  being quite heavy, only the tail part of the  $\rho$  can contribute. Therefore it does not enjoy much of phase space to decay into  $\pi$ - $\eta$ .

As has been mentioned before, there is an experimental uncertainty in the determination of the  $a_0$ - $\pi$ - $\eta$  coupling constant. The measured value is in the range of 50–100 MeV [51]. One could argue that the calculation of Ref. [127] puts a bias toward the smaller side of this range. In any case, Fig. 4.10 shows the dependence of the dilepton productions on this parameter against the background contribution. It is observed that the signal with mixing ranges from visible peaks to a strong enhancement in the region between the  $\omega$  and the  $\phi$ .

It does seem reasonable to conclude that  $\rho$ - $a_0$  mixing provides a promising kinetic window in the invariant mass spectra to study exclusive in-medium effects.

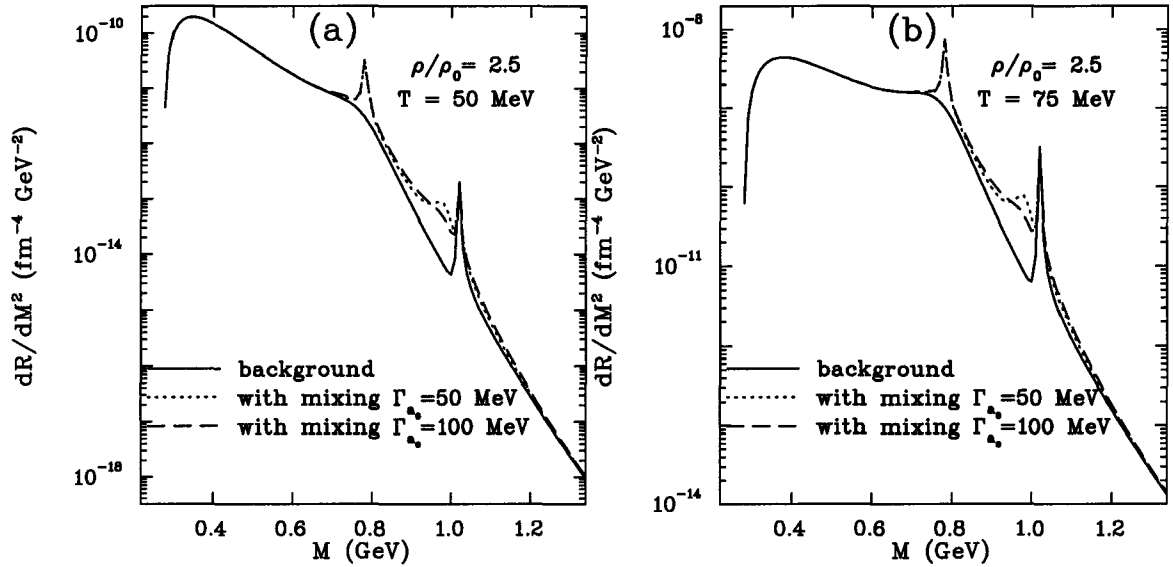


Figure 4.10: Rates at  $T = 50$  MeV (a) and  $75$  MeV (b) for the two limiting cases of  $a_0$ - $\pi$ - $\eta$  coupling corresponding to the decay width  $50$  MeV and  $100$  MeV represented by the dotted and dashed lines respectively. The solid line shows dilepton production through channels other than the ones associated with mixing.

#### 4.5.2 Isoscalar Channel Mediated by $\omega$ - $\sigma$ Mixing

For completeness, we also show the channel opened by  $\omega$ - $\sigma$  mixing *viz.*  $\pi + \pi \rightarrow e^+e^-$  through  $n$ - $n$  excitations. Fig. 4.11 shows the Feynman diagram of such a process. For the description of the  $\sigma\pi\pi$  vertex we use [49]

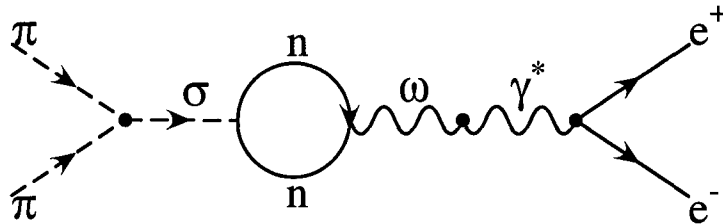


Figure 4.11: The Feynman diagram of the process  $\pi + \pi \rightarrow e^+e^-$  mediated by  $\omega$  -  $\sigma$  mixing.

$$\mathcal{L} = \frac{1}{2} f_{\sigma\pi\pi} m_\pi \phi_\sigma \vec{\phi}_\pi \cdot \vec{\phi}_\pi \quad (4.35)$$

where for later convenience we define  $g_{\sigma\pi\pi} = f_{\sigma\pi\pi}m_\pi$ .

The cross section for this process can be expressed in terms of the momentum-dependent mixing amplitude

$$\sigma_{\pi\pi\rightarrow\sigma/\omega\rightarrow e^+e^-} = \frac{2\pi\alpha^2}{3q_z^2 M} \frac{g_{\sigma\pi\pi}^2}{g_\omega^2} \frac{F_\omega(M^2)G_\sigma(M^2)}{k_\sigma} |\Pi_0|^2$$

where,  $\Pi_0$  is given by Eq. 3.95, and

$$F_\omega(M^2) = \frac{m_\omega^4}{(M^2 - m_\omega^2)^2 + m_\omega^2 \Gamma_\omega^2}, \quad G_\sigma(M^2) = \frac{1}{(M^2 - m_\sigma^2)^2 + m_\sigma^2 \Gamma_\sigma^2(M)},$$

$$k_\sigma = \frac{\sqrt{(M^2 - 4m_\pi^2)}}{2}.$$

For  $\omega$  we used a constant width of 8.43 MeV and for the sigma meson width we adopt the same mass (550 MeV) and width (300 MeV) as Ref. [52]. The invariant mass dependence of the decay width of the  $\sigma$  meson is presented below:

$$\Gamma_\sigma(M) = \frac{3g_{\sigma\pi\pi}^2}{32\pi} \frac{\sqrt{(1 - (\frac{2m_\pi}{M})^2)}}{M}. \quad (4.36)$$

Recent discussions of this issue may be found also in Refs. [128, 129, 130].

The results presented in Fig. 4.12 show an important effect induced by  $\omega$ - $\sigma$  mixing on the dilepton spectrum from a medium denser than the normal nuclear matter. However, unlike  $\rho$ - $a_0$  mixing, this effect is important only in a small range of invariant mass around the  $\omega$  pole. We also have checked the effect of form factor by considering the same as Ref. [47] which is normalized to one for the on-shell particle. Effects found are small.

Next we concentrate on the isoscalar channel effect of  $\sigma$ - $\omega$  mixing at finite temperature and density or, in other words, on the dilepton production rate. As the mixing amplitude now involves the  $\omega$  propagator we observe a sharp peak in the vicinity of

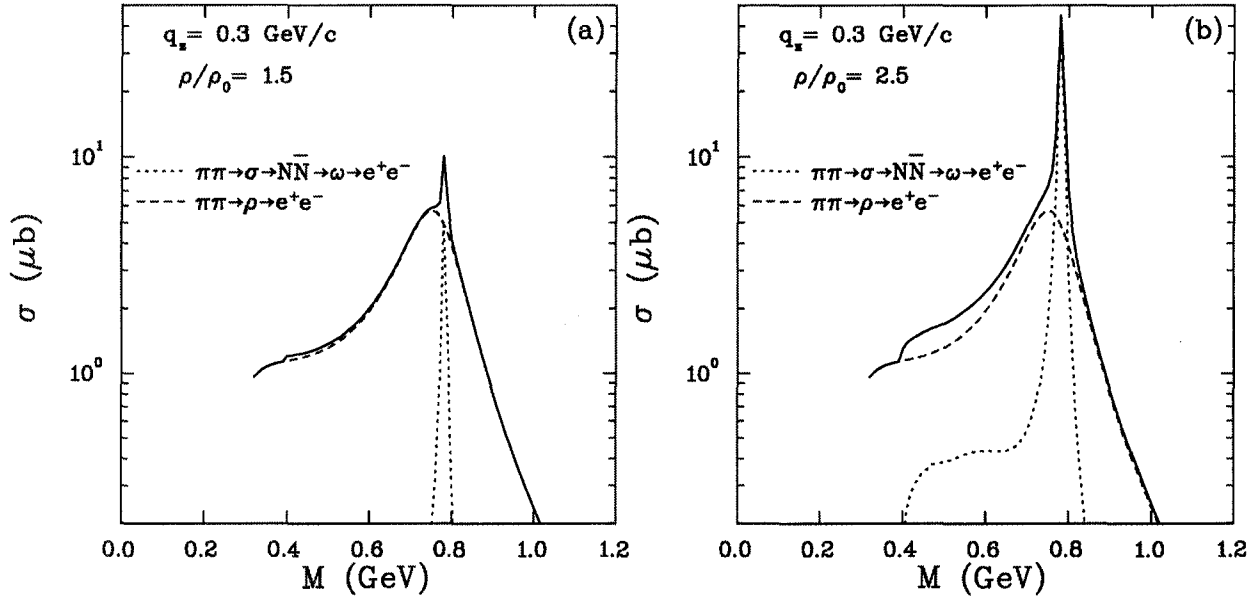


Figure 4.12: Dilepton spectrum of  $\pi + \pi \rightarrow e^+ + e^-$  considering matter induced  $\omega - \sigma$  mixing and the direct channel

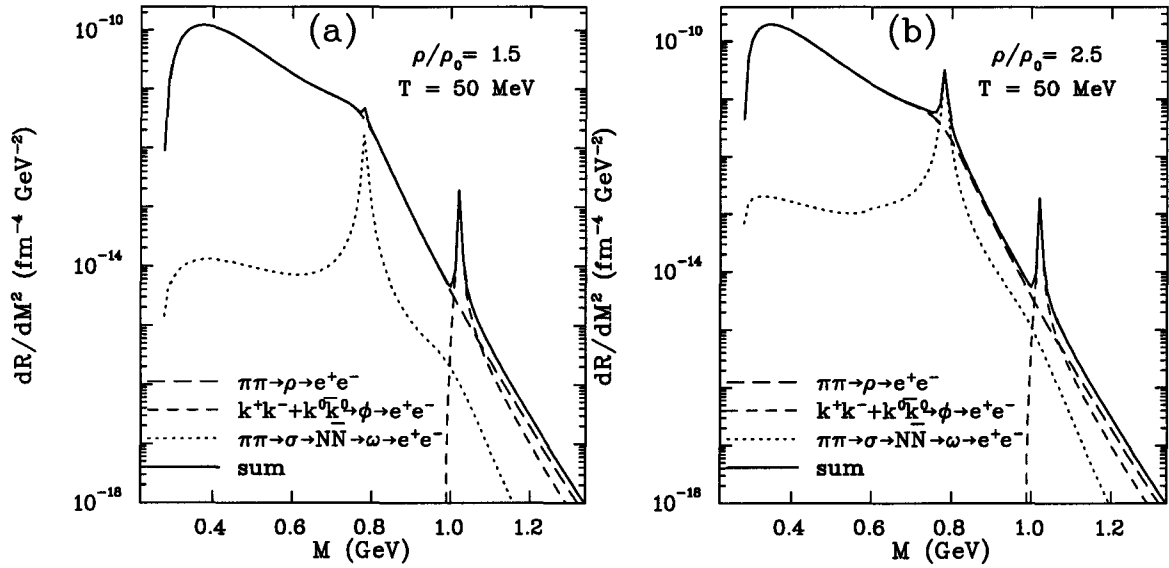


Figure 4.13: Effect of  $\sigma$ - $\omega$  mixing on the dilepton production rate at  $T = 50$  MeV for two different densities as mentioned in the legend.

the  $\omega$  mass. Obviously this mixing amplitude depends on the density and the temperature. The effects are more pronounced in the left panel of Fig. 4.13 where we have higher density. No such peak is observed for the  $\sigma$  meson which is sufficiently broad. We also plot the rates for  $\pi$ - $\pi$  and  $K$ - $\bar{K}$  annihilation for comparison. The left panel shows the results at  $\rho/\rho_0 = 1.5$  and the right panel shows the same for  $\rho/\rho_0 = 2.5$ . Fig. 4.14 shows the results for the isoscalar channel at a higher temperature. It is

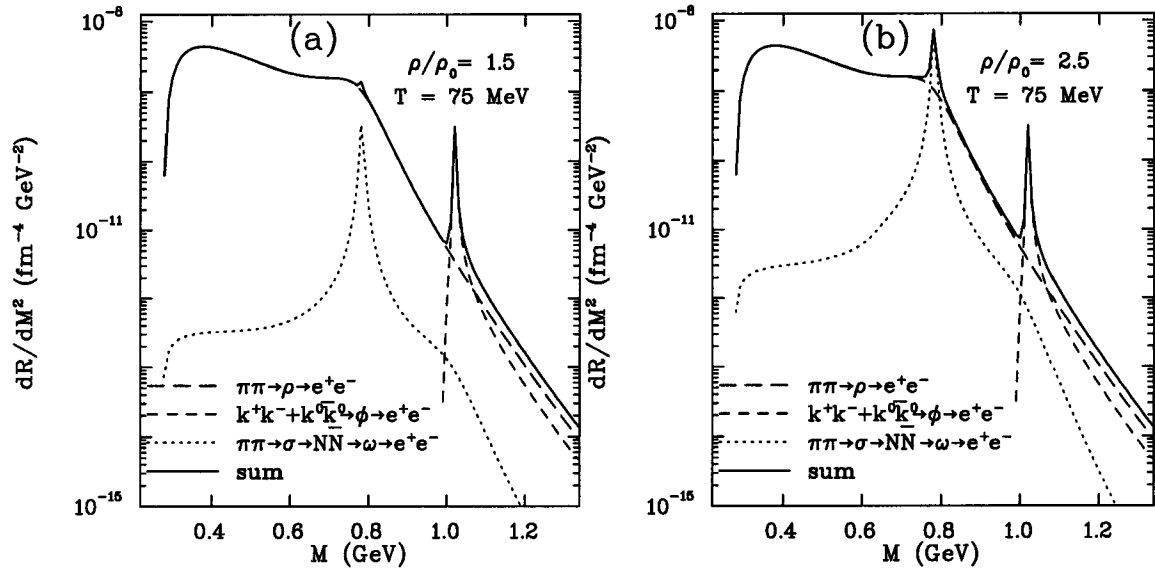


Figure 4.14: Same as Fig. 4.13 but for  $T=75$  MeV

evident that at higher density the effect of mixing is also high.

It is to be noted that to calculate the dilepton rate we have used tree level propagator for  $\omega$  and  $\sigma$ . In Ref. [47] it is argued that  $\sigma$ - $\omega$  mixing broadens the  $\omega$  decay width substantially in nuclear matter at high density. This is understandable as now  $\omega$  thorough nucleon-antinucleon (hole) excitations can decay into pion pairs as opposed to vacuum because of G-parity violation in matter. Therefore in matter this decay channel enjoys a larger phase space and becomes as broad as  $\rho$  as its vacuum mass is almost degenerate with that of  $\rho$  meson. But at the one loop level the diagonal

elements of the mixed propagator would also reduce its mass (off-diagonal elements have little effect on the effective mass). Now if one considers the broadening induced by the off-diagonal element of the dressed propagator of the  $\omega$  meson, then to be consistent one should also take the medium modified mass for the  $\omega$  meson. We have seen that in Walecka model  $\omega$  meson mass also drops, which would again reduce the phase space and, consequently, the decay width decreases. These two competing effects are not expected therefore to change the in-medium width of  $\omega$  significantly. Our focus here was to see the effect of mixing on the dilepton production and how it compares with  $\pi$ - $\pi$  annihilation. However, in Chapter 5 we consider the in-medium modification on the  $\omega$  meson propagator and we postpone the discussion on the changes this effect brings to the total dilepton yield.

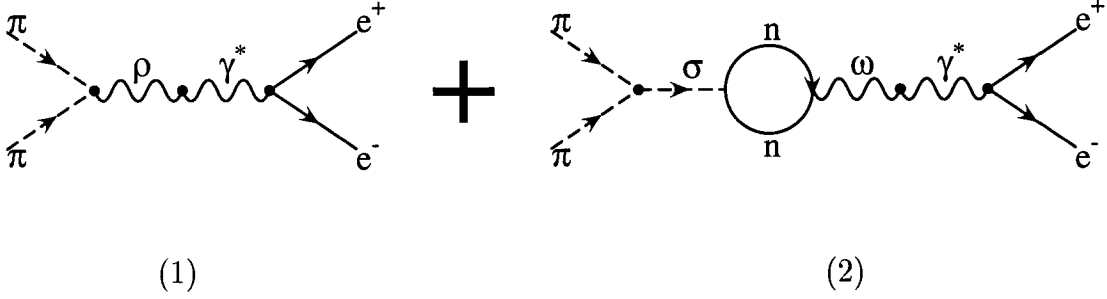
#### 4.6 *Interference Between the Direct and Mixing-Induced Channel in the Pion Annihilation into Dileptons*

The direct dilepton channel of the  $\pi\pi$  annihilation and the channel opened by  $\sigma$ - $\omega$  mixing have the same initial and final components. Therefore, in order to evaluate the total production of  $\pi\pi \rightarrow e^+e^-$  we need to add the interference term to the individual evaluated channels. Let's understand how to evaluate such term by starting with the production rate formula

$$\begin{aligned} \frac{R_{12}^{e^+e^-}}{dM^2} &= \int d\Phi_{12} \int \frac{d^3p_-}{(2\pi)^3 2E_-} \frac{d^3p_+}{(2\pi)^3 2E_+} (2\pi)^4 \\ &\quad \times \delta^4(k_1 + k_2 - p_+ - p_-) |\mathcal{M}_{12 \rightarrow e^+e^-}|^2 \\ d\Phi_{12} &= \frac{d^3k_1}{(2\pi)^3 2E_1} f_1(E_1) \frac{d^3k_2}{(2\pi)^3 2E_2} f_2(E_2) \delta[M^2 - (k_1 + k_2)^2] . \end{aligned} \quad (4.37)$$

Because for both processes shown in fig. 4.15 have the same initial and final states we, therefore, have a composed matrix element for the  $\pi$ - $\pi$  annihilation into dileptons

$$\mathcal{M}_{\pi\pi \rightarrow e^+e^-} = \mathcal{M}_1 + \mathcal{M}_2 \quad (4.38)$$

Figure 4.15: The two processes interfering in the  $\pi\pi$  annihilation into dileptons.

$$|\mathcal{M}_{\pi\pi \rightarrow e^+e^-}|^2 = |\mathcal{M}_1|^2 + |\mathcal{M}_2|^2 + \mathcal{M}_1^\dagger \mathcal{M}_2 + \mathcal{M}_2^\dagger \mathcal{M}_1$$

where we could define the square of the matrix element corresponding to interference

$$|\mathcal{M}_{int}|^2 = \mathcal{M}_1^\dagger \mathcal{M}_2 + \mathcal{M}_2^\dagger \mathcal{M}_1 \quad . \quad (4.39)$$

Evaluating the Feynman diagrams 4.15 we get after some simplification

$$\mathcal{M}_1 = (4\pi\alpha) g_{\rho\pi\pi} \frac{m_\rho^2}{g_\rho} \frac{1}{q^2} \frac{1}{q^2 - m_\rho^2 + im_\rho\Gamma_\rho} \bar{u}^{(s)} \gamma^\mu v^{(s)} (k_1 - k_2)_\mu \quad (4.40)$$

$$\mathcal{M}_2 = (4\pi\alpha) g_{\sigma\pi\pi} \frac{m_\omega^2}{g_\omega} \frac{1}{q^2} \frac{1}{q^2 - m_\omega^2 + im_\omega\Gamma_\omega} \frac{\bar{u}^{(s)} \gamma^\mu v^{(s)}}{q^2 - m_\sigma^2 + im_\sigma\Gamma_\sigma} \Pi_\mu \quad . \quad (4.41)$$

$$(4.42)$$

We could now make use of the following identities,

$$(\bar{u} \gamma^\mu v)^\dagger = \bar{v} \gamma^\mu u \quad (4.43)$$

$$\sum_s u^s(p) \bar{u}^s(p) = \not{p} + m \quad \sum_s v^s(p) \bar{v}^s(p) = \not{p} - m \quad (4.44)$$

$$\sum_{s,s'} \bar{v}^{s'}(p') \gamma^\mu u^s(p) \bar{u}^s(p) \gamma^\nu v^{s'}(p') = \text{Tr}[(\not{p}' - m) \gamma^\mu (\not{p} + m) \gamma^\nu] \quad (4.45)$$

and, we get after summing over the final spin states of the electrons

$$|\mathcal{M}_{int}|^2 = (4\pi\alpha)^2 \frac{m_\omega^2}{g_\omega} \frac{m_\rho^2}{g_\rho} \frac{g_{\rho\pi\pi} g_{\sigma\pi\pi}}{q^4} \quad (4.46)$$

$$\times \frac{\text{Tr}[(\not{p}_+ - m) \gamma^\mu (\not{p}_- + m) \gamma^\nu]}{(q^2 - m_\rho^2 + im_\rho\Gamma_\rho)(q^2 - m_\omega^2 + im_\omega\Gamma_\omega)} \Pi_\mu \frac{(k_1 - k_2)_\nu}{q^2 - m_\sigma^2 + im_\sigma\Gamma_\sigma} + c.c. \quad .$$

Therefore, the contribution of this interference to the production rate will be

$$\begin{aligned} \frac{dR_{int}}{dM^2} &= \int d\Phi_{12} \int \frac{d^3p_-}{(2\pi)^3 2E_-} \frac{d^3p_+}{(2\pi)^3 2E_+} (2\pi)^4 \\ &\times \delta(k_1 + k_2 - p_+ - p_-) |\mathcal{M}_{int}|^2 . \end{aligned} \quad (4.47)$$

and using

$$Tr[(\not{p}_+ - m)\gamma^\mu(\not{p}_- + m)\gamma^\nu] = 4[p_+^\mu p_-^\nu + p_+^\nu p_-^\mu - g^{\mu\nu}(p_+ \cdot p_-)] \quad (4.48)$$

$$= L^{\mu\nu} \quad (4.49)$$

$$\int \frac{d^3p_-}{(2\pi)^3 2E_-} \frac{d^3p_+}{(2\pi)^3 2E_+} (2\pi)^4 \quad (4.50)$$

$$\times \delta^4(q - p_+ - p_-) L^{\mu\nu} = \frac{q^\mu q^\nu - q^2 g^{\mu\nu}}{6\pi} \quad (4.51)$$

we get

$$\begin{aligned} \frac{dR_{int}}{dM^2} &= -\frac{(4\pi\alpha)^2 m_\omega^2 m_\rho^2 g_{\rho\pi\pi} g_{\sigma\pi\pi}}{6\pi g_\omega g_\rho q^2} \\ &\times \int d\Phi_{12} \frac{[\Pi_0(E_1 - E_2) - \mathbf{\Pi} \cdot (\mathbf{k}_1 - \mathbf{k}_2)]}{(q^2 - m_\rho^2 + im_\rho\Gamma_\rho)(q^2 - m_\omega^2 + im_\omega\Gamma_\omega)(q^2 - m_\sigma^2 + im_\sigma\Gamma_\sigma)} + c.c. . \end{aligned} \quad (4.52)$$

To be noted here that for this expression we have used the current conservation relation  $q_\mu \Pi^\mu = 0$ . We also note that the second term does not survive the angular integration over the initial pion states. The expression left is only function of the initial pion energies and could be evaluated numerically in the same way as in section 4.3. For reference we will also give the similar expressions for the direct channels.

$$\begin{aligned} \frac{dR_{\pi\pi \rightarrow \rho \rightarrow e^+ e^-}}{dM^2} &= \frac{g_{\rho\pi\pi}^2 (4\pi\alpha)^2}{6\pi g_\rho^2} \frac{m_\rho^4}{(q^2 - m_\rho^2)^2 + m_\rho^2 \Gamma_\rho^2} \left(1 - \frac{4m_\pi^2}{q^2}\right) \int d\Phi_{12} \quad (4.53) \\ \frac{dR_{\pi\pi \rightarrow \sigma \rightarrow \omega \rightarrow e^+ e^-}}{dM^2} &= \frac{g_{\sigma\pi\pi}^2 (4\pi\alpha)^2}{6\pi q^2 g_\omega^2} \frac{m_\omega^4}{(q^2 - m_\omega^2)^2 + m_\omega^2 \Gamma_\omega^2} \frac{1}{(q^2 - m_\sigma^2)^2 + m_\sigma^2 \Gamma_\sigma^2} \\ &\times \int d\Phi_{12} |\Pi_0|^2 \end{aligned} \quad (4.54)$$

where  $|\Pi_0|^2$  is the same as in section 3.5. Again that current conservation was used to cancel the first term produced by the integration of the leptonic tensor 4.51 as well as  $q \cdot (k_1 - k_2) = 0$ .

In the present case, the contribution from the interference term is small and, therefore, we do not present separately the numerical results. However, for completeness, we include this effect in the calculation of the total dilepton yield.

### 4.7 Thermal Rates at Finite Temperature and Density

We show in Figs. 4.16 and 4.17 the total dilepton yield with the combined effects of mixing in both the isoscalar and isovector channels. It is important to see that rates induced by mixing are significant in certain windows of density and temperature. For completeness we have also evaluated the contribution  $\pi N \rightarrow \omega N \rightarrow N e^+ e^-$ . It was found to be negligible, in agreement with a previous estimate [131].

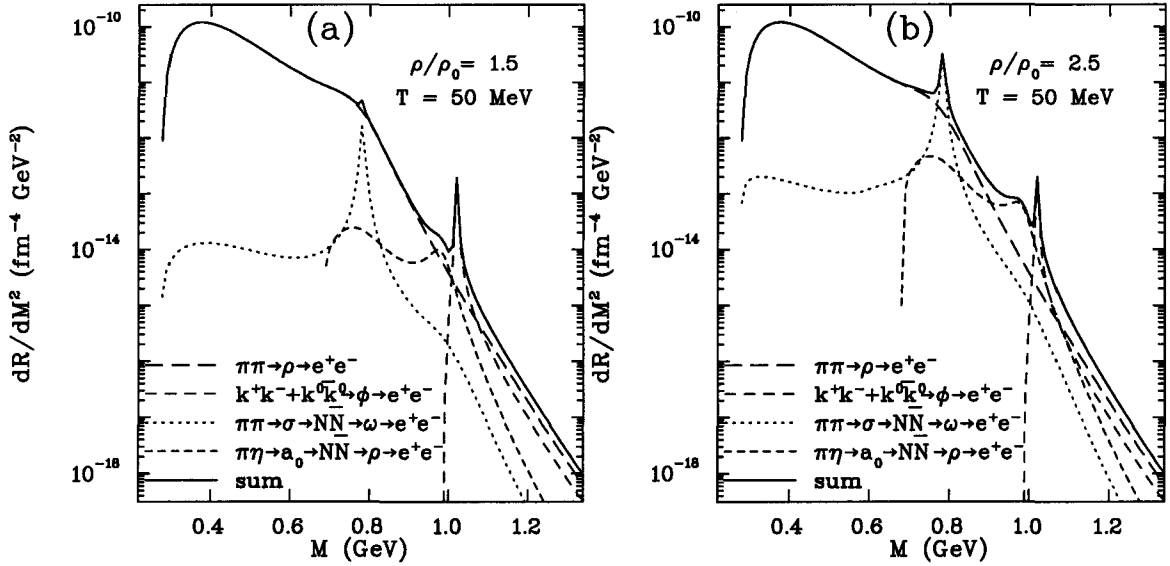
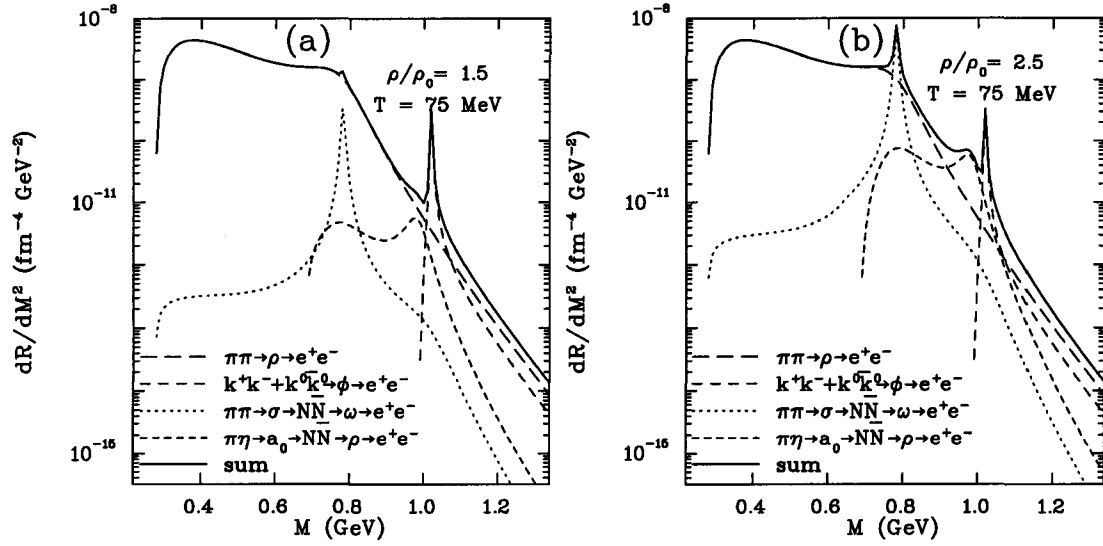
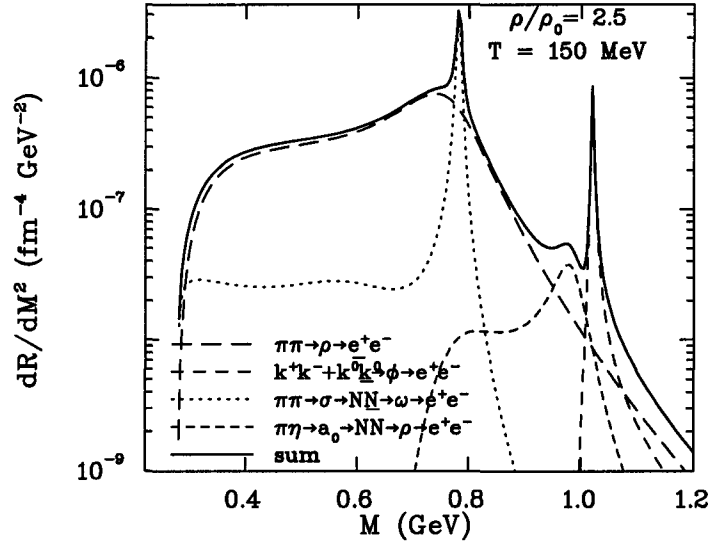


Figure 4.16: Rates at  $T=50$  MeV with mixing in both isoscalar and isovector channels.

We present in Fig. 4.18 the results of the total dilepton yield from thermal mesons with mixing at a temperature of 150 MeV. Interestingly enough the dilepton yield induced by the mixing in the isovector channel at higher temperature also seems to be significant as evident from the Fig. 4.18.

Figure 4.17: Rates at  $T = 75$  MeV with mixing in both isoscalar and isovector channels.Figure 4.18: Rates at  $T = 150$  MeV with mixing in both isoscalar and isovector channels.

It should be noted that the contribution from  $\sigma$ - $\omega$  mixing does not change the resultant spectra much except for a small peak representing  $\omega$  meson pole in the transition amplitude. However, in experiments we expect an  $\omega$  peak in the dilepton

spectra even in the absence of meson mixing as a resultant of direct decays of the thermally produced  $\omega$  mesons. The situation, as one can easily notice, is different for the isovector mode. There, the dominant contributions are distributed near the tail of the  $\pi$ - $\pi$  annihilation spectra ( $\rho$  spectral function). On the other hand if  $\rho$  spectral function gets sufficiently broadened this effect might become more visible near the  $\omega$  peak region where additional contributions would come from the mixing.

---

## Summary

In this chapter, we have estimated the dilepton production rates arising from scalar and vector meson mixing in different isospin channel involving nucleon -hole (or anti-nucleon) excitations as intermediate states. The rates have been compared against the  $\pi$ - $\pi$  annihilation in the p-wave channel ( $\rho$ -channel) and  $K$ - $\bar{K}$  annihilation. Higher yield of dileptons in the invariant mass region between the  $\rho$  and the  $\phi$  peaks are expected. The mixing in the isoscalar channel contributes mostly between the two-pion threshold and the  $\omega$  peak but is small compared to the  $\pi$ - $\pi$  annihilation contribution. On the other hand, the isovector channel seems to provide a better probe as it contributes near the tail region of the two pion annihilation contribution. It should be stressed here that broadening or dropping  $\rho$  meson mass would even favour our observation. In that case the  $\pi$ - $\pi$  background would be pushed more towards lower invariant mass region bringing the  $a_0$  peak into a clearer relief. Finally, it is important to realize that mixing effects only appear in the longitudinal part of the vector meson spectral function and therefore there should be no effect of the mixing on the photon spectra which involves the transverse part of the vector meson polarization tensor.

The effects studied here are density driven and can therefore be observed in en-

vironments where one has high baryonic chemical potential and comparatively lower temperature. The most relevant experiments to observe this kind of medium-induced phenomenon are the ones to be performed at GSI using the HADES detector where the density might reach up to three times the normal nuclear matter density at temperatures of  $T = 60 - 90$  MeV [132, 133]. Ref. [134] also indicates a similar range of densities and temperatures at SIS/GSI energies. Those observations have guided our choice of the temperatures and densities used in this section.

---



---

## SPACE-TIME EVOLUTION AND THE DILEPTON SPECTRA

---



---

As we discussed in the introduction, the highly relativistic collisions of heavy ions can produce matter in the form of a hot hadronic gas. So far we have discussed the rate of dilepton emission per unit time from unit volume from a thermal system made up of hadronic matter at a fixed temperature and baryonic density. However, the highly excited state of matter produced at a high temperature will expand and cool, emitting dileptons in the process. This process will continue as long as the mean free paths of the constituents become comparable to the size of the system and freeze-out occurs. So, in order to compare the yield with experiments we must integrate the static rates over the space time volume of the collision from formation till freeze-out. The total yield is hence

$$\frac{dN}{d^4q} = \int_{\text{formation}}^{\text{freeze-out}} d^4x \frac{dR(\rho_B, T(x))}{d^4q} \quad (5.1)$$

where  $T(x)$  is the local temperature, assuming that the produced matter is in local thermal equilibrium.  $x$  is the space-time coordinate and  $d^4x = d\mathcal{V}dt$  where  $\mathcal{V}$  is the three-volume. As is evident from Eq. (5.1) the key ingredients that we now need in order to carry through our program are firstly, the initial conditions namely the initial temperature and the initial volume and the number of participating baryons, and secondly, the temperature and volume as a function of space-time or, in other

words the equation of state (EOS).

## 5.1 *Relativistic Thermal Model*

The space-time expansion will be done a relativistic thermal model similar with Refs. [24, 33] but we will not consider a free Fermi gas model for the equation of state. Instead, we will use the Walecka model as described in chapter 2 to determine the equation of state at a given time. The dilepton data will be compared with the results of the CERES experiment and we will make predictions for HADES experiment under development at GSI.

Our thermal model assumes, for simplicity, that the hot matter formed has a cylindrical shape and it expands in both radial and longitudinal directions [50]. We parameterize the fire-cylindrical expansion in the following manner [33]

$$V_{FC}(t) = 2(z_0 + v_z t + \frac{1}{2}a_z t^2)\pi(r_0 + \frac{1}{2}a_\perp t^2)^2 \quad (5.2)$$

where the fire-cylinder is expanding in both  $\pm z$  directions. This model have been employed to allow for a sufficient spread in the particle rapidity distributions [40]. We have several parameters involved in this expansion. These parameters are adjusted to fit results from transport models or hydrodynamic simulations while these calculations consider experimental observables like charge multiplicity and particle ratios. Of course, the baryonic number of the plasma is considered constant and therefore the time dependence of the baryonic density will be inversely-proportional to the volume dependence.

Some approaches in thermal models also parameterize the temperature evolution in accordance with microscopic transport simulations [33]. Instead, we assume local thermal equilibrium with the nuclear matter equation of state deduced in the Walecka model and the entropy conservation is imposed during expansion [50]. This, along

with the baryonic density functional in time, will provide us with the temperature dependence in a similar manner as in [24]. Therefore, during whole process we have an interacting hadron gas in sustained thermal equilibrium until the thermal freezeout is reached when hadrons cease to interact.

## 5.2 Results for CERES/SPS

CERES is an experiment dedicated to the measurement of low-mass electron-positron pairs and direct photons in ultra-relativistic heavy-ion collisions at the CERN Super Proton Synchrotron (SPS). The CERES spectrometer is optimized to measure low-mass electron pairs from about  $50 \text{ MeV}/c^2$  up to beyond  $2 \text{ GeV}/c^2$ , limited at the upper end by statistics [135, 136]. It covers the pseudorapidity region  $2.1 < \eta < 2.65$  with  $2\pi$  azimuthal symmetry and accepts a very broad range of  $p_t$ .

CERES has completed a systematic physics program including the measurements of electron pairs in p-Be and p-Au collisions at  $450 \text{ GeV}/c$  [137, 138], S-Au collisions at  $200 \text{ A GeV}$  [139] and Pb-Au collisions at  $158 \text{ A GeV}$  [75]. The p-nucleus experiments can be well reproduced by final state hadron decays with known abundances, the so-called “hadronic cocktail”. We show in Fig. 5.1 the invariant mass spectra of dileptons measured by CERES collaboration in p-Be and p-Au experiments and the hadronic cocktail which explains quite well the hadronic spectrum within the systematic uncertainty.

Things become different for nucleus-nucleus collisions and the dilepton production is strongly underestimated if one considers only final state hadronic decays. As mentioned in Chapter 4, due to the abundant production of pions,  $\pi\pi \rightarrow l^+l^-$  is expected to bring the most important contribution in the low-mass region. Indeed, several works on nucleus-nucleus collisions using a relativistic transport model [141], a thermal model [33, 24] or an hydrodynamic model [142], show agreement with ex-

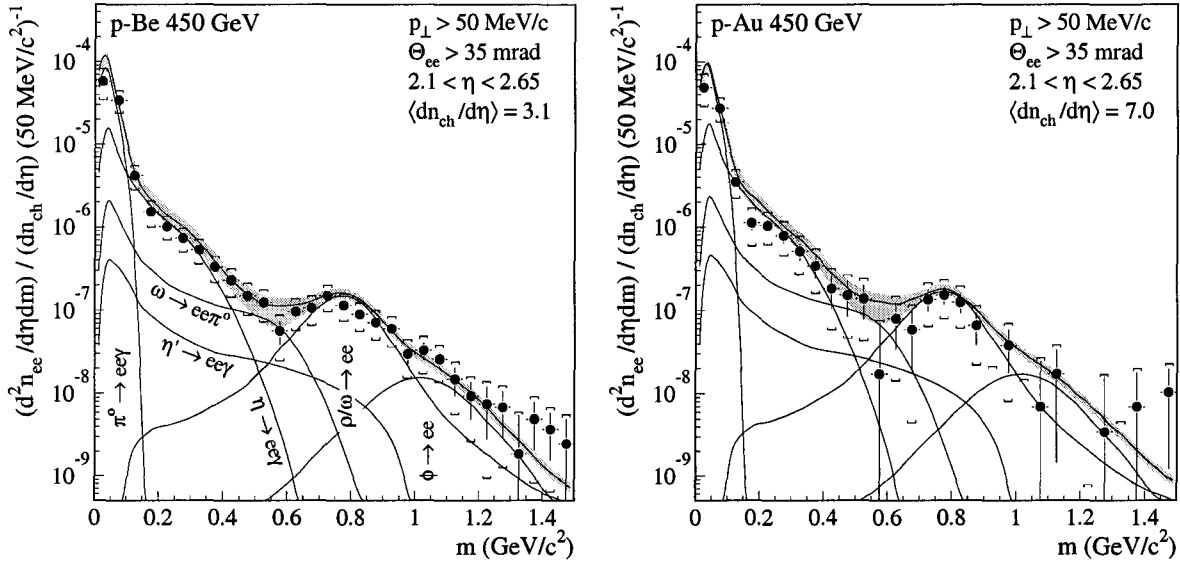


Figure 5.1: Invariant mass spectra of dileptons measured by CERES collaboration in p-Be and p-Au experiments and the hadronic cocktail. The shaded area shows the systematic uncertainty in the cocktail. Figures are taken from [140].

perimental results, all considering in-medium modification of the  $\rho$  meson properties when they evaluate  $\pi\pi \rightarrow l^+l^-$  channel.

In the present calculation we would like to include the effect of meson mixing in addition to the channels induced by thermal meson collisions. The integration over the space-time evolution of the plasma formed in the collision is done by using a relativistic thermal model. Our attempt will be to adjust the parameters of our model to match experimental values where available or various simulations available for CERN-SPS experiments.

Figure 5.2 shows the time dependence of baryonic density and temperature dependence for a typical Pb(158GeV)+Au collision with an impact parameter  $b=5$  fm. Guided by hydrodynamical simulations [143], the initial velocity describing the longitudinal expansion of the fire-cylinder is taken to be  $v_z^0 = 0.5c$  for Pb(158GeV)+Au collisions. Longitudinal and transverse accelerations are fixed to give the final velocities  $v_z^f = 0.75c$  and  $v_\perp^f = 0.6c$  as borne out from experiment [24, 144]. If we consider

a transverse expansion of 3-4 fm we get a fire-cylinder lifetime of about 10-12 fm/c, consistent with HBT analyses [145]. The parameter  $r_0$  denotes the initial overlap radius and is, e.g.,  $r_0=4.6$  fm for the given impact parameter where there are  $N_b = 260$  participant baryons in the collision as consistent with transport calculations [126]. The same transport calculations provide us the initial baryonic density for a given impact parameter. This parameter in turn is implied by the measured number of charged particles emergent from the collisions. For instance, for an average number of charged particles in unit pseudorapidity  $\langle dN_{ch}/d\eta \rangle = 250$ , we have an impact parameter  $b = 5$  fm and an initial baryonic density  $\rho_B = 3.0\rho_0$ . From the initial baryonic density we also can find  $z_0$ , a parameter equivalent to a formation time. For these

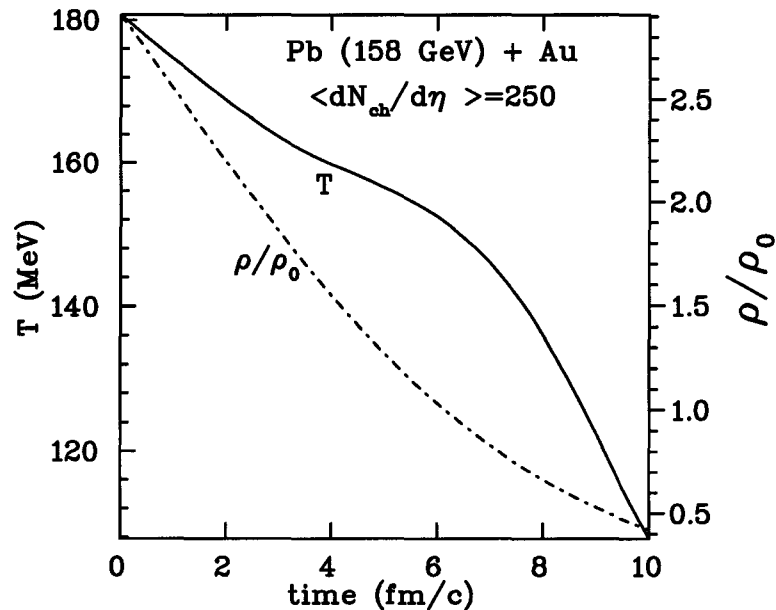


Figure 5.2: The temperature and nuclear density time dependence for Pb(158GeV)+Au collisions with  $\langle dN_{ch}/d\eta \rangle = 250$  in our thermal model.

parameters, we choose an initial temperature of  $T=180$  MeV and a freeze-out temperature  $T=110$  MeV [33]. We notice a slower drop of temperature as compared to [33] followed by a faster drop in the later stages of expansion. In figure 5.3 we show the

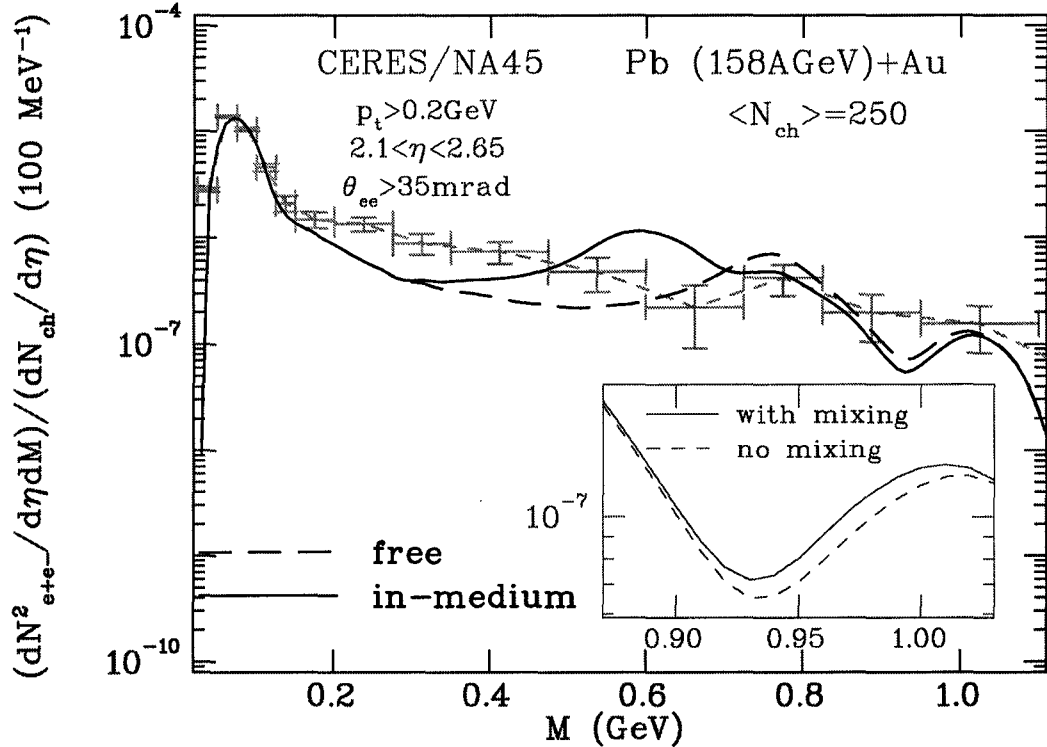


Figure 5.3: Dilepton spectra in a CERES/SPS scenario for Pb(158GeV)+Au collisions with  $\langle dN_{ch}/d\eta \rangle = 250$ . In the main plot, we present the dilepton spectrum with free  $\rho$  spectral function and also the in-medium effects evaluated in Walecka model. In the secondary plot, we show explicitly the effect of mixing.

CERES results [75] for Pb(158GeV)+Au collisions compared with our model. Even though the  $\rho$ - $a_0$  mixing channel wins over the background, we notice that the effect of mixing is small and cannot be observed in this experiment due to large experimental errors and with the CERES detector having a poor resolution. With the addition of the Time Projection Chamber (TPC) in the CERES setup, resolution is expected to improve in the analysis of the data of the Pb(158GeV)+Au run, which are now on tape and will be analyzed next year. The effect of  $\omega$ - $\sigma$  mixing was found to be small. If a larger decay width of the  $\omega$  meson is used at high temperatures [146, 147], the effect becomes even smaller. In any case, for SPS energies, the latter mixing effect

does not present practical importance.

### 5.3 Prediction for Experiments at HADES/GSI

The High Acceptance DiElectron Spectrometer (HADES) [148] is a second-generation apparatus that just came into operation at the Gesellschaft für Schwerionenforschung (GSI), in Darmstadt. It is a detector dedicated to the investigation of the in-medium modification of hadron properties with special focus on the light vector mesons  $\rho$ ,  $\omega$  and  $\phi$ , by studying the dilepton spectra in proton-nucleus and nucleus-nucleus collisions [133]. HADES will investigate collisions at Synchrotron for Heavy Ions (SIS) energies of 1-2 GeV/nucleon. At these energies, it is expected that a high-density matter is created at relatively low temperatures as compared to the experiments at the CERN SPS [149]. Another particularity of HADES detector is an excellent momentum resolution of about 1% with a large acceptance [150].

In our study an 1GeV Au+Au collision is considered where the initial baryonic density formed is considered to be three times normal nuclear matter density at an initial temperature of 90 MeV. Refs. [132, 133, 134] support our choice of density and temperature. One also could make reasonable assumptions for the initial and final transverse velocities, and the fire-cylinder lifetime can be taken about 20 fm [151].

We show in Fig. 5.4 our calculation for the time dependence of the temperature and baryonic density in the present model. We consider the freeze-out temperature at about 31 MeV at a density of 0.65 normal nuclear matter density. We notice a slower relative drop of the baryonic density in the early stages of the expansion as compared to the scenario at SPS energies, mainly due to the lower initial expansion assumed.

We present in Fig. 5.5 the  $\rho$ - $a_0$  mixing channel as compared to the dominant channel in the range of invariant mass 0.6-1.0 GeV,  $\pi$ - $\pi$  annihilation. We observe

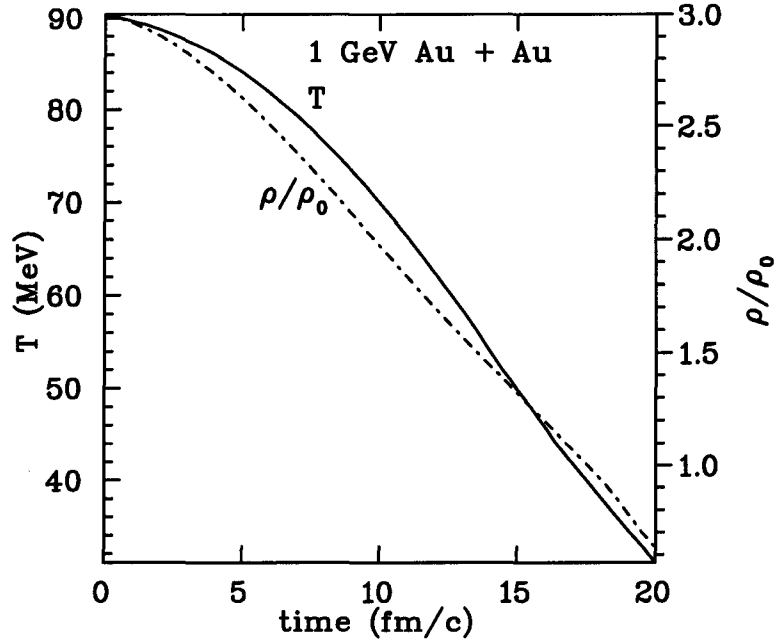


Figure 5.4: The temperature and nuclear density time dependence for 1 GeV Au+Au collisions in our thermal model.

that the mixing channel is almost an order of magnitude above the background at the  $a_0$  peak and, therefore, expected to appear as a considerable enhancement on the dilepton spectrum around 1 GeV. The new channel substantially increases the dilepton production over a span of almost 100 MeV. The same feature can be seen if one considers the in-medium effects on the meson masses. Fig. 5.6 shows the expected dilepton spectrum if we invoke in-medium changes on the properties of vector mesons evaluated in Walecka model. We observe the shift of  $\rho$  and  $a_0$  peaks due to their modified in-medium masses. Still, the enhancement due to the  $\rho$ - $a_0$  mixing effect is strong enough to be detected, but, this time, the new channel peaks at about 0.8 GeV. The isoscalar channel, mediated by  $\sigma$ - $\omega$  mixing, is observed as a sharp peak near the  $\rho$  pole. If the in-medium effects are considered on the  $\omega$  meson properties, the contribution of this mixing effect is spread over a large range in the invariant mass spectrum as a result of the shifting of the omega meson mass with the

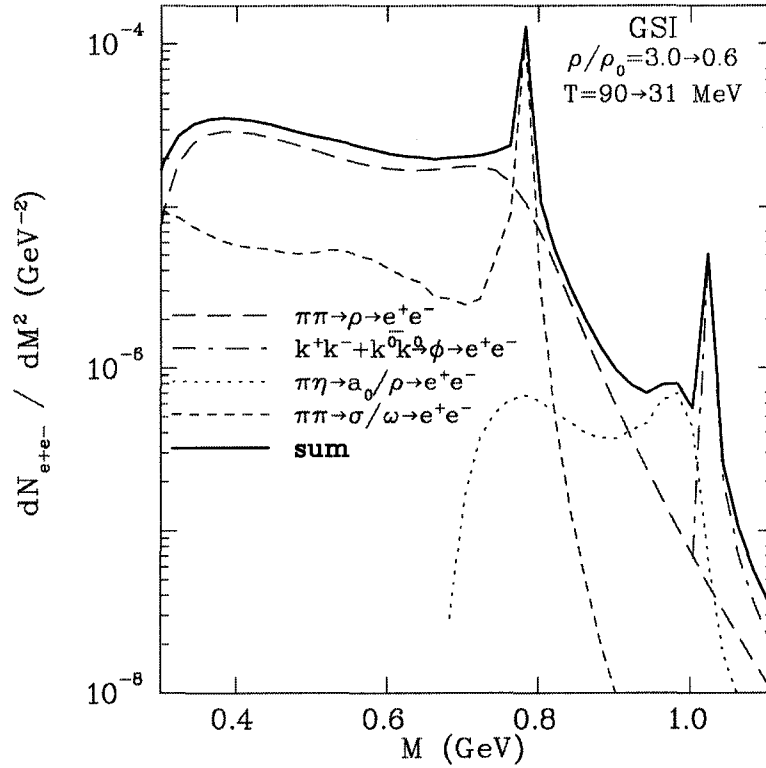


Figure 5.5: Dilepton spectra in a HADES/SIS scenario for 1 GeV  $Au + Au$  collisions with free masses and decay widths.

density during expansion. Consequently, instead of a sharp peak, we have a rather broad distribution in the region where  $\rho$  decay into dileptons is dominant. Therefore, the dilepton signal of the mixing effect in the isoscalar channel will be shadowed by the pion annihilation as evident from Fig. 5.6. We should also note that the  $\phi$  mass does not change importantly in matter [104, 105]. Therefore, its correspondent peak is not apparent in Fig. 5.6 where we are concerned with the dilepton production below the invariant mass of about 0.9 GeV.

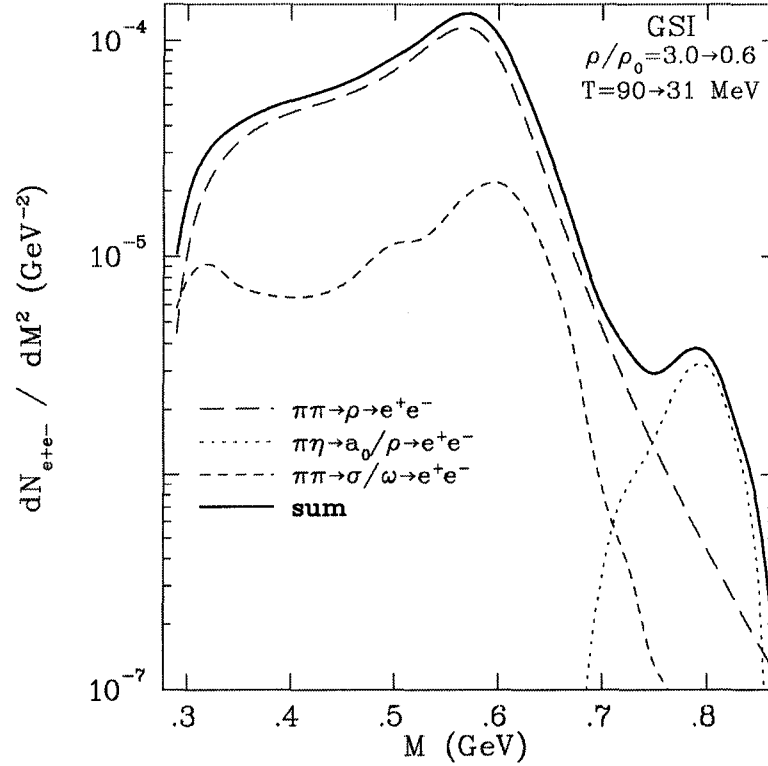


Figure 5.6: Dilepton spectra in a HADES/SIS scenario considering in-medium modifications for 1 GeV Au+Au collisions.

---

## Summary

We have evaluated the dilepton production from thermal mesons in the low invariant mass region in two scenarios: CERES/SPS and HADES/SIS. We have seen that the effect of scalar-vector meson mixing effects are important even in heavy ion collisions at SPS energies, but does not modify dramatically the dilepton spectrum. At SIS energies, signatures of  $\rho$ - $a_0$  meson mixing can be detected as a distinctive peak in the dilepton spectrum. We have presented our findings in two hypothesis, one assuming free meson masses and one considering the in-medium modification of

the meson masses in Walecka model. The detection of the signatures of  $\sigma$ - $\omega$  mixing is questionable since the shifting of vector meson mass due to in-medium effects produce a broad distribution around  $\rho$  peak and the signal is consequently masked by the decay of the latter.

We should point here that the results does not show a strong dependence on our arbitrary choice of the freeze-out parameters. We have checked, and, a change of about 10 MeV for the freeze-out temperature does not change qualitatively the results since the main contribution to the dilepton spectrum comes from the initial stages where temperatures is higher. Also, one could argue that pion or  $\eta$  chemical potential should be introduced in the calculation. Our  $\pi/\eta$  ratio at the thermal freeze-out is by a large amount over-estimated if compared with particle ratios obtained at SIS energies [149, 152] . Therefore, the addition of chemical potentials will only increase the effect of mixing pointed out in the present section. Same argument applies for CERES data [153, 154] but here the mixing effect is not strong enough to produce a noticeable difference.

---

---

# 6

---

---

## CONCLUSIONS AND SUMMARY

---

---

We have discussed in Chapter 1 the importance of studying nuclear matter at high densities and temperatures. One of the main concerns was related to the physics of heavy ion collisions, an innovative way to produce nuclear matter at extreme conditions of temperature and density in the laboratory. There was emphasized that dilepton and photon signals are the only direct probes of these evolving strongly interacting systems, due to their electromagnetic nature. Afterwards, the importance of studying the in-medium properties of hadrons was discussed and special emphasis was put on the light vector mesons due to their decays into dileptons.

In Chapter 2 the formalism to model nuclear matter at finite density and temperature was introduced. The nuclear matter properties in the Walecka model were further presented. We have evaluated the nucleon properties, finding a dropping mass as function of density and the particularities of the temperature dependence were explained. Also, a complete study of the equation of state as function of temperature has been performed.

Knowing the properties of nuclear matter, we were able to discuss in Chapter 3 the properties of  $\rho$ ,  $\omega$ ,  $a_0$  and  $\sigma$  mesons in nuclear matter. The main work consisted in the evaluation of the meson modifications induced by  $n$ - $n$  excitations in nuclear matter at the one-loop level. We have shown that the meson masses drop with increasing baryon density and it was noticed a similar feature as in the case of the nucleon mass

in a changing temperature scenario. We have shown for the first time the possibility of scalar-vector meson mixing in the isovector channel:  $\rho$ - $a_0$  mixing in dense nuclear matter. A detailed study has been developed to uncover the properties of this mixing effect and show the modified dispersion curves and mixing angles. The same studies have been done as part of the present thesis in the case of the isoscalar channel:  $\omega$ - $\sigma$  meson mixing. Last part of this chapter deals with temperature modifications on the light vector meson properties including a discussion of the matter-induced modification of the  $\rho$  meson decay width.

Having completed the relevant studies on the in-medium modification of mesons in nuclear matter, we are now able to evaluate the dilepton spectrum produced by thermal mesons having vector mesons as intermediate stage. In Chapter 4 it is explained the vector meson decay into dileptons in the Vector Meson Dominance model. One of the central subjects of this thesis is to establish the meson mixing effects on the dilepton spectrum. Indeed, we show in Chapter 4 that the mixing effects become important if the nuclear matter densities exceed about normal nuclear matter densities. At higher densities, these channels dominate over the conventional channels around mesonic peaks. For instance,  $\rho$ - $a_0$  mixing induces a peak in the dilepton spectrum in the vicinity of the  $\phi$  meson mass. Similarly,  $\omega$ - $\sigma$  mixing induce a peak close to the  $\rho$  pole, but, due to the broad  $\rho$  spectrum and very sharp  $\omega$ , this channel could be masked in experiments with poor resolution.

The main purpose of Chapter 5 is to expose our findings to a more realistic scenario. We try to model the space-time expansion in a relativistic fireball with relevant parameters adjusted to the experimental values when available, or to transport simulations. In this model, the meson mixing effects are presented in two cases: CERES/SPS and HADES/SIS. We show that the mixing effects wins over background in CERES/SPS experiments, but does not produce a detectable signal at the available resolutions in Pb(158 GeV)+Au experiments. Our predictions for the SIS

energies of 1-2 GeV Au+Au is very encouraging, and the dilepton spectrum shows a very strong enhancement induced by  $\rho$ - $a_0$  mixing in both scenarios, free mass or dropping mass evaluated at mean field level. We expect to see this signal in the forthcoming experiments with the HADES detector. Less promising, but still important, is the  $\omega$ - $\sigma$  mixing since our predictions show that the dilepton signal corresponding to this channel is masked by the pion annihilation. Still, we expect the HADES experiment to bring light on the properties of  $\omega$  meson, especially its mass at finite density, and consequently, help us say the final word related to the isoscalar mixing channel.

A natural extension of the present work is the calculation of the complete spectral densities of the vector mesons with the inclusion of meson mixing effects. Since this is a higher order effect, the work require calculations at higher loop level. Also, the effects of nuclear resonances on the vector meson spectral density should also be further addressed. Recent evaluations of the rho meson spectral function in a non-relativistic nuclear resonance model [33] or assuming linear density approximation (LDA) for the evaluation of the  $\rho$  polarization function [155] show a broadening of the  $\rho$  meson induced by these effects. Our recent calculations in this direction [156] show an important departure from the LDA results for densities above normal nuclear matter density. However, all the above mentioned works are limited to the one loop level, and therefore, does not permit to include consistently the mixing effects. Moreover, another difficulty of this calculation is the limited knowledge of the  $a_0$  meson coupling to nuclear resonances. The work on the above topics continues.

---

---

# A

---

---

## PROPERTIES OF FINITE TEMPERATURE GREEN'S FUNCTION

---

---

In the present appendix, some properties of the Green's function at finite temperature are highlighted in the imaginary-time formalism. For a more complete and detailed study on this issue the reader should address to Ref. [102].

For two operators  $A$  and  $B$  in the Heisenberg picture we can write the following thermal average

$$\langle A(t)B(t') \rangle_\beta = Z^{-1}(\beta)Tr[\rho(\beta)A(t)B(t')] \quad (\text{A.1})$$

where  $\rho_B = e^{-\beta\mathcal{H}}$  is the density matrix of the system, and  $Z^{-1}(\beta) = Tr e^{\beta\mathcal{H}}$  is the partition function of the system. By introducing the identity operator  $1 = e^{+\beta\mathcal{H}}e^{-\beta\mathcal{H}}$  between the two operators ( $A$  and  $B$ ) and considering the time dependence of the operators in Heisenberg picture ( $A(t) = e^{i\mathcal{H}t}Ae^{-i\mathcal{H}t}$ ), we get

$$\langle A(t)B(t') \rangle_\beta = Z^{-1}(\beta)Tr[A(t+i\beta)e^{-\beta\mathcal{H}}B(t')] \quad (\text{A.2})$$

Re-arranging the terms by using the cyclic properties of the trace we finally get

$$\langle A(t)B(t') \rangle_\beta = \langle B(t')A(t+i\beta) \rangle_\beta \quad (\text{A.3})$$

The two point Greens function is defined in the imaginary time formalism similarly with the zero temperature Greens function in the Heisenberg picture if we identify  $t = -i\tau$ ,  $0 < \tau < \beta$  [102],

$$G_\beta = \langle \mathcal{T}(\phi(\tau)\phi^\dagger(\tau')) \rangle \quad (\text{A.4})$$

where  $\phi$  is a bosonic or fermionic field and  $\mathcal{T}$  is the ordering operator, like the time ordering at zero temperature,

$$\mathcal{T}[\phi(\tau)\phi^\dagger(\tau')] = \theta(t-t')\phi(\tau)\phi^\dagger(\tau') \pm \theta(t'-t)\phi^\dagger(\tau')\phi(\tau) \quad (\text{A.5})$$

where the minus sign is for fermionic fields.

If  $\tau > 0$ , because of the properties of the thermal correlation function of two operators (A.3) we get by straightforward calculation

$$G_\beta(0, \tau) = \pm G_\beta(\beta, \tau) \quad (\text{A.6})$$

We observe that is a (anti)periodic function and therefore will develop discrete values of frequencies when it is Fourier transformed.

$$G_\beta(\tau, 0) = \frac{1}{\beta} \sum_n e^{-i\omega_n \tau} \bar{G}_\beta(\omega_n, 0) \quad (\text{A.7})$$

where, due to the different behavior, periodic or anti-periodic for bosons and fermions, we have

$$\omega_n = \begin{cases} \frac{2n\pi}{\beta} & \text{for bosons} \\ \frac{(2n+1)\pi}{\beta} & \text{for fermions} \end{cases}$$

These are commonly called the Matsubara frequencies. If we introduce the space variable we get for fermions,

$$S_\beta(0, \mathbf{x}; \tau, \mathbf{y}) = -S_\beta(\beta, \mathbf{x}; \tau, \mathbf{y}) \quad (\text{A.8})$$

By a similar procedure we get the following expansion

$$\begin{aligned} S_\beta(\tau, \mathbf{x}) &= \frac{1}{\beta} \sum_n e^{-i\omega_n \tau} \int d^3 p e^{i\mathbf{p} \cdot \mathbf{x}} S_\beta(\omega_n, \mathbf{p}) \\ S_\beta(\omega_n, \mathbf{p}) &= \int_0^\beta d\tau e^{i\omega_n \tau} \int d^3 x e^{-i\mathbf{p} \cdot \mathbf{x}} S_\beta(\tau, \mathbf{x}) \\ \omega_n &= \frac{(2n+1)\pi}{\beta} \end{aligned} \quad (\text{A.9})$$

If we define the following Green functions

$$G_{\beta}^{<}(x_0, \mathbf{x}) \quad ix_0 < 0 \quad (\text{A.10})$$

$$G_{\beta}^{<}(x_0, \mathbf{x}) \quad ix_0 > 0 \quad (\text{A.11})$$

We can similarly show that

$$G_{\beta}^{<}(x_0, \mathbf{x}) = G_{\beta}^{>}(x_0)(x_0 - i\beta, \mathbf{x}) \quad (\text{A.12})$$

---



---

# B

---



---

## SOME PROPERTIES OF SPIN-1 BOSON SELF-ENERGY

---



---

We would like to show that

$$\Pi_{\beta}^{>\mu\nu}(q) = e^{\beta q_0} \Pi_{\beta}^{<\mu\nu}(q) \quad (\text{B.1})$$

we start with

$$\Pi_{\beta}^{>\mu\nu}(q) = \int d^4x e^{i(q_0(x_0) - \mathbf{q} \cdot \mathbf{x})} \theta(x_0) \langle i | j^{\mu}(x) j^{\nu}(0) | i \rangle_{\beta} \quad (\text{B.2})$$

this, accordingly to eq. A.3 is

$$\begin{aligned} \Pi_{\beta}^{>\mu\nu}(q) &= \int d^4x e^{i(q_0 x_0 - \mathbf{q} \cdot \mathbf{x})} \langle i | j(0) j(x_0 + i\beta, \mathbf{x}) | i \rangle_{\beta} \\ \Pi_{\beta}^{>\mu\nu}(q) &= \int d^4x e^{i(q_0 x_0 - \mathbf{q} \cdot \mathbf{x})} \Pi_{\beta}^{<\mu\nu}(x_0 + i\beta, \mathbf{x}) \\ \Pi_{\beta}^{>\mu\nu}(q) &= e^{\beta q_0} \int d^4x e^{iqx} \Pi_{\beta}^{<\mu\nu}(x) \\ \Pi_{\beta}^{>\mu\nu}(q) &= e^{\beta q_0} \Pi_{\beta}^{<\mu\nu}(q) \end{aligned} \quad (\text{B.3})$$

---

---

## BIBLIOGRAPHY

---

---

- [1] J.I. Kapusta, *Finite Temperature Field Theory* (Cambridge University Press, Cambridge, 1989).
- [2] S. Gottlieb *et al.*, Phys. Rev. **D35**, 3972 (1987).
- [3] M. Fukugita and A. Ukawa, Phys. Rev. Lett. **57**, 503 (1986).
- [4] M. C. Ruivo, C. A. de Sousa, B. Hiller, and A. H. Blin, Nucl. Phys. **A575**, 460 (1994).
- [5] H. Kurasawa and T. Suzuki, Prog. Theor. Phys. **84**, 1030 (1990).
- [6] G. E. Brown, Comments Nucl. Part. Phys. **A19**, 185 (1990).
- [7] W. K. Wilson *et al.*, Nucl. Phys. A **566**, 387c (1994).
- [8] G. S. F. Stephans, Nucl. Phys. **A583**, 653c (1995).
- [9] E. V. Shuryak, Nucl. Phys. **A661**, 119 (1999).
- [10] A. Balanda, Heavy Ion Phys. **7**, 119 (1998).
- [11] S. A. Bass *et al.*, Phys. Rev. **C60**, 021901 (1999).
- [12] K. J. Eskola and X.-N. Wang, Phys. Rev. **D49**, 1284 (1994).
- [13] H. Von Gersdorff, L. McLerran, M. Kataja, and P. V. Ruuskanen, Phys. Rev. **D34**, 794 (1986).

- [14] L. D. McLerran, M. Kataja, P. V. Ruuskanen, and H. von Gersdorff, *Phys. Rev.* **D34**, 2755 (1986).
- [15] X. Cai, X. R. Wang, C. B. Yang, and Z. M. Zhou, *Nucl. Phys. Proc. Suppl.* **71**, 319 (1999).
- [16] S. A. Bass *et al.*, *Phys. Rev.* **C60**, 021902 (1999).
- [17] Y. Iwasaki *et al.*, *Phys. Rev.* **D54**, 7010 (1996).
- [18] D. Teaney and E. V. Shuryak, *Phys. Rev. Lett.* **83**, 4951 (1999).
- [19] L. P. Csernai, J. I. Kapusta, G. Kluge, and E. E. Zabrodin, *Z. Phys.* **C58**, 453 (1993).
- [20] S. Sarkar *et al.*, *Nucl. Phys.* **A634**, 206 (1998).
- [21] S. Sarkar, *Photons From Ultrarelativistic Heavy Ion Collisions* (Ph. D. Thesis, University of Calcutta, India, 2000).
- [22] J. Cleymans and K. Redlich, *Phys. Rev.* **C60**, 054908 (1999).
- [23] N. Xu *et al.*, *Nucl. Phys.* **A610**, 175c (1996).
- [24] R. Rapp and J. Wambach, *Eur. Phys. J.* **A6**, 415 (1999).
- [25] J. Alam *et al.*, *Annals Phys.* **286**, 159 (2001).
- [26] L. D. McLerran and T. Toimela, *Phys. Rev.* **D31**, 545 (1985).
- [27] K. Kajantie, J. Kapusta, L. McLerran, and A. Mekjian, *Phys. Rev.* **D34**, 2746 (1986).
- [28] A. Dumitru *et al.*, *Phys. Rev. Lett.* **70**, 2860 (1993).

- [29] A. Majumder and C. Gale, Phys. Rev. **D63**, 114008 (2001).
- [30] X-Jin, D. B. Leinweber, Phys. Rev. C **52**, 3344 (1995).
- [31] H. Shiomi and T. Hatsuda, Phys. Lett. **B334**, 281 (1994).
- [32] H. C. Jean, J. Piekarewicz, and A. G. Williams, Phys. Rev. **C49**, 1981 (1994).
- [33] R. Rapp, G. Chanfray, and J. Wambach, Nucl. Phys. **A617**, 472 (1997).
- [34] J. Stroth and others, *Hadrons in Nuclear Matter, Proceedings of the International Workshop XXII* (GSI, Darmstadt, 1995), p. 202.
- [35] R. A. Broglia, P. Kienle and P. F. Bartignon, *Probing the Nuclear Paradigm with Heavy Ion Reactions* (World Scientific, Singapore, 1994), p. 463.
- [36] G. Roche, Phys. Lett. B **226**, 228 (1989).
- [37] C. Nandet, Phys. Rev. Lett. **62**, 2652 (1989).
- [38] B.M. Freedman and G.S. Blanpied, CEBAF report **PR-89-001**, (1989).
- [39] G.Q. Li, C.M. Ko and G.E. Brown, Phys. Rev. Lett. **75**, 4007 (1995).
- [40] R. Rapp and J. Wambach, Adv. Nucl. Phys. **25**, 1 (2000).
- [41] G. E. Brown and M. Rho, Phys. Rev. Lett. **66**, 2720 (1991).
- [42] T. Hatsuda and S.H. Lee, Phys. Rev. C **46**, 34 (1992).
- [43] C. M. Shakin and Wei-Dong Sun, Phys. Rev. C **49**, 1185 (1994).
- [44] M. Herrmann, B. L. Friman and W. Nörenberg, Z. Phys. A **343**, 119 (1992).
- [45] S. A. Chin, Ann. Phys. **108**, 301 (1977).

- [46] G. E. Brown and M. Rho, Phys. Lett. **B237**, 3 (1990).
- [47] G. Wolf, B. Friman and M. Soyeur, Nucl. Phys. A **640**, 129 (1998).
- [48] O. Teodorescu, A. K. Dutt-Mazumder, and C. Gale, Phys. Rev. **C61**, 051901 (2000).
- [49] O. Teodorescu, A. K. Dutt-Mazumder, and C. Gale, Phys. Rev. **C63**, 034903 (2001).
- [50] O. Teodorescu, A. K. Dutt-Mazumder, and C. Gale, Phys. Rev. C (in prep.) .
- [51] Particle Data Group, Euro. Phys. J. C **3**, (1998).
- [52] K. Saito, K. Tsushima, A. W. Thomas, A. G. Williams, Phys. Lett. B **433**, 243 (1998).
- [53] B. D. Serot and J. D. Walecka, Adv. Nucl. Phys **16**, 1 (1986).
- [54] J.D. Walecka, Ann. Phys. **83**, 491 (1974).
- [55] J. D. Walecka, *Theoretical Nuclear Physics* (Oxford University Press, New York, 1995).
- [56] K. Erkelenz, Phys. Rept. **13**, 191 (1974).
- [57] M. A. Preston and R. K. Bhaduri, *Structure of the Nucleus* (Addison-Wesley, Reading, Massachusetts, 1975).
- [58] M. E. Peskin and D. V. Schroeder, *An Introduction to Quantum Field Theory* (Addison-Wesley, Reading, Massachusetts, 1995).
- [59] J. J. Sakurai, *Modern Quantum Mechanics* (Addison-Wesley, Reading, Massachusetts, 1994).

- [60] B. D. Serot and J. D. Walecka, *Int. J. Mod. Phys.* **E6**, 515 (1997).
- [61] A. L. Fetter and J. D. Walecka, *Theoretical Mechanics of Particles and Continua* (McGraw-Hill, New York, 1980).
- [62] Cheryl Grant and Joseph Kapusta, *Phys. Rev. C* **32**, 663 (1985).
- [63] R. K. Pathria, *Statistical Mechanics* (Oxford, Boston, 1996).
- [64] B. M. Waldhauser *et al.*, *Phys. Rev.* **C36**, 1019 (1987).
- [65] R. J. Furnstahl and B. D. Serot, *Phys. Rev.* **C41**, 262 (1990).
- [66] H. Mueller and B. D. Serot, *Nucl. Phys.* **A606**, 508 (1996).
- [67] E. V. Shuryak, *The QCD Vacuum, Hadrons and the Superdense Matter* (World Scientific, Singapore, 1988).
- [68] G. E. Brown, *Proceedings of the Nuclear Physics Conference* (Sao Paulo, Brazil, 1989), Vol. 2, pp. 3–34.
- [69] A. Hosaka, *Phys. Lett.* **B244**, 363 (1990).
- [70] K. Saito and A. W. Thomas, *Phys. Rev.* **C51**, 2757 (1995).
- [71] Y. Koike, *Phys. Rev.* **C51**, 1488 (1995).
- [72] M. Asakawa, C. M. Ko, P. Levai, and X. J. Qiu, *Phys. Rev.* **C46**, 1159 (1992).
- [73] A.K. Dutt-Mazumder, *Nucl. Phys. A* **611**, 442 (1996).
- [74] R. Rapp, G. Chanfray, J. Wambach, *Phys. Rev. Lett.* **76**, 368 (1996).
- [75] G. Agakishiev *et al.*, *Phys. Lett.* **B422**, 405 (1998).

- [76] Michel Le Bellac, *Thermal Field Theory* (Cambridge University Press, Great Britain, 1996).
- [77] J.-P. Blaizot and E. Iancu, (2001), arXiv:hep-ph/0101103.
- [78] Pines, D., *The Many-Body Problem* (W. A. Benjamin, New York, USA, 1961).
- [79] Fetter, A. L. and Walecka, J. D., *Quantum Theory of Many-Particle Systems* (McGraw-Hill, New York, USA, 1971).
- [80] V. N. Tsytovich, Soviet Physics JTEP **13**, 1249 (1961).
- [81] J. J. Sakurai, *Currents and Mesons* (University of Chicago Press, Chicago, 1969).
- [82] R. Machleidt, Adv. Nucl. Phys. **19**, 198 (1989).
- [83] T. Ericson and W. Weise, *Pions and Nuclei* (Clarendon Press, Oxford, 1988).
- [84] H. Yamamoto and T. Matsubara, Prog. Theor. Phys. **54**, 920 (1975).
- [85] V.M. Galitskii and A.B. Migda, Sov. Phys. JETP **34**, 96 (1958).
- [86] A.B. Migdal, Phys. Rev. Lett. **31**, 247 (1973).
- [87] E. S. Fradkin, Nucl. Phys. **12**, 465 (1959).
- [88] Ta-Pei Cheng and Ling-Fong Li, *Gauge Theory of Elementary Particles* (Clarendon Press, Oxford, 1984).
- [89] J. C. Caillon and J. Labarsouque, Phys. Lett. **B311**, 19 (1993).
- [90] T. Hatsuda, H. Shiomi, and H. Kuwabara, Prog. Theor. Phys. **95**, 1009 (1996).

- [91] A. K. Dutt-Mazumder, B. Dutta-Roy, and A. Kundu, Phys. Lett. **B399**, 196 (1997).
- [92] W. Broniowski and W. Florkowski, Phys. Lett. **B440**, 7 (1998).
- [93] W. Greiner and J. A. Maruhn, *Nuclear Models* (Springer, Berlin, 1996).
- [94] R. P. Feynman, *Photon Hadron Interactions* (W. A. Benjamin, Reading, Massachusetts, USA, 1972).
- [95] R. D. Pisarski, *Workshop on Finite Temperature QCD and Quark-Gluon Transport Theory* (PRC, Wuhan, 1994).
- [96] C. Song, Phys. Rev. **D53**, 3962 (1996).
- [97] M. Harada and A. Shibata, Phys. Rev. **D55**, 6716 (1997).
- [98] A.K. Dutt-Mazumder, A. Kundu, T. De and B. Dutta-Roy, Phys. Lett. B **378**, 35 (1996).
- [99] A.K. Dutt-Mazumder, J. Alam, B. Dutta-Roy and B. Sinha, Phys. Lett. B **396**, 264 (1997).
- [100] R. L. Kobes and G. W. Semenoff, Nucl. Phys. **B260**, 714 (1985).
- [101] F. Gelis, Nucl. Phys. **B508**, 483 (1997).
- [102] Ashok Das, *Finite Temperature Field Theory* (World Scientific, Singapore, 1997).
- [103] V. L. Eletsky and J. I. Kapusta, Phys. Rev. **C59**, 2757 (1999).
- [104] K. L. Haglin and C. Gale, Nucl. Phys. **B421**, 613 (1994).
- [105] C. Song, Phys. Lett. **B388**, 141 (1996).

- [106] Rückl, R., Phys. Lett. **B64**, 39 (1976).
- [107] J. Jalilian-Marian and V. Koch, Phys. Rev. **C58**, 3763 (1998).
- [108] K. Haglin and C. Gale, Proceedings of the 9<sup>th</sup> Winter Workshop on Nuclear Dynamics, Key West, 264 (1976).
- [109] S. D. Drell and T.-M. Yan, Phys. Rev. Lett. **25**, 316 (1970).
- [110] C. Spieles *et al.*, Eur. Phys. J. **C5**, 349 (1998).
- [111] K. Geiger, Phys. Rept. **258**, 237 (1995).
- [112] P. Aurenche, F. Gelis, R. Kobes, and H. Zaraket, Phys. Rev. **D60**, 076002 (1999).
- [113] J. I. Kapusta and S. M. H. Wong, Phys. Rev. **C62**, 027901 (2000).
- [114] K. L. Haglin and C. Gale, Phys. Rev. **C63**, 065201 (2001).
- [115] B. Kampfer, O. P. Pavlenko, and K. Gallmeister, Phys. Lett. **B419**, 412 (1998).
- [116] R. H. Dalitz, Proc. Phys. Soc. (London) **A64**, 667 (1951).
- [117] B. E. Lautrup and J. Smith, Phys. Rev. **D3**, 1122 (1971).
- [118] J. J. Sakurai, Annals Phys. **11**, 1 (1960).
- [119] R. K. Bhaduri, *Models of the Nucleon: from Quarks to Soliton* (Addison-Wesley, Redwood City, USA, 1988), pp. 261–286.
- [120] Y. Nambu, Phys. Rev. **106**, 1366 (1957).
- [121] N. M. Kroll, T. D. Lee, and B. Zumino, Phys. Rev. **157**, 1376 (1967).
- [122] N. P. Landsman and Ch. G. van Weert, Phys. Rep. **145**, 141 (1987).

- [123] C. Gale and J. Kapusta, Nucl. Phys. B **357**, 65 (1991).
- [124] C. Gale and J. Kapusta, Phys. Rev. C **35**, 2107 (1987).
- [125] C. Gale and P. Lichard, Phys. Rev. D **49**, 3338 (1994).
- [126] H. Sorge, Phys. Lett. **B373**, 16 (1996).
- [127] M. Kirchbach and L. Tiator, Nucl. Phys. **A604**, 385 (1996).
- [128] N. A. Tornquist and M. Roos, Phys. Rev. Lett. **76**, 1575 (1996).
- [129] M. Harada, F. Sannino, and J. Schechter, Phys. Rev. **D54**, 1991 (1996).
- [130] M. Harada, F. Sannino, and J. Schechter, Phys. Rev. Lett. **78**, 1603 (1997).
- [131] L. Xiong, Z.G. Wu, C.M. Ko and J.Q. Wu, Nucl. Phys. **A512**, 772 (1990).
- [132] J. Friese, Nucl. Phys. **A654**, 311 (1999).
- [133] J. Friese, Prog. Part. Nucl. Phys. **42**, 235 (1999).
- [134] A. Devismes, *Proceedings of the International Workshop XXVIII on Gross Properties of Nuclei and Nuclear Excitations, Hirschegg, Austria* (GSI, Darmstadt, 2000).
- [135] G. Agakishiev *et al.*, Nucl. Phys. **A638**, 159 (1998).
- [136] A. Drees, *Proceedings of the International Workshop XXIII on Gross Properties of Nuclei and Nuclear Excitations, Hirschegg, Austria* (GSI, Darmstadt, 1995).
- [137] G. Agakishiev *et al.*, Eur. Phys. J. **C4**, 231 (1998).
- [138] G. Agakishiev *et al.*, Eur. Phys. J. **C4**, 249 (1998).
- [139] G. Agakishiev *et al.*, Phys. Rev. Lett. **75**, 1272 (1995).

- [140] P. Wurm *et al.*, Nucl. Phys. **A590**, 103c (1995).
- [141] G. Q. Li, C. M. Ko, G. E. Brown, and H. Sorge, Nucl. Phys. **A611**, 539 (1996).
- [142] S. Sarkar, J. Alam, and T. Hatsuda, (2000).
- [143] C. M. Hung and E. Shuryak, Phys. Rev. **C57**, 1891 (1998).
- [144] H. Appelshauser, Prog. Part. Nucl. Phys. **42**, 311 (1999).
- [145] U. A. Wiedemann, Nucl. Phys. **A661**, 65c (1999).
- [146] J.-e. Alam *et al.*, Phys. Rev. **C59**, 905 (1999).
- [147] V. L. Eletsky, M. Belkacem, P. J. Ellis, and J. I. Kapusta, Phys. Rev. **C64**, 035202 (2001).
- [148] P. Salabura *et al.*, Nucl. Phys. Proc. Suppl. **44**, 701 (1995).
- [149] J. Cleymans, H. Oeschler, and K. Redlich, J. Phys. G **G25**, 281 (1999).
- [150] R. Schicker *et al.*, Nucl. Instrum. Meth. **A380**, 586 (1996).
- [151] H. Oeschler, Acta Phys. Polon. **B31**, 227 (2000).
- [152] J. Cleymans, H. Oeschler, and K. Redlich, Phys. Rev. **C59**, 1663 (1999).
- [153] R. Albrecht *et al.*, Phys. Lett. **B361**, 14 (1995).
- [154] Y. A. Tarasov, Phys. Lett. **B441**, 453 (1998).
- [155] M. Post, S. Leupold, and U. Mosel, Nucl. Phys. **A689**, 753 (2001).
- [156] O. Teodorescu, A. K. Dutt-Mazumder, and C. Gale, Phys. Rev. C (in prep.) .